Distribution Agreement

In presenting this thesis or dissertation as a partial fulfillment of the requirements for an advanced degree from Emory University, I hereby grant to Emory University and its agents the non-exclusive license to archive, make accessible, and display my thesis or dissertation in whole or in part in all forms of media, now or hereafter known, including display on the world wide web. I understand that I may select some access restrictions as part of the online submission of this thesis or dissertation. I retain all ownership rights to the copyright of the thesis or dissertation. I also retain the right to use in future works (such as articles or books) all or part of this thesis or dissertation.

Signature:

Jeffrey B. Schriber	Date

Development of Selected Configuration Interaction Methods for Problems in Strong Correlation

By

Jeffrey B. Schriber
Doctor of Philosophy

Chemistry

Dr. Francesco Evangelista, Ph.D
Advisor

Dr. Joel Bowman, Ph.D
Committee Member

Dr. James Kindt, Ph.D
Committee Member

Accepted:

Lisa A. Tedesco, Ph.D
Dean of the James T. Laney School of Graduate Studies

Date

Development of Selected Configuration Interaction Methods for Problems in Strong Correlation

By

Jeffrey B. Schriber
B.S., University of Richmond, 2014

Advisor: Dr. Francesco Evangelista, Ph.D

An abstract of
A dissertation submitted to the Faculty of the
James T. Laney School of Graduate Studies of Emory University
in partial fulfillment of the requirements for the degree of
Doctor of Philosophy
in Chemistry
2019

Abstract

Development of Selected Configuration Interaction Methods for Problems in Strong Correlation

By Jeffrey B. Schriber

In this dissertation, we develop and apply the adaptive configuration interaction (ACI) method to enable computations on large chemical systems with potentially many strongly correlated electrons. ACI is a new variant of selected CI methods that provides the user with *a priori* control over the error in the total energy by an iterative, cumulative determinant screening algorithm. We benchmark the ACI on the dissociation of N_2 and on the singlet-triplet splittings of oligoacenes up to decacene, achieving sub kcal mol^{-1} accuracy in comparison to density matrix renormalization group data. We then extend the ACI to compute excited states both by optimizing determinantal spaces for each electronic state, and by using a single determinantal space optimized for several states. We test these methods using excited states of methylene, the avoided crossing in LiF, and challenging excited states in long polyenes. To connect the ACI to a dynamical correlation treatment, we then use ACI as an affordable substitute for complete active space CI (CASCI) in combination with the multireference driven similarity renormalization group perturbatively expanded to second order (ACI-DSRG-MRPT2). The ACI-DSRG-MRPT2 uses specialized techniques to recover both static and dynamical electron correlations, and we are able to treat active spaces with as many as 30 electrons in 30 orbitals in a total basis of 1350 orbitals. We apply this method to the oligoacenes and achieve good agreement with experimental singlet-triplet splittings, and the dynamical correlation treatment causes a significant reduction in the observed radical character compared to active space methods. Finally, we introduce a real time-dependent ACI (TD-ACI) which uses ACI to generate a fixed basis for propagating an initial state in real time. We apply the TD-ACI to study charge migration dynamics following ionization, and we can reproduce experimental migration frequencies in iodoacetylene with minimal computational effort.

Development of Selected Configuration Interaction Methods for Problems in Strong Correlation

By

Jeffrey B. Schriber
B.S., University of Richmond, 2014

Advisor: Dr. Francesco Evangelista, Ph.D

A dissertation submitted to the Faculty of the
James T. Laney School of Graduate Studies of Emory University
in partial fulfillment of the requirements for the degree of
Doctor of Philosophy
in Chemistry
2019

Acknowledgement

First, I would like to thank my undergraduate research advisor, Dr. Carol Parish, for taking me into her group when I was just a distracted and generally confused freshman. She introduced me to computational chemistry and got me hooked on problems in strong correlation right away. Without her mentorship and belief in my potential, I certainly would not have been able to succeed in research and genuinely enjoy learning as much as possible about theoretical chemistry. I am thankful for our frequent attendance of conferences, particularly one long drive we made to SETCA hosted at UGA in 2012, where I was especially intrigued by a talk given by a post-doc working in the Tully group at Yale. Little did I know, I'd be one of his early students at Emory just two years following.

That said, I would like to thank my advisor, Dr. Francesco Evangelista, for being a great mentor, educator, and scientist. His ability to endlessly come up with new, interesting ideas is astounding, and I will always be grateful for how he has guided me in becoming a better scientist. I would look forward to his daily visits at our desks (or more commonly at the espresso machine), where he would nonchalantly list off a handful of research ideas that would often send me into a week-long reading and prototyping binge. I thank him for fostering a lab environment not driven by competition, but by open collaboration. I also thank my committee members, Dr. Joel Bowman and Dr. James Kindt, for their helpful advice and mentorship. I often fondly think about our discussion following my original research proposal a year ago, which has stuck with me and left me more prepared to seriously pursue a career in science.

It is an impossible task to properly express my gratitude towards the Evangelista group members I worked with in my tenure at Emory. The early years can be especially tough due to the constant flow of new material to master, and I certainly would not have been able to get through them without the help and companionship from Kevin Hannon and Tianyuan (Sam) Zhang. I thank Kevin for constantly encouraging me to evaluate my scientific ideas, desires, and overall happiness and for being there to answer my many questions when I was (wrongfully) too embarrassed to ask anyone else. I thank Sam for our many memorable collaborative work sessions and for being more helpful than Google. I am also thankful for the guidance from Dr. Wallace Derricotte and Dr. Chenyang (York) Li, who both set the model of productivity, while still maintaining such calm and easygoing demeanors. I also want to thank the newer group members, Nick Stair, Nan He, Shuhe Wang, and Renke Huang—the future of the lab is clearly in good hands. I am thankful for many conversations with Nick that always serve as a constant source of insight, stoke, and growth.

I thank my parents, Rufus and Kathy Schriber, and my sister, Sarah Schriber, for constant love and support and for always encouraging me to pursue things that are interesting, challenging, and helpful. To Rebecca, I thank for endless patience and love and for providing balance in my life. I would not have made it here without their support.

My final acknowledgement is to the late Dr. James Aldridge, who first instilled a desire in me to become an intellectual of any sort.

– Jeff

Table of Contents

1 Introduction 1
1.1 Introduction 1
1.2 Electronic Structure Theory 3
1.2.1 Second Quantization 5
1.2.2 An exact solution 6
1.2.3 Single-reference Approaches 8
1.3 Multireference Methods 11
1.3.1 Active Space Treatments 13
1.3.2 Multireference Methods for Dynamical Correlation 18
1.3.3 The Driven Similarity Renormalization Group 22
1.4 Selected Configuration Interaction 25
1.4.1 Early Selected CI Methods 26
1.4.2 Modern Selected CI 28
1.5 Prospectus 31

2 The Adaptive Configuration Interaction Method 44
2.1 Introduction 44
2.2 The Adaptive Configuration Interaction Method 45
2.3 Numerical Tests and Applications 48
2.3.1 The Dissociation of N_2 48
2.3.2 Singlet-Triplet Splittings in Oligoacenes 50
2.4 Conclusions 52

3 ACI for Computing Challenging Excited States 58
3.1 Introduction 58
3.2 Theory 62
3.2.1 Brief review of ground-state ACI 62
3.2.2 Excited State Methods in ACI 66
3.3 Results and Discussion 72
3.3.1 Methylene 72
3.3.2 LiF avoided crossing 75
3.3.3 Extended polyenes 79
3.4 Conclusions 84

4 Combining ACI with DSRG 96
4.1 Introduction 96
4.2 Theory 98
4.2.1 Adaptive CI 98
4.2.2 Implementation of RDMs 100
4.2.3 DSRG-MRPT2 101
4.3 The Oligoacenes. 105
4.3.1 Computational Details 106
4.3.2 Singlet-Triplet Splittings 109
4.3.3 Emergent Radical Character 113
4.3.4 Analysis of Spin-Spin Correlation 115
4.4 Conclusions 117

5 Real-Time Propagation of Selected Configuration Interaction Wave Functions Applied to Charge Migration. 126
5.1 Introduction 126
5.2 Theory 129
5.2.1 Time-Dependent ACI 129
5.3 Results and Discussion 133
5.3.1 Valence Ionization of Benzene 133
5.3.2 Charge Migration in Iodoacetylene 137
5.4 Conclusions and Future Challenges. 140

6 Conclusions and Future Directions 150

List of Figures

1.1 Squared magnitude of CI expansion coefficients computed from FCI and CISD wave functions. Determinants are ordered based on magnitude in the FCI expansion, and determinants with squared coefficient less than 10^{-12} are not shown. 12

2.1 Evolution of determinant spaces in the ACI algorithm. Each node represents a determinant, and the edges represent coupling through the Hamiltonian between two nodes. The edges are weighted by the magnitude of this coupling, and the nodes are weighted proportionally to the square modulus of the determinant coefficient ($|C_\mu|^2$). 45

2.2 Ground-state potential energy curve of N_2 computed with the cc-pVDZ basis set. (A) Energy errors with respect to FCI for the ACI, MR-CISD, and MR-CISD+Q. (B) Energy errors with respect to FCI for the ACI plus the second-order energy correction [Eq. (2.9)]. ACI results used restricted Hartree–Fock orbitals while MR-CISD and MR-CISD+Q results are based on a CASSCF(6,6) reference. The 1s-like orbitals of nitrogen were frozen in all correlated computations. 50

3.1 Squared expansion coefficients computed from full CI wave functions of the three lowest singlets of methylene. The DZ basis was used without freezing orbitals, resulting in a CAS(8e,14o) and 239,259 determinants. The squared coefficients are sorted by magnitude, and vertical lines represent where the accumulation of squared coefficients reaches 0.999 for each state. 60

3.2 Comparison of ACI excited state methods for three electronic states of methylene. The points shown are computed for $\sigma = 0.5$, 0.25, 0.1, 0.05, and 0.005 eV. All computations used the modified cc-pVDZ basis set as described in Ref. 105 with no frozen orbitals. 74

3.3 Absolute energy errors (mE_h) for the avoided crossing of LiF computed with various methods. For all ACI methods, values of $\sigma = 10$ and 1.0 mE_h are used and plotted as grey dashed lines. Solid lines represent errors in the ground $X\ ^1\Sigma^+$ state, while dashed lines represent errors in the $2\ ^1\Sigma^+$ excited state. The custom basis from Ref. 112 was used with two 1s-like molecular orbitals frozen. 77

3.4 Absolute energy errors (mE_h) and number of determinants required for the lowest eight singlets of octatetraene computed with all excited state ACI methods with $\sigma = 1.0$. The ground electronic state is labeled in each calculation, while all excited states are unlabeled. 81
3.5 Vertical excitation energies (eV) for five polyenes computed with OC-ACI(10) and with CASCI for the first three polyenes. 84

4.1 Summary of batched screening algorithm. (**A**) Determinants in the first batch are generated from a subset of the single and double excitations from the reference P space. The excited determinants in the batch are sorted and screened using a scaled σ value, with only selected ones being stored. (**B**) The procedure in **A** is repeated for all batches sequentially, with all selected determinants stored. (**C**) These selected determinants are merged and sorted, and a final screening is done to ensure that the total correlation energy ignored corresponds to the original σ value. 99
4.2 Size consistency errors $[E_n(\sigma) - n \times E_1(\sigma)]$ for n non-interacting benzene molecules computed with relaxed ACI-DSRG-MRPT2 using CAS(6n,6n) active spaces and a cc-pVDZ basis set. Each curve is labeled by its σ value in mE_h. 104
4.3 Absolute energy, singlet-triplet splitting, and norm of the T_1 amplitudes as a function of s, computed for pentacene with ACI-DSRG-MRPT2 using a CAS(22,22) and $\sigma = 5$ mE_h. Red and dark blue curves represent singlet and triplet states, respectively, and solid (dashed) lines represent relaxed (unrelaxed) energies. The vertical black line indicates the $s = 0.5$ E_h^{-2} value used in the remainder of this work. 108
4.4 ACI-DSRG-MRPT2 error in adiabatic singlet-triplet splitting of n-acenes ($2 \leq n \leq 6$) with respect to experiment using cc-pVDZ (left) and cc-pVTZ (right) basis sets and unrelaxed (top) and relaxed (bottom) references. The shaded area indicates a ± 1 kcal mol^{-1} error window, and no zero-point vibrational energy correction is included. 109
4.5 Number of unpaired electrons for the ground state singlets of the oligoacenes computed from unrelaxed (dashed line) and relaxed (solid line) ACI-DSRG-MRPT2 wave functions. Sigma values are chosen to produce a constant 190 μE_h error per electron. 114
4.6 Log-plot of the spin-spin correlation function using carbons 1 and 6 as references, computed for the ground state singlet of pentacene with a relaxed ACI-DSRG-MRPT2 wave function. 115
4.7 Spin correlation densities plotted from unrelaxed and relaxed references, in addition to the difference of relaxed and unrelaxed results. We show two reference sites, marked with "*", corresponding to central and terminal carbons consistent with the labeling in Figure 4.6, with all reference sites plotted in the SI. 116

5.1 Sorted squared magnitudes of all determinants in the FCI wave function. The wave function is computed for a lithium dimer separated by 1.0 Å, computed with the STO-3G basis and propagated using the exact exponential propagator. Each curve shows the coefficients at 10, 100, 1000, and 10000 as snapshots. We also plot a labeled vertical dotted line at the number of determinants that recover 99% of the exact FCI wave function. . . 128
5.2 Active space used in all benzene computations. Orbitals are computed with restricted Hartree–Fock using C_1 symmetry, though we use D_{2h} labels here for convenience. 134
5.3 Error in propagated wave functions computed with various σ values using one, two, or three reference states in computing the cationic basis. The error is defined as the deviation between unity and the overlap of the approximate wave function with the exact wave function, for which $|M^{N-1}| = 3920$ determinants. Each error curve is labeled with the number of determinants in the cationic space. The exact wave functions are propagated with the exact propagator, and TD-ACI wave functions are propagated with the fourth order Runge–Kutta propagator. 135
5.4 Hole occupations of $1b_{1u}$ (red), $1b_{2g}$ (blue), and $1b_{3g}$ (green) orbitals computed using TD-ACI with various sizes of M^{N-1} optimized for 1, 2, and 4 states. The top row shows occupations computed using the exact propagator, and the bottom row used the fourth order Runge–Kutta propagator. Each plot shows the exact occupations with a grey line. 137
5.5 Hole occupations of the $5p$-like molecular orbital on iodine (red) and the π on the acetylene (blue) in the same plane. Below the plot we show the migration of the hole using the representation of the hole density defined in the text. The snapshots selected for the densities shown correspond to maxima, minima and intersection of the hole occupation curves. 139

List of Tables

2.1 Errors with respect to FCI (ΔE, in mE_h), number of variational parameters (N_par), and non-parallelism error (NPE = $|\Delta E(r=3) - \Delta E(r=1.1)|$) for the ground state of N_2 at r = 1.1 and 3 Å computed with the cc-pVDZ basis set. ACI and MR-CI computations used restricted Hartree–Fock and CASSCF(6,6) orbitals, respectively. The 1s-like orbitals of nitrogen were frozen in all correlated computations. For $\sigma = 1$, we also report ACI results computed using MP2 natural orbitals (NO) and CASSCF(6,6) orbitals (CAS). 51

2.2 Singlet-triplet splittings of the acene series computed with the ACI , DMRG, and v-2RDM methods using the STO-3G basis set. All carbon π orbitals were correlated. 51

2.3 Number of determinants required for the ACI wave functions used for the oligoacenes in this work. 52

3.1 Comparison of excited state ACI methods. 70

3.2 Methylene vertical excitation energies (eV) obtained with truncated CI, EOM-CCSD, CC3, and ACI methods. All computations use restricted Hartree–Fock orbitals and the modified cc-pVDZ basis described in Ref. 105 with no frozen orbitals, resulting in a CAS(8e,27o). 73

3.3 Comparison of LiF avoided crossing curves. We report the average error for the lowest two Σ^+ states, the non paralellism error (NPE)[a], the standard deviation ($\sigma_{\Delta E}$) with respect to FCI, and the average number of variational parameters (N_p) required for each computation. For OC-ACI computations, the two numbers represent the average number of determinants required for ground and excited states, respectively. All values are reported in mE_h, and computed from seven bond distances from 8.5 a.u. to 14.5 a.u. incremented by 1 a.u. in order to enable comparison with PMC-SD and SA-MCCI. We do not show data for MS-ACI and SC-ACI as they diverge near the avoided crossing. All ACI computations used restricted Hartree–Fock orbitals and the custom basis set defined in Ref. 112, with the two 1s-like molecular orbitals frozen on each atom resulting in a CAS(8,27). 76

3.4 Comparison of excited state ACI methods for the lowest eight singlet electronic states of octatetraene (C_8H_{10}) computed with $\sigma = 1$ and 10 mE_h. All computations use split-localized orbitals, with an active space including all sixteen π orbitals defined in the cc-pVDZ basis. We report both the excitation energy errors (ΔE_{ex}) and absolute energy errors (ΔE_{abs}) with respect to FCI in mE_h. 80

3.5 Vertical excitation energies (eV) for the polyene series ($C_{2n}H_{2n+2}$) computed with various methods. All ACI, CASCI, and DRMG methods use a CAS($2n$,$2n$), and the NOCI calculation was performed with 10 nonorthogonal determinants as described in Ref 129. The OC-ACI computation uses σ = 10 mE_h. 83

4.1 Adiabatic singlet-triplet splittings (kcal mol^{-1}) of the acene series computed with ACI and ACI-DSRG-MRPT2 with both unrelaxed and relaxed references. 111

4.2 Comparison of the best ACI-DSRG-MRPT2 adiabatic singlet-triplet splittings (kcal mol^{-1}) of the acene series with selected literature values . . 112

5.1 Hole migration times (as) for various dimensions of M^{N-1} optimized with respect to one, two, or three electronic states. 140

Chapter 1

Introduction

1.1 Introduction

As famously summarized by Paul Dirac, quantum mechanics, even at its inception, had the capacity to describe chemical phenomena but contained equations too complicated to be practically solved. Thus, he continued, approximations are required to reduce the mathematical complexity while still conserving the desired properties of a particular molecular system.[1] The exponential growth of available computational power since then has rendered parts of Dirac's early prognostications obsolete; nonetheless, modern applications of quantum mechanics to chemical problems still rely on appropriately chosen approximations. Unfortunately, no single set of approximations has produced a theory or equation which can adequately and tractably predict the behavior of molecules, despite the laws governing the interaction of electrons and nuclei being known for decades.

The central goal of the modern quantum chemist is to develop predictive theories whose range of applicability is, at best, broad and, at worst, well-understood. To achieve this goal, a new theory needs to be traceable to an exact or near-exact theory through a series of systematic, well-understood, and controllable approximations. The first approximations commonly invoked in quantum chemistry are defined by our scope of interest, namely that the desired chemical information we seek is largely determined by the behavior of the electrons in a molecular system. Thus, we invoke the Born-Oppenheimer approximation

and assume nuclei are fixed in space, so that mathematically we only need to solve for an electronic wave function in a field of fixed nuclei. Furthermore, if we restrict our range of applicability to moderately light elements, we can safely ignore the relativistic effects of fast-moving electrons in the cores of heavy atoms, which can also greatly complicate the mathematics.

This set of initial approximations together comprise the subfield known as electronic structure theory, which is primarily concerned with obtaining the electronic energy and wave function of a molecular system. These quantities arise from the solution of the time-independent Schrödinger equation, which produces the electronic energy, E_n, and wave function, Ψ_n for a particular state n, using the electronic Hamiltonian operator, $\hat{H}$,

$$\hat{H}\left|\Psi_n\right\rangle = E_n\left|\Psi_n\right\rangle, \tag{1.1}$$

which is a simple hermitian eigenvalue problem. The electronic Hamiltonian is written as,

$$\hat{H} = -\sum_i \frac{1}{2}\nabla_i^2 - \sum_{i,A}\frac{Z_A}{r_{i,A}} + \sum_{i,j}\frac{1}{r_{ij}}, \tag{1.2}$$

where i and A label electrons and nuclei, respectively, ∇_i^2 is the Laplace operator, r is an inter-particle distance, and Z_A is the nuclear charge.[2] Correspondingly, the first term is the kinetic energy of each electron, the second term is the Coulombic attraction between electrons and nuclei, and the final term is the electron-electron repulsion. This final term simultaneously couples all pairs of electrons and correspondingly requires a wave function that contains all 2-, 3-, ..., up to N-body correlations. An exact solution to the Schrödinger equation is thus impossible for systems with more than one electron because the wave function becomes impossibly complex. Accurately approximating the electron repulsion is a central challenge of electronic structure theory, and it is typically done by initially assuming the electrons are essentially non-interacting and introducing electron-electron interactions—called electron correlation—in a tractable way.

The goal of this thesis is to find new ways to solve the Schrödinger equation in cases

where approximating electron correlation is particularly difficult due to the presence of a phenomenon called *strong correlation*. In the remainder of this chapter, we will present more details on electronic structure theory such that a precise definition of strong electron correlation is reached. We will then provide a brief review of conventional techniques for solving the Schrödinger equation for molecules with strongly-correlated electrons, with particular attention paid to selected configuration interaction methods.

1.2 Electronic Structure Theory

As introduced previously, electronic structure theory is the branch of quantum chemistry primarily concerned with solving the time-independent electronic Schrödinger equation. Particularly challenging is handling the many-body nature of the exact wave function that arises due to the electron repulsion term of the electronic Hamiltonian. A common approximation to circumvent this many-body problem is to express the wave function in a basis of one-electron wave functions, called spin orbitals, and to replace the electron repulsion term of the Hamiltonian with some yet-undefined one-body potential between each electron and an average field of the remaining electrons. Operating under this assumption of an averaged field, we can write a solution for the wave function as a normalized and antisymmetrized product of $2N$ spin orbitals, corresponding to N spatial orbitals,

$$|\Psi_n\rangle = |\Phi_n\rangle \equiv \frac{1}{\sqrt{2N!}} \begin{vmatrix} \phi_1(\mathbf{x_1}) & \phi_1(\mathbf{x_2}) & \cdots & \phi_1(\mathbf{x_{2N}}) \\ \phi_2(\mathbf{x_1}) & \phi_2(\mathbf{x_2}) & \cdots & \phi_2(\mathbf{x_{2N}}) \\ \vdots & \vdots & \ddots & \vdots \\ \phi_{2N}(\mathbf{x_1}) & \phi_{2N}(\mathbf{x_2}) & \cdots & \phi_{2N}(\mathbf{x_{2N}}) \end{vmatrix} \tag{1.3}$$

where $\phi_i(\mathbf{x_j})$ is a spin orbital with associated spatial and spin coordinates $\mathbf{x_j}$ for electron j. Writing the wave function as a determinant ensures indistinguishability of electrons and antisymmetry of the wave function, as swapping two electrons corresponds to swapping columns in the determinant to produce the necessary change of sign. This wave function is called a Slater determinant, $|\Phi\rangle$, and it defines a particular occupation of a set of spin orbitals, or in more chemical terms, a single electronic configuration.

To get the single Slater determinant that best approximates the Schrödinger equation, we invoke the variational principle which states that the optimal Slater determinant minimizes the total energy, defined as $E = \langle \Phi_n | \hat{H} | \Phi_n \rangle$ for a normalilzed Φ_n. The optimizable parameters in the variational minimization are the orbitals that compose the Slater determinant. Furthermore, we cannot use a Hamiltonian with the complete electron repulsion term, but instead we need to use an operator that replaces this term with an averaged electrostatic field. Hartree–Fock (HF) theory defines such an operator in terms of the orbitals themselves, which requires an iterative procedure to optimize both the orbitals and the effective electrostatic field self-consistently (SCF).[2] What results is a set of orbitals that are variationally optimal for a single-determinantal solution to the electronic Schrödinger equation. Furthermore, this set of Hartree–Fock orbitals defines molecular orbital theory, invaluable to chemists, which relies on this foundational approximation that electrons are essentially noninteracting and respond only to an external field.

This simplified picture of electrons does not adequately represent reality. Electrons are negatively charged particles that continuously move in a concerted effort to minimize mutual repulsions. Such a complex correlation of motion is not described under the Hartree–Fock approximation. This phenomenon is termed *dynamical correlation* and it defines the short-range cusp structure of the wave function in addition to long range dispersion.[3] A second failure of Hartree–Fock theory results from its single-determinantal form. If energetic degeneracies among occupied and virtual orbitals exist in the Hartree-Fock solution, then numerous electronic configurations (Slater determinants) can become equally important in the exact wave function. Moreover, if electron-electron repulsion is large and similar in magnitude to combined kinetic and electron-nuclear repulsion energies, then electrons are less energetically "fixed" to the occupation defined in a single determinant and will correspondingly occupy other orbitals. This situation, called *static* or *strong correlation*, points to a more fundamental failure of the mean-field description of electronic repulsion, which cannot produce a qualitatively correct wave function as a simple product of orbitals

when these orbitals contain degeneracies.[3–5] Strong correlation commonly occurs in bond-breaking processes, open-shell transition metal species, electronically excited states, and in large organic molecules with a high degree of orbital degeneracy.[6–11] Cases of static correlation can also indicate entanglement of electrons in the exact wave function, which is defined by their inability to be described by a product of one-electron states. Therefore, a wave function ansatz more flexible and complex than the single Slater determinant is required to describe this phenomena. Unfortunately, the concept of static correlation is rather *ad hoc* in that its definition is intimately tied to the failure of Hartree–Fock in comparison to the exact wave function, which is generally not known.

1.2.1 Second Quantization

Before discussing the various methods for adding a correlation treatment to a Hartree–Fock reference, we will briefly introduce the language of second quantization which conveniently keeps track of orbital occupations and phase factors. We define the Fermi vacuum, $|-\rangle$, as an empty state void of electrons. The creation operator, $\hat{a}_i^\dagger$, creates a particle in orbital ϕ_i, and the annihilation operator, $\hat{a}_i$, destroys a particle in the corresponding orbital. When acting on the vacuum state, the annihilation operator sends the state to zero, e.g.,

$$\hat{a}_i^\dagger |-\rangle = |\phi_i\rangle \tag{1.4}$$

$$\hat{a}_i |-\rangle = 0. \tag{1.5}$$

The creation and annihilation operators obey the following anticommutation relations,

$$\{\hat{a}_i, \hat{a}_j^\dagger\} = \delta_{ij} \tag{1.6}$$

$$\{\hat{a}_i^\dagger, \hat{a}_j^\dagger\} = 0. \tag{1.7}$$

These anticommutation rules provide consistency in determining the sign resultant from an operation, and they enforce the antisymmetry requirement of the wave function. We can

then write an N-particle Slater determinant as,

$$|\Phi\rangle = \hat{a}_1^\dagger \hat{a}_2^\dagger \ldots \hat{a}_N^\dagger |-\rangle . \tag{1.8}$$

Using this notation, the electronic Hamiltonian in the spin-orbital basis can be written as,

$$\hat{H} = \sum_{pq} h_{pq} \hat{a}_p^\dagger \hat{a}_q + \frac{1}{4} \sum_{pqrs} \langle pq||rs\rangle \, \hat{a}_p^\dagger \hat{a}_q^\dagger \hat{a}_s \hat{a}_r, \tag{1.9}$$

where $p, q, r, s, \ldots$ index all spin-orbitals, and we define the one- and antisymmetrized two-electron integrals, respectively,

$$h_{pq} = \int \phi_p^*(\mathbf{x}) h(\mathbf{x}) \phi_q(\mathbf{x}) \mathrm{d}\mathbf{x} \tag{1.10}$$

$$\langle pq||rs\rangle = \langle pq|rs\rangle - \langle pq|sr\rangle \tag{1.11}$$

with the two-electron integrals in physicist's notation defined as,

$$\langle pq|rs\rangle = \int \phi_p^*(\mathbf{x}) \phi_q^*(\mathbf{x}') r_{12}^{-1} \phi_r(\mathbf{x}) \phi_s(\mathbf{x}') \mathrm{d}\mathbf{x} \mathrm{d}\mathbf{x}'. \tag{1.12}$$

From equation 1.9, we can see that the Hamiltonian contains one- and two- body terms and will only produce non-zero expectation values for determinants that differ by no more than four occupations, corresponding to the excitation of two electrons.

1.2.2 An exact solution

The language of second quantization simplifies how we write equations in improving the correlation treatment of Hartree–Fock theory. Specifically, improvements to Hartree–Fock are generally made by using excitations of electrons to model both the correlated motion of electrons and any significant electronic configurations indicative of strong correlation. A simple way to add correlation to a Hartree–Fock reference is to represent the electronic wave function as a linear combination of Slater determinants, and solve the Schrödinger equation in the basis of these determinants. This approach, denoted configuration interaction (CI), is particularly attractive in that its solution arises from simply

diagonalizing the Hamiltonian in a basis of determinants, producing energies and associated wave functions as the eigenvalues/eigenvectors of ground and excited states.[12] The CI wave function is a linear combination of determinants, $|\Phi_I\rangle$,

$$|\Psi\rangle = \sum c_I |\Phi_I\rangle , \tag{1.13}$$

with corresponding expansion coefficients labeled by determinant index, c_I, determined in the diagonalization of $\hat{H}$. In fact, one can build the complete set of determinants for a given number of orbitals (n_o) and electrons (n_e) by generating a determinant for every possible combination of n_e orbitals. When this complete basis of determinants is used, the resultant wave function and energy are formally exact within the orbital basis, a procedure called full CI (FCI). We can write the FCI wave function in terms of the Hartree-Fock reference, denoted Φ_0, and second-quantized operators,

$$|\Psi_{\text{FCI}}\rangle = (c_0 + \sum_{pq} c_q^p \hat{a}_p^\dagger \hat{a}_q + \sum_{pqrs} c_{rs}^{pq} \hat{a}_p^\dagger \hat{a}_q^\dagger \hat{a}_s \hat{a}_r + \sum_{pqrstu} c_{stu}^{pqr} \hat{a}_p^\dagger \hat{a}_q^\dagger \hat{a}_r^\dagger \hat{a}_u \hat{a}_t \hat{a}_s + \dots) |\Phi_0\rangle , \tag{1.14}$$

where expansion coefficients c are labeled with orbital indices and the series includes all n-body excitation strings up to the simultaneous excitation of all n_e electrons. In writing the FCI wave function in terms of the Hartree–Fock determinant, we can clearly see that FCI is formally exact in the fixed orbital basis because all possible excitations—and thus all possible correlations—are considered. Analyzing the FCI expansion coefficients can give valuable insight into the nature of correlation in a particular computation. Most importantly, the value of the coefficient for the Hartree–Fock determinant, c_0, can indicate any strong correlation if its square is smaller than about 0.9. If one could use FCI in a basis of infinitely many orbitals, then the exact solution of the electronic Schrödinger equation—complete CI—would be obtained.

Unfortunately, FCI is prohibitively expensive for all but trivially small systems. The number of determinants in a FCI expansion,N_{FCI}, defines a Hilbert space ($\mathscr{H}$) and grows

combinatorially as the number of electrons in a set of orbitals,

$$N_{\mathrm{FCI}} = \binom{n_o}{n_\alpha}\binom{n_o}{n_\beta}, \tag{1.15}$$

where n_α and n_β are the numbers of electrons with α and β spin, respectively. Even with the most sophisticated diagonalization algorithms, n_α, n_β, and n_o are restricted to produce no more than about 60 billion determinants.[13–15] While this number is in many ways an impressive feat, it limits computations to systems with tens of electrons, typically nothing larger than diatomic molecules. For example, the largest FCI computation we are aware of was done on the carbon dimer using 8 electrons in 66 orbitals, which required about 64 billion determinants.[15]

1.2.3 Single-reference Approaches

For cases where HOMO/LUMO gaps are large and strong correlation effects are expected to be small, the structure of the FCI wave function can be approximated fairly straightforwardly. In other words, if the Hartree-Fock determinant is a reasonably good approximation to FCI, then the only required corrections to achieve quantitative accuracy are for dynamical correlations. This strategy of correcting a Hartree–Fock reference for dynamical correlation defines a class of techniques called single-reference methods, which generally come in variational, perturbative, or projective forms.

A common approach for single-reference methods is to only compute contributions from determinants that couple directly to the Hartree-Fock determinant. From equation 1.9, we can see that these contributions are only the single and double excitations from the reference, a space of determinants called the first order interacting space (FOIS). Note that the concept of FOIS is general, and can be applied to a set determinants in addition to a single reference. A very natural approximation to FCI is then to only include singly and doubly excited determinants from the Hartree–Fock reference in the wave function. This procedure, called CI with singles and doubles (CISD), uses a linear combination of

determinants,

$$|\Psi_{\text{CISD}}\rangle = (c_0 + \sum_{pq} c_q^p \hat{a}_p^\dagger \hat{a}_q + \sum_{pqrs} c_{rs}^{pq} \hat{a}_p^\dagger \hat{a}_q^\dagger \hat{a}_s \hat{a}_r) |\Phi_0\rangle \,, \tag{1.16}$$

and produces variationally optimized expansion coefficients by diagonalizing the Hamiltonian in only the basis of the reference and FOIS. Since the CISD wave function is built variationally from a subset of the FCI determinantal space, the CISD energy is always an upper bound to the exact energy. In fact, this principle holds for any truncated CI wave function built from the same one-electron basis. The CI ansatz is most commonly employed in this order-by order fashion, where triples and possibly higher excitations can be added to increase the accuracy of the energy and wave function.

As we will discuss in great detail throughout this thesis, CI truncated by excitation order suffers from many drawbacks. A technical problem with all truncated CI methods, except CIS, is that they are not formally size consistent nor size extensive. Size consistency refers to the numerical property that a computation on a bipartite system, AB, with A and B completely noninteracting, gives the same energy as the energies summed from two separate computations on A and B. This property is typically associated with the failure of many CI variants to properly dissociate a diatomic molecule. Size consistency is usually met when the form of the wave function includes products of excitations such that the total wave function can be written as a product of subsystem wave functions. Size extensivity is achieved when the scaling of the energy error in a computation with respect to the number of electrons is constant, and it only occurs when products in the energy expression contain no instances of mismatched numbers of indices, also known as disconnected terms. Finally, CI truncated by excitation order is generally very inefficient with respect to the number of parameters required for a given accuracy. For example, CISD scales already as $\mathcal{O}(n_o^6)$, with the exponent increasing by two for each order of excitation added, and 95% of the correlation energy is not typically reached for small di- and triatomics at their equilibrium geometries until triple excitations are included.[12] In general, double excitations contribute the most to the correlation energy, but numerous, small magnitude excitations higher than

doubles are needed for quantitative accuracy. Despite this need for higher excitations, many determinants at each excitation order end up being relatively unimportant in the exact FCI wave function. Put another way, CI wave functions are usually very sparse when all excitations of each given order are included.

An elegant improvement to CI methods is to replace the linear wave function ansatz with an exponential representation as is done in coupled cluster theory (CC),[16,17]

$$|\Psi_{\mathrm{CC}}\rangle = e^{\hat{T}} |\Phi_0\rangle , \tag{1.17}$$

where $\hat{T}$ is the cluster operator and is composed of n-orbital excitation operators up to order k,

$$\hat{T} = \sum_{n=1}^{k} \hat{T}_n. \tag{1.18}$$

We can write a general n-orbital excitation operator as,

$$\hat{T}_n = \frac{1}{(n!)^2} \sum t_{ij\ldots}^{ab\ldots} \hat{a}_a^\dagger \hat{a}_b^\dagger \ldots \hat{a}_j \hat{a}_i, \tag{1.19}$$

where $a, b, \ldots$ index virtual orbitals, $i, j, \ldots$ index occupied orbitals, and $t_{ij\ldots}^{ab\ldots}$ are the cluster amplitudes determined by projection of a manifold of excited determinants, $|\Phi_{ij\ldots}^{ab\ldots}\rangle = \hat{a}_a^\dagger \hat{a}_b^\dagger \ldots \hat{a}_j \hat{a}_i |\Phi_0\rangle$, onto the Schrödinger equation,

$$\langle \Phi_{ij\ldots}^{ab\ldots} | \hat{H} e^{\hat{T}} |\Phi_0\rangle = E \langle \Phi_{ij\ldots}^{ab\ldots} | e^{\hat{T}} |\Phi_0\rangle . \tag{1.20}$$

If the cluster operator includes all n-orbital excitations, then the theory is formally equivalent to FCI. Similar to CI methods, we can manage the size of the coupled cluster wave function representation, and thus the cost to solve the CC equations, by truncating the cluster operator to a given rank. For example, we can represent the CCSD wave function in a way analogous to the CISD wave function,

$$|\Psi_{\mathrm{CCSD}}\rangle = \exp\Big(\sum_{pq} t_i^a \hat{a}_a^\dagger \hat{a}_i + \sum_{abij} t_{ij}^{ab} \hat{a}_a^\dagger \hat{a}_b^\dagger \hat{a}_j \hat{a}_i\Big) |\Phi_0\rangle . \tag{1.21}$$

The exponentiation of the excitation operators produces not only single and double excita-

tions, but also products of these excitation operators called the disconnected contributions to the wave function.[16,17] These disconnected excitations differentiate the CC wave function from a CI wave function with the same orders of excitation included, and they are responsible for the multiplicative separability of the CC wave function not possible in the case of CI. Therefore, if a size consistent reference is used, then the CC method is size consistent. Analysis of the coupled cluster equations, which we will not do here but is summarized nicely in ref. 16, reveals that the CC method is also size extensive. Beyond these formal properties, CCSD generally outperforms CISD, even though both methods are parameterized by the same number of variables.[12] Finally, the CCSD method can be corrected perturbatively for triple excitations in a method denoted CCSD(T), which is considered the "gold standard" of quantum chemistry due to its high accuracy and moderate cost.[18–20]

1.3 Multireference Methods

While both CI and CC approaches can systematically approach the FCI limit where all correlation is recovered, static correlation is typically not recovered adequately until impractically high excitation operators (at least quadruples) are included. Correspondingly, single-reference methods truncated to only doubles will rarely be accurate for computations involving strongly correlated electrons. As an example, Figure 1.1 shows the square of the expansion coefficients computed with FCI and CISD for the nitrogen dimer near equilibrium and at dissociation. This computation used the STO-3G basis set, and the set of orbitals used to construct the correlated wave functions come only from the three π bonding and three π^* anti-bonding orbitals from a restricted Hartree–Fock reference. Near equilibrium, the Hartree–Fock reference is clearly dominant in the FCI wave function, with the squared magnitudes for excited determinants falling off rather quickly compared to the coefficient of the Hartree–Fock determinant. This distribution of coefficients indicates that the Hartree–Fock reference is a reasonable approximation to FCI, and a single-reference

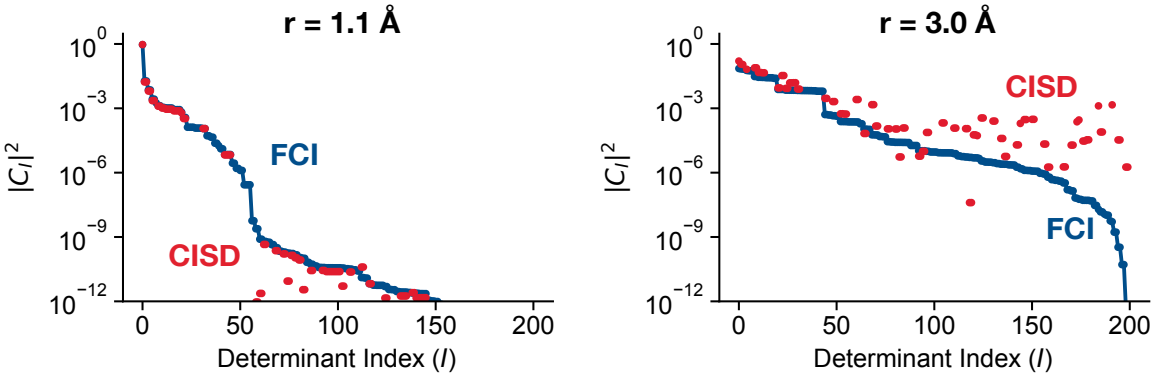

Figure 1.1: Squared magnitude of CI expansion coefficients computed from FCI and CISD wave functions. Determinants are ordered based on magnitude in the FCI expansion, and determinants with squared coefficient less than 10^{-12} are not shown.

method is appropriate. Indeed, we see that CISD does fairly well in capturing the most important determinants, though we can see it still ignores some minorly important determinants and includes numerous determinants with near-zero weight.

Upon dissociation, the FCI wave function looks quite different. Most notably is that the Hartree–Fock reference has a small squared coefficient (≈ 0.2) and is one of eight determinants that capture most of the wave function. In this case, Hartree–Fock alone qualitatively fails to describe the ground state, and a single-reference method is bound to fail. As we can see, the CISD wave function ignores several of the most important determinants, namely the single and double excitations from those determinants with similar coefficient to the reference. The errors in the CISD wave function in this strongly-correlated system are also seen in the total energy, where the error with respect to FCI is 0.35 E_h, an incredibly high amount, compared to the more reasonable 8 mE_h error produced at equilibrium. Clearly, single-reference methods fail to treat strong correlation primarily due to the qualitatively incorrect region of Hilbert space they tend to span.

To begin building a theory capable of treating strong correlation, a fairly fundamental shift in perspective is necessary. The notion of occupied and virtual orbitals in a Hartree–Fock reference is no longer pertinent because multireference theories need to always consider multiple reference occupations in an unbiased way. Instead, a reference state is typ-

ically defined by partitioning the orbitals into three sets: core (**C**), active (**A**), and virtual (**V**). The core orbitals are occupied in all reference determinants, the virtual orbitals are always unoccupied, and the active orbitals are allowed variable occupation. This partitioning defines a reference wave function in what is commonly called a *genuine* multireference method, where an active space is used to define and treat strong correlation, and the dynamical correlation is computed by coupling this space with core and virtual orbitals.

1.3.1 Active Space Treatments

A multireference approach is defined usually from two theories, one specialized for each type of correlation. The most common treatment for the active orbitals is simply FCI, particularly since the number of orbitals and electrons in many applications are manageable. This procedure is also called complete active space CI (CASCI) since it exactly recovers correlation in the active space. CASCI is commonly combined with orbital optimization such that the active orbitals are optimized along with the CI coefficients in an approach called CASSCF.[21–23] Since the static correlation is solved usually with CASSCF or CASCI, the number of active orbitals (N_A) and active electrons (N_e) are typically limited to CAS(16,16), where we adopt the conventional notation of CAS(N_e,N_A) to define active space dimensions.

Chemists are interested in molecular processes where the strong correlation can manifest CAS spaces larger than CAS(16,16), for example, in biologically relevant transition-metal catalysts and large, conjugated organic chromophores.[24–26] To enable studies utilizing active spaces larger than the conventional CAS(16,16) limit, approximate CASCI theories that do not rely on a single-reference ansatz are needed. The simplest approximate CASCI theory is realized by further partitioning the active space into smaller subspaces, and restricting the occupations within each subspace.[12] The first method of this type is the restricted active space method (RAS), which adds two orbital spaces around the active space and only allows single and double excitations into and out of these auxillary spaces.

The RAS concept was generalized to an arbitrary number of active space partitions with any user-defined set of occupation rules in both the occupation-restricted-multiple-active-space (ORMAS)[27] and generalized active space (GAS)[28,29] methods. Though these methods do enable large active space computations, the selection of active space partitioning schemes is neither straightforward nor intuitive, where changing a partitioning scheme to include more determinants does not guarantee a more accurate reference.[30] Development of approximate CAS techniques is an active area of research and is one of the main components of this thesis.

The Density Matrix Renormalization Group

The most commonly used approximate CAS method is an algorithm called the density matrix renormalization group (DMRG), and it achieves a compact representation of CASCI wave functions using a nonlinear matrix product state ansatz.[31–34] Consider a FCI wave function written in terms of a FCI coefficent tensor, $C^{n_1 n_2 \ldots n_k}$,

$$|\Psi_{\mathrm{FCI}}\rangle = \sum_{\{n\}} C^{n_1 n_2 \ldots n_k} |n_1 n_2 \ldots n_k\rangle , \tag{1.22}$$

where we have represented a Slater determinant in terms of the occupations (n_i) of all orbitals (i), and the sum is over all possible combinations of occupations. For a given orbital, four possible occupations exist ($n_i \in \{|0\rangle , |\alpha\rangle , |\beta\rangle , |\alpha\beta\rangle\}$). This tensor contains exactly the same information as the FCI expansion coefficients; only their organization is changed from a vector indexed by determinant number to a multidimensional array indexed by each orbital and its possible occupations. As such, the FCI tensor has a dimension of 4^k, and becomes intractably large already for about 14-15 orbitals. The approach of DMRG is to factorize this tensor into a series of products,

$$|\Psi_{\mathrm{DMRG}}\rangle = \sum A^{n_1}_{a_1} A^{n_2}_{a_1,a_2} A^{n_3}_{a_2,a_3} \ldots A^{n_k}_{a_{k-1}} |n_1 n_2 \ldots n_k\rangle , \tag{1.23}$$

where each rank-3 site tensor $A^{n_i}_{a_{i-1},a_i}$ represents an orbital i with associated virtual bond dimension a_i, and has a dimension $4 \times a_{i-1} \times a_i$. The first and last site tensors are ma-

trices with only one bond dimension so that contraction of all tensors for a given set of occupations n_i yields the expansion coefficient for a given determinant. For simplicity, the virtual bond dimension at all sites is truncated to M, which is defined by the user and allows DMRG computations to be systematically improved. For the case of $M = 1$, the decomposition of the FCI tensor is approximated as a simple product of vectors containing one coefficient for each occupation, and thus does not correlate the occupations of different sites (no entanglement). As M is increased, correlation is introduced between sites up to an arbitrarily high accuracy. The most clever aspect of the MPS wave function is exactly this feature, where complexity of the wave function can be smoothly introduced without assuming any element sparsity of the FCI vector.

Practically, the DMRG algorithm variationally optimizes the MPS wave function by sweeping through each site and minimizing the total energy by varying elements in the site tensor one at a time. Moreover, each orbital site is optimized individually with respect to all other orbital sites at every iteration in the sweep algorithm, resembling the SCF procedure in Hartree–Fock theory. The contraction of two neighboring sites directly correlates their occupations, and correlations beyond the neighboring site are thus accounted for indirectly. As a result, the DMRG method is extremely well-suited to treat local correlation in one dimension, present in most strongly correlated linear systems. Perhaps the biggest drawback of DMRG is that it accordingly cannot treat correlation as efficiently when it spans more than one dimension. This problem is related to the fact that the site tensors in the wave function need to be local and have a canonical ordering. Ordering the orbitals in such a way as to maximize correlation between sites is a significant challenge—an NP-hard problem—that in general limits the applicability of DMRG to near one-dimensional systems.[34–36] Nonetheless, the DMRG has seen a lot of success in enabling large active space computations using over 50 orbitals in complex applications,[25,37,38] and it has also been coupled with orbital-optimization schemes to yield accurate approximations to CASSCF wave functions.[34,38,39]

FCI Quantum Monte Carlo

Another approach to approximate a CASCI wave function is to stochastically solve the Schrödinger equation within an active space. Quantum Monte Carlo (QMC) methods achieve this by stochastically integrating the imaginary time-dependent Schrödinger equation,

$$\frac{\partial \Psi}{\partial \tau} = -\hat{H}\Psi, \tag{1.24}$$

which is achieved by propagating a initial state, usually a Hartree–Fock reference, to the infinite imaginary time limit,

$$|\Psi\rangle = \lim_{\tau\to\infty} e^{-\tau(\hat{H}-E_0)} |\Phi_0\rangle , \tag{1.25}$$

where E_0 is the exact ground state energy. Stochastic approaches are particularly useful in this context because they are able to sample the imaginary time propagator very efficiently with straightforward implementations on parallel architectures.[40–46] Of numerous manifestations of QMC methods, FCIQMC is especially well-suited in approximating CASCI because it operates in a basis of orthogonal Slater determinants and as a result does not suffer from the fermionic sign problem, which causes artificial propagation to bosonic states and plagues other QMC variants.[47–53]

The FCIQMC algorithm uses the dynamics of walkers to approximate the FCI wave function. The walkers are signed and populate a set of Slater determinants, and the sum of the walkers on a given determinant weighted by their sign is directly proportional to the CI expansion coefficient for that determinant in the FCIQMC wave function. At each imaginary time step, a walker can spawn a new determinant with a probability related to the Hamiltonian matrix element between the new determinant and the parent determinant. If this probability is greater than a randomly selected threshold between 0 and 1, then the new walker is spawned. Similarly, walkers on determinants can be annihilated in a stochastic process to prevent determinants with low importance from persisting in the simulation. More details on the algorithm are presented in reference 47. FCIQMC has been success-

fully applied to molecules using CAS(24,24) active spaces including orbital optimization, in addition to being applied to excited states.[47–55] While the stochastic nature of FCIQMC allows for efficient implementations, it makes the method susceptible to random noise in converging the wave function and the energy. The FCIQMC algorithm can also be susceptible to convergence issues, particularly for studying near-degenerate states of the same symmetry.

The Variational Reduced Density Matrix Method

An interesting alternative to the wave function-based CASCI approximations we have discussed is the variational two-particle reduced density matrix method (v-2RDM), which does not use a wave function at all.[56–59] To avoid the exponential scaling of the exact solution, v-2RDM seeks to directly compute the 2-particle reduced density matrix,

$$\gamma_{rs}^{pq} = \langle \Psi | \hat{a}_p^\dagger \hat{a}_q^\dagger \hat{a}_s \hat{a}_r | \Psi \rangle , \tag{1.26}$$

for active orbital indicies p, q, r, s and a general wave function Ψ composed of determinants defined by active orbital occupations.[60–62] The total energy can be written in terms of the one- and two-particle RDMs, so the strategy of the v-2RDM method is to treat elements of the RDMs as the variational parameters rather than the exponentially-many parameters in the wave function. The number of variational parameters in the 2-RDM scales only as roughly the fourth power of the number of active orbitals, making its direct optimization a very attractive option.

Unfortunately, this approach is not without its complications. Left to freely optimize, the RDMs can produce artificially low energies because they may not correspond to antisymmetric N-electron wave functions and would thus be unphysical. In this case, the RDMs are not N-representable. As a result, the v-2RDM method is defined by a variational optimization of the RDMs subject to a series of constraints, so-called N-representability conditions, that approximately ensure that the RDMs map to a physical wave function. Along with constraints that conserve the symmetry, total spin, and number of active elec-

trons, the RDMs are constrained to meet a set of p-positivity conditions, where unique spin components of the 2-particle, 2-hole, and particle-hole RDMs are required to be positive semidefinite. Practically, this optimization is achieved using the technique of semidefinite programming, causing an overall scaling of approximately the sixth power of the number of active orbitals. More accurate results can be obtained by applying constraints to higher-order RDMs.

Recently, the v-2RDM method has shown promise in large active space computations, and it has been combined with orbital optimization[63] and a density functional theory-based treatment of dynamical correlation.[64] It was applied to the polyacene series, requiring up to a CAS(50,50), and is very well-suited to study strong correlation in the ground states of molecules.[26,62] Unfortunately, extension of this theory to electronic excited states is very complicated, relying either on linear response approaches or on the derivation of active space and state-specific representability conditions.

1.3.2 Multireference Methods for Dynamical Correlation

Multireference methods use specialized techniques to separately treat static and dynamical correlation, which in combination recover the total correlation. As mentioned, this separation is realized by partitioning orbitals into an active set and a combined set of core and virtual orbitals. A multideterminantal reference wave function, $|\Psi_0\rangle$ is then computed either exactly or with one of the approximate methods discussed previously, and it is corrected with a theory of dynamical correlation. The dynamical correlation contribution can be written generally as a wave operator, $\hat{\Omega}$, which is applied to the reference to yield a totally correlated wave function,

$$|\Psi\rangle = \hat{\Omega}\,|\Psi_0\rangle\,. \tag{1.27}$$

The function of the wave operator is to couple the reference wave function with determinants containing core-active, core-virtual, and active-virtual excitations. By using various forms of the wave operator, multireference versions of single-reference theories can be

developed.

Perhaps the simplest formulation of the wave operator is a sum of quantized operators that generate an explicit set of Slater determinants involving all single and double excitations among core, active, and virtual spaces. This formulation, called MR-CISD, corresponds to CISD generalized for a multideterminantal reference.[11] MR-CISD provides a protocol to produce a determinantal basis for diagonalizing the Hamiltonian that does not rely on defining a Hartree–Fock reference and is thus well-suited for problems in strong correlation. MR-CISD wave functions tend to be very large, and even with efficiency tricks like internal contraction,[65,66] can only be applied to relatively small molecules. Also, issues with size-consistency are still present, requiring *a posteriori* corrections. Nonetheless, MR-CISD is extremely useful in computing potential energy surfaces and thermodynamics of chemical systems involving less than ten atoms, in addition to producing benchmark photochemical data for the excited states of similarly small molecules.[11,67]

Drawing from its superior performance in single-reference contexts, an attractive alternative to MR-CISD is a mutlireference generalization of coupled cluster theory (MRCC).[5,10] The main challenge in developing MRCC methods is in formulating an affordable theory that conserves properties of size consistency and extensivity. This challenge is further complicated by the lack of a single ansatz for parameterizing the wave function. Specifically, one can choose to apply the exponentiated cluster operator to a multideterminantal reference, i.e. $\hat{\Omega} = e^{\hat{T}}$ in equation 1.27, to produce an internally-contracted MRCC wave function (ic-MRCC).[68–70] Alternatively, individual exponentiated cluster operators can be applied to each determinant in the reference space to produce essentially a linear combination of single reference coupled cluster wave functions, known as the Jeziorski–Monkhorst (JM) ansatz.[71] Because excitations of different reference determinants can produce the same excited determinant, the JM ansatz suffers from a redundancy of parameters that limits its application to only small active spaces. In cases where small active spaces are appropriate, a particular state-specific, numerically stable formulation of JM MRCC by Mukherjee *et al.*

(Mk-MRCC) has provided valuable benchmark data for systems as large as naphthalene-based diradicals.[72–74] To access larger active spaces, the more tractable ic-MRCC approach is required. In addition to being practically very complex (routine applications can easily lead to equations with over 100,000 terms), ic-MRCC suffers from numerical instabilities associated with linearly-dependent excitations associated with all internally contracted theories. Both MRCC formulations have their complications and relatively high costs but remain among the most accurate multireference theories available.[69,75]

Due to its reduced cost compared to MRCI and MRCC methods, multireference perturbation theories (MRPT) are the most commonly used multireference methods in general applications.[76–78] The general approach in MRPT is to define a zeroth-order Hamiltonian, $\hat{H}_0$ solved exactly using a multideterminantal reference, and a perturbation defined as $V = \hat{H} - \hat{H}^{(0)}$. For example, using a CAS reference Ψ_0 one can derive a simple uncontracted Epstein–Nesbet MRPT energy expression by defining the zeroth Hamiltonian as,

$$H^{(0)} = \sum_{\Phi_I, \Phi_J \in \Psi_0} \hat{H} \left|\Phi_I\right\rangle \left\langle\Phi_J\right|, \tag{1.28}$$

where Φ_I is a determinant in the reference wave function, and defining the perturbation V as the part of the FCI Hamiltonian that couples the reference wave function to its first order interacting space, F. We can then write expressions for the first-order correction to the wave function and the second-order correction to the energy, respectively, as

$$\left|\Psi^{(1)}\right\rangle = \sum_{\Phi_K \in F} \frac{\left\langle\Phi_K\right| \hat{H} \left|\Psi_0\right\rangle}{\left\langle\Psi_0\right| \hat{H} \left|\Psi_0\right\rangle - \left\langle\Phi_K\right| \hat{H} \left|\Phi_K\right\rangle} \left|\Phi_K\right\rangle \tag{1.29}$$

$$E^{(2)} = \sum_{\Phi_K \in F} \frac{\left|\left\langle\Phi_K\right| \hat{H} \left|\Psi_0\right\rangle\right|^2}{\left\langle\Psi_0\right| \hat{H} \left|\Psi_0\right\rangle - \left\langle\Phi_K\right| \hat{H} \left|\Phi_K\right\rangle}, \tag{1.30}$$

which are much simpler to compute than corresponding quantities from MRCI or MRCC methods. More common MRPT methods including CASPT2[79–81] and the N-electron valence state perturbation theory (NEVPT2) are formulated in a similar way, but using different definitions of the zeroth-order Hamiltonian.[82] For example, CASPT2 uses a mul-

tireference generalization of the Fock operator as a zeroth-order Hamiltonian, so that the theory behaves like Moller–Plesset perturbation theory in the single-determinant limit. NEVPT2 takes a similar approach, but uses a zeroth-order Dyall Hamiltonian. CASPT2 and NEVPT2 thus use perturbing determinants that are no longer orthogonal, and a costly diagonalization of the 3-body cumulant is required. Furthermore, evaluation of the energy of the excited determinants in CASPT2 an NEVPT2 requires the 4-RDM, a quantity with an associated scaling $\mathcal{O}(N_A^8)$ for N_A active orbitals, which results in an overall computational scaling of $\mathcal{O}(N_A^9)$.

The requirement of the reference 4-RDM has a large impact on the scope of MRPT2 methods. Namely, this requirement limits the size of the active space in a computation to about 25 orbitals, despite the treatment of many core and virtual orbitals being possible. Approximating the the 4-RDM using products of lower-order RDMS can significantly reduce this bottleneck, but not without introducing uncontrollable and potentially significant errors.[83–85]

Aside from cost considerations, the most troubling issue plaguing both MRPT and internally contracted MRCC methods is the so-called intruder state problem. The intruder state problem occurs in perturbation theories when excitations outside of the reference become energetically degenerate or near-degenerate with the reference state itself, and they cause incurable problems with convergence in MRCC in the form of multiple solutions.[5] This problem is best understood from the perspective of MRPT, specifically in equations 1.29 - 1.30, where intruders occur when the energy of an excited determinant, Φ_K, is nearly equal to the reference energy, causing the denominators to go to zero and the corresponding contributions to the energy and wave function to be unphysically large. In the case of MRPT2, this problem can be partially ameliorated by modifying the zeroth-order Hamiltonian or by shifting the denominator by an arbitrary value.[86] For MRCC, however, these instabilities largely remain an unsolved problem.

1.3.3 The Driven Similarity Renormalization Group

Finding a solution to the intruder state problem has been one of the major thrusts of our research group. In the final part of this chapter, we will give a basic overview of our intruder-free strategy for dynamical correlation, the driven similarity renormalization group (DSRG), and we will provide more explicit details relevant to this work in Chapter 4.

The DSRG is based on the SRG method of Glazek and Wilson[87,88] and Wegner,[89,90] which is defined by a continuous unitary transformation to bring a bare Hamiltonian, $\hat{H}$, to a block diagonal form.[91] A time-like parameter, s, called the *flow parameter*, controls the continuous transformation to produce the SRG Hamiltonian, $\bar{H}(s)$,

$$\bar{H}(s) = \hat{U}(s)\hat{H}\hat{U}(s)^{\dagger}, \tag{1.31}$$

where $\bar{H}(0) = \hat{H}$ and $\bar{H}(\infty)$ is fully block-diagonalized. This transformation decouples the reference space from its excited configurations to produce an effective Hamiltonian, defined as the subset of $\bar{H}$ corresponding to the reference space. As a result, the correlation effects of the decoupled excitations are folded into the effective Hamiltonian, which can be diagonalized to produce ground and excited state wave functions. Moreover, if the reference space is chosen to capture all static correlation effects, then one can think of the continuous block diagonalization as a way to progressively fold dynamical correlation effects into the computation of a multideterminantal reference.

Our main purpose with the SRG, and by extension the DSRG, is to perform this block diagonalization to a finite value of s such that the individual excitations responsible for the intruders and instabilities are not included in constructing the effective Hamiltonian.[91] The evolution of the SRG Hamiltonian is governed by a differential equation,

$$\frac{\partial \bar{H}(s)}{\partial s} = [\eta(s), \bar{H}(s)], \tag{1.32}$$

where the *flow generator*, $\eta(s) = \frac{\partial \hat{U}(s)}{\partial s}\hat{U}^{\dagger}$, is anti-Hermitian and is usually defined in terms

of the diagonal [$\bar{H}(s)^{\mathrm{d}}$] and off-diagonal [$\bar{H}(s)^{\mathrm{od}}$] parts of the SRG Hamiltonian,[89]

$$\eta(s) = [\bar{H}(s)^{\mathrm{d}}, \bar{H}(s)^{\mathrm{od}}]. \tag{1.33}$$

The SRG equations can be solved by numerically integrating equation 1.32 while updating $\eta(s)$ with equation 1.33. Approximate solutions can be obtained at a significantly reduced cost by only retaining the 1- and 2-body interactions resultant from equations 1.32 and 1.33, and additionally a perturbative analysis of these equations is also possible. For a single-determinantal reference, we can write the second order perturbative SRG energy correction, $E^{(2)}(s)$,

$$E^{(2)}(s) = \frac{1}{4}\sum_{ij}^{\mathrm{occ}}\sum_{ab}^{\mathrm{vir}} \frac{|\langle ij||ab\rangle|^2}{\Delta_{ab}^{ij}}\left(1 - e^{-2s(\Delta_{ab}^{ij})^2}\right), \tag{1.34}$$

where we again write the two-electron integrals in physicist's notation and introduce the Moller–Plesset denominator, $\Delta_{ab}^{ij} = \varepsilon_i + \varepsilon_j - \varepsilon_a - \varepsilon_b$, written in terms of orbital energies. Equation 1.34 can be viewed as the standard second-order Moller–Plesset perturbative energy correction (MP2) with a multiplicative regularization term dependent on s. While vanishing denominators ($\Delta_{ab}^{ij} \to 0$) usually destroy the numerical stability of PT2 theories, we see that the SRG elegantly suppresses these unphysically large contributions.

We have seen that the SRG is capable of providing numerical stability in formulating a theory of dynamical correlation. However, its general application requires the solution of complicated ordinary differential equations which can introduce numerical instabilities themselves. The DSRG improves upon the SRG by recasting the differential equation in terms of coupled polynomial equations.[91,92] The unitary transformation that block-diagonalizes the Hamiltonian is written in terms of unitary exponential operators,

$$\bar{H}(s) = e^{-\hat{A}(s)}\hat{H}e^{\hat{A}(s)}, \tag{1.35}$$

where $\hat{A}(s)$ is an n-particle rank operator written in terms of cluster operators, $\hat{A}(s) = \sum_{k=1}^{n}\hat{T}_k(s) - \hat{T}_k^{\dagger}(s)$. To drive the transformation, we equate the off diagonal block of the

DSRG Hamiltonian (labeled "od") to a yet undetermined source operator, $\hat{R}(s)$,

$$[\bar{H}(s)]^{\mathrm{od}} = [^{-\hat{A}(s)}\hat{H}e^{\hat{A}(s)}]^{\mathrm{od}} = \hat{R}(s). \tag{1.36}$$

At $s = 0$, the source operator must leave the bare Hamiltonian unchanged, $\hat{R}(0) = [\hat{H}]^{\mathrm{od}}$, and it must completely block diagonalize it as s approaches infinity, $\hat{R}(\infty) = 0$. To build the DSRG many-body conditions, $\hat{A}(s)$ is truncated to contain only one- and two- body operators, and $\hat{R}(s)$ is defined to match the SRG flow equation to second order.[91–93]

The DSRG allows us to build an effective Hamiltonian for a fixed value of s without numerical integration. By using different truncations to $\hat{A}(s)$ and various approximations to the evaluation of the exponential transformation of the bare Hamiltonian, a hierarchy of intruder-free perturbative and nonperturbative multireference methods can be derived. In any DSRG variant, the ground state energy can be computed by taking the expectation value of the effective Hamiltonian, $E(s) = \langle \Psi_0 | \bar{H}(s) | \Psi_{0)} \rangle$, or by rediagonalizing the effective Hamiltonian in the reference space. The former approach is denoted the *unrelaxed* energy, and the latter approach is the *relaxed* energy since the reference wave function is allowed to relax in response to the dynamical correlation treatment.

With a carefully chosen value of s, the DSRG is able to recover dynamical correlation effects without exposing the computation to intruder states. The strong correlation effects are captured in the reference wave function, usually computed with CASSCF, CASCI, or an approximate version of either method. In connecting the reference to the DSRG, RDMs appear in the energy and amplitude expressions, similar to previously discussed multireference theories. Unlike CASPT2 and NEVPT2 which require the 4-RDM, the DSRG only requires up to the 3-RDM and enables the use of reference wave functions that span large active orbital spaces unfeasible with similar many-body theories. The large active spaces accessible to the DSRG also require approximations to the CASCI wave function, like those previously discussed.

1.4 Selected Configuration Interaction

In the previous section, we provided a broad overview of current available multireference methods. As discussed, a major challenge in developing multiereference theories is to enable the use of large active spaces by formulating new approximations both in computing active space wave functions and in the dynamical correlation treatment. One of the central topics of this dissertation is the development and application of a new approximate CASCI technique designed for large active spaces. This method, called the Adaptive CI (ACI) is built upon decades of previous research in a class of wave function-based theories called selected configuration interaction (sCI). In the remainder of this chapter, we will give some historical perspective and current review of sCI methods, and finish with an outline of the remainder of this dissertation.

The conventional CI approach is to build a model space of determinants by considering all excitations of a preselected order, i.e. all singles, doubles, etc. with respect to a Hartree–Fock reference. This approach, as we saw in Figure 1.1, is inefficient in the weakly correlated regime and qualitatively wrong when strongly correlated electrons are present. Selected CI methods take an alternative approach in truncating the FCI wave function, whereby determinants are included in the model space based on a well-defined, determinant-specific importance criterion. In addition to a selection criterion, sCI methods are also defined by a screening algorithm that samples Hilbert space so that the most important determinants in the FCI wave function are considered for selection. Though challenging to efficiently formulate, a good sCI method can be an extremely powerful tool for exploiting sparsity in a FCI wave function regardless of the degree of static or dynamical correlation present. Early sCI techniques were designed to recover the total correlation energy in small molecules, while more recent versions of the theory use it to replace CASCI in computing reference wave functions for multireference computations.

1.4.1 Early Selected CI Methods

To our knowledge, the first published method that fits our sCI definition was done in 1952 by Bernal and Boys,[94] where they used second-order perturbative energy estimates, $\varepsilon(\Phi_I)$,

$$\varepsilon(\Phi_I) = \left| \frac{\left| \langle \Phi_0 | \hat{H} | \Phi_I \rangle \right|^2}{E_0 - E_I} \right|, \tag{1.37}$$

based on a Hartree–Fock reference, Φ_0, to determine if an excited determinant, Φ_I, should be included in a CI expansion. This procedure was used to study Na^+, Li, and F^- atoms, and they were able to use a 5s4p1d STO basis and a CI wave function with 17 configurations, representing one of the largest variational computations done at the time. Their method produces an extremely truncated CISD wave function, and was one of the only viable ways to build a configuration space without hand-picking determinants based on chemical intuition. This idea of determinant selection by perturbative estimates was used soon after in a similar context to reduce the cost of conventional CISD,[95–99] but it was not until a 1969 study by Whitten and Hackmeyer where a more rigorous selection algorithm was combined with a determinant-based criterion.[100] In their method, they begin with a small set of reference determinants, $\{\Phi_k^{(1)}\}$, that describe one or more electronic state, and augment the reference with determinants from the FOIS, Φ_I, with a perturbative energy correction,

$$\varepsilon(\Phi_I) = \left| \frac{\left| \langle \Phi_J^{(1)} | \hat{H} | \Phi_I \rangle \right|^2}{E_j - E_I} \right| \tag{1.38}$$

above a user-specified threshold for at least one $\Phi_J \in \{\Phi_k^{(1)}\}$. The Hamiltonian is diagonalized in this space, and a user-defined number of the energetically lowest roots are used to define a new reference. The screening process is then repeated once more using this updated reference. The first iteration of this method corresponds to a kind of selected MR-CISD, but the second iteration allows for possibly higher excitations to be included.

Soon after this work of Whitten and Hackmeyer, some of the most well-known sCI

methods were introduced which still find applications today. Improving upon the method of Whitten and Hackmeyer, Huron, Malrieu, and Rancurel introduced a new sCI method in 1973 called *configuration interaction by perturbation with multiconfigurational zeroth order wave function selected by iterative process* (CIPSI).[101] CIPSI starts with a reference wave function, usually a single Hartree–Fock determinant, which is perturbed to first order, producing a set of singly and doubly excited determinants with perturbatively determined coefficients. The excited determinants whose first-order contribution to the wave function is greater than a threshold η are added to the reference, and the Hamiltonian is diagonalized in this updated basis to produce a new reference. This procedure is iterated until the updated references stabilize, or until they become prohibitively large. CIPSI was initially used to generate a zeroth-order reference wave function for a larger perturbative treatment, but it has since evolved into the "grandparent" of all sCI methods, where any new sCI theory can be reasonably defined as a modified CIPSI variant. The key improvement that CIPSI contributed is that it is iterative, and in principle does not converge until an appropriately large amount of Hilbert space has been explored.

A year after CIPSI was introduced, Buenker and Peyerimhoff published an alternative sCI method, called MRD-CI, which does not use perturbation theory to compute determinant importance criteria.[102,103] The MRD-CI relies on the assumption that the most important part of the wave function can be easily determined based on an analysis of molecular orbital theory. Importance criteria for the excited determinants in the FOIS of the reference are computed by solving numerous small secular equations involving the reference and each excited determinant individually. Their importance criterion thus corresponds to the energy lowering a given configuration contributes to the reference, and only determinants whose lowering is greater than a threshold are included in the wave function. The MRD-CI can be considered a selected MRCI method where the reference is not determined by an active space but by hand. While these energy lowerings are more expensive to compute than the perturbative estimates in CIPSI, they are useful in providing an accurate approxi-

mation to the correlation energy *not* described in the final wave function. These accurately computed energy lowerings are very valuable in reliably extrapolating the energy to the zero-threshold limit.

Since these foundational sCI developments, the popularity of these methods has waned with the emergence of efficient coupled cluster methods in quantum chemistry. Furthermore, sCI even lost favor in multireference cases since it is more expensive than the small-CAS based methods we discussed previously, particularly in large basis sets. Motivated by the need for near-FCI accuracy for benchmarking small chemical systems, a few developments in sCI did occur in the two decades following its initial emergence. CIPSI, for example, underwent modifications to increase its flexibility in treating different classes of determinants,[104] in addition to improvements to the perturbative treatment of CIPSI references.[105] Starting with work by Knowles *et al.*, a large effort was also put in to making direct CI and diagonalization routines more efficient for sCI methods, where previously developed graphical and string-based methods in FCI had to be modified.[13,106–118] In 1991, Harrison introduced a new sCI algorithm closely related to CIPSI, but which used second order perturbative energy estimates rather than corrections to the wave function, possibly leading to accurate energies but not guaranteeing accurate wave functions. This method, called CI+PT, also uses configuration state functions rather than Slater determinants, so that all CI wave functions built are guaranteed to be eigenfunctions of $\hat{S}^2$ without any artificial modifications.[119] Other interesting sCI developments include size-consistent formulations[120] and sCI methods tailored for the computation of excited states.[121–123] A more complete review of sCI methods in this era can be found in Ref 12.

1.4.2 Modern Selected CI

Over the past decade or so, sCI methods have been undergoing a revival inspired primarily by the limitations in CASCI. To specify, CASCI requires the user to identify a set of active orbitals responsible for strong correlation, with the constraint that the number of

active orbitals be small (≤ 16). Owing to its flexibility, sCI has emerged as a very attractive alternative, either because it can partially lift this small active space constraint or remove the CAS paradigm entirely.

Central to the renewed success of sCI methods has been the improved efficiency of determinant screening, which is required to rigorously sample the FCI wave function. One interesting approach that has received renewed attention is to, at each iteration, add a manageable number of randomly generated excited determinants to a reference, diagonalize the Hamiltonian in this basis, and define a new reference using a subset of the wave function with the largest coefficients. This method, called Monte Carlo Configuration Interaction (MCCI), takes advantage of an efficient, easily parallelized Monte Carlo algorithm that does not require computation of determinant-specific importance criteria.[124–131] Other interesting screening algorithms use new concepts of compressed sensing usually applied in signal processing, where the sCI wave function is formulated as a functional minimization of the energy and a penalty function that controls sparsity.[132,133] A number of new sCI methods have appeared recently that use similar algorithms to CIPSI, but with some modifications to the selection criterion.[134–139]

The combination of sCI wave functions with perturbation theory was done with the introduction of CIPSI, and most sCI methods do provide a means of approximating the correlation energy ignored from unselected determinants. This methodological structure, usually called sCI+PT, allows any strong correlation and a portion of dynamical correlation effects to be described rigorously by a CI wave functions, and any remaining correlations can be described more affordably. With the high cost and low flexibility of CASCI, sCI+PT seems like a very attractive option for diverse chemical systems so long as the total FCI wave function is well sampled by the sCI and PT algorithms. Again, the use of stochastic approaches has been very useful in this context. Recently, a new implementation of CIPSI has been used to produce a reliable nodal structure for diffusion Monte Carlo,[41,46,140,141] enabling accurate computations of metal-containing compounds using large basis sets.[142,143]

One of the most promising sCI+PT methods is the heat-bath CI (HBCI) method developed by Holmes, Umrigar, Sharma, and coworkers.[144–146] HBCI uses the observation that screening the double excitations from the reference is frequently the computational bottleneck in sCI variants of CIPSI, and it addresses this bottleneck with two changes to CIPSI. The first is in the determinant importance criteria ($\varepsilon(\Phi_I)$), which they take to be just part of the numerator in the amplitude expression of CIPSI,

$$\varepsilon(\Phi_I) = \max_{\Phi_J \in \Psi_0} |\langle \Phi_I | \hat{H} | \Phi_J \rangle c_J|, \tag{1.39}$$

where Φ_J is a determinant in the reference with expansion coefficient c_J. This criteria is very efficient to compute since it does not require computation of the energy for external determinants, and they show it behaves similarly to the full amplitude expression. Rather than checking this criteria for all double excitations, HBCI sorts the two-electron integrals and only generates an excited determinant for cases where $\langle \Phi_I | \hat{H} | \Phi_J \rangle$ is known to be relatively large beforehand. This presorting is not too computationally demanding, and it leads to a sCI algorithm that screens determinants with near-perfect efficiency, in that it does not waste very much time in generating determinants that will not end up in the updated reference. In addition to this efficient sCI algorithm, HBCI has been combined with deterministic, stochastic, and semistochastic perturbative treatments to in principle recover static and dynamical correlation.[145,147,148] Due to these algorithmic improvements, HBCI with perturbative corrections is able to treat up to 30 electrons in about 100 orbitals,[149] and it has been applied to the ground state of transition metal-containing compounds using a CAS(28,22).[145]

While various manifestations of sCI+PT can produce near FCI accuracy for a wide range of chemical systems, many interesting cases containing strongly correlated electrons are still out of reach. For example, to study correlation effects in heptacene using a triple-zeta basis set would require treatment of 138 electrons in over 1000 orbitals, too large for any sCI+PT algorithm. As a result, the approach of genuine multireference methods, which

requires partitioning orbitals into core, virtual, and active sets, is required. In this context, sCI can be used to access active spaces much larger than the CAS(16,16) limit imposed for CASCI. In this spirit, many sCI methods report results using the CAS(N_e, N_a) notation, and Smith *et al.* has reported a HBCI extension which incorporates orbital optimization analogous to an approximate CASSCF.[150] While approximating CASSCF and CASCI is an often-cited goal and motivation for the development of new sCI methods, the only reported example where an sCI method was coupled to a many-body dynamical correlation treatment spanning a different (inactive) set of orbitals was performed by us,[151] and is topic of Chapter 4. The lack of published work in this area is somewhat surprising given the success of other approximate CAS methods, namely DMRG, in this context.[39,64,85,152–155] Connecting large CAS sCI methods to theories of dynamical correlation has its challenges, but it represents one of the few viable options to treat strong and dynamical correlation in large molecules and will accordingly see much more development in the future.

1.5 Prospectus

In chapter 2, we introduce our new sCI method called the Adaptive CI (ACI), which provides a flexible CI expansion whose energy error can be reliably predetermined by the user. We apply this method to the dissociation of molecular nitrogen and to the singlet-triplet splittings of the oligoacene series, treating only the strongly correlation electrons in the latter case. In chapter 3, we develop several algorithms to compute electronically excited states using the ACI with the goal of conserving the predictive energy properties for any type of electronic state (doube-excitation, charge-transfer, etc.). We benchmark these excited state algorithms on the lowest three singlet states of methylene and on the avoided crossing in the dissociation of lithium fluoride. As a final test, we study the lowest four singlets of increasingly large all-*trans* polyenes, comparing excitation energies to CASCI values when possible. In chapter 4, we combine ACI with the second-order perturbative version of the driven similarity renormalization group (ACI-DSRG-MRPT2). We use this

method to revisit the oligoacene series, where the addition of dynamical correlation produces singlet-triplet splittings that agree well with experimental data. Furthermore, analysis of the wave function shows that dynamical correlation effects reduce the predicted radical character in the ground states. In chapter 5, we introduce some preliminary work on time propagation of selected CI wave functions. We benchmark a new strategy to use single-state and state-averaged ACI algorithms to build a determinantal basis for propagating a cationic wave packet. This real-time dependent ACI is then applied to charge migration resultant from ultrafast near-valence ionization. Specifically, we study charge migration following ionization in the π/π^* manifold in benzene and in the experimentally studied iodoacetylene.

Bibliography

[1] P. A. M. Dirac. "Quantum mechanics of many-electron systems." *Proc. R. Soc. Lond. Ser. A.* **123**, 714 (1929).

[2] A. Szabo and N. S. Ostlund. *Modern quantum chemistry: introduction to advanced electronic structure theory* (2012).

[3] D. K. W. Mok, R. Neumann, and N. C. Handy. "Dynamical and Nondynamical Correlation." *J. Phys. Chem.* **100**, 6225 (1996).

[4] J. W. Hollett and P. M. W. Gill. "The two faces of static correlation." *J. Chem. Phys.* **134**, 114111 (2011).

[5] F. A. Evangelista. "Perspective: Multireference coupled cluster theories of dynamical electron correlation." *J. Chem. Phys.* **149**, 030901 (2018).

[6] M. W. Schmidt and M. S. Gordon. "The construction and interpretation of MCSCF wavefunctions." *Annu. Rev. Phys. Chem.* **49**, 233 (1998).

[7] F. Neese, D. G. Liakos, and S. Ye. "Correlated wavefunction methods in bioinorganic chemistry." *J. Biol. Inorg. Chem.* **16**, 821 (2011).

[8] R. J. Bartlett. "To multireference or not to multireference: That is the question?" *Int. J. Mol. Sci.* **3**, 579 (2002).

[9] W. Jiang, N. J. DeYonker, and A. K. Wilson. "Multireference character for 3d transition-metal-containing molecules." *J. Chem. Theor. Comput.* **8**, 460 (2012).

[10] D. I. Lyakh, M. Musiał, V. F. Lotrich, and R. J. Bartlett. "Multireference nature of chemistry: the coupled-cluster view." *Chem. Rev.* **112**, 182 (2012).

[11] P. G. Szalay, T. Müller, G. Gidofalvi, H. Lischka, and R. Shepard. "Multiconfiguration self-consistent field and multireference configuration interaction methods and applications." *Chem. Rev.* **112**, 108 (2012).

[12] C. D. Sherrill and H. F. Schaefer III. "The configuration interaction method: Advances in highly correlated approaches." *Adv. Quant. Chem.* **34**, 143 (1999).

[13] P. J. Knowles and N. C. Handy. "Unlimited full configuration interaction calculations." *J. Chem. Phys.* **91**, 2396 (1989).

[14] J. Olsen, P. Jørgensen, and J. Simons. "Passing the one-billion limit in full configuration-interaction (FCI) calculations." *Chem. Phys. Lett.* (1990).

[15] Z. Gan, R. H. S. P. o. t. . ACM, and 2005. "Calibrating quantum chemistry: A multi-teraflop, parallel-vector, full-configuration interaction program for the Cray-X1." *iee-explore.ieee.org* (2005).

[16] T. D. Crawford and H. F. Schaefer. *An Introduction to Coupled Cluster Theory for Computational Chemists*, volume 45 of *Lipkowitz/Reviews*. John Wiley & Sons, Ltd, Hoboken, NJ, USA (2007).

[17] I. Shavitt and R. J. Bartlett. "Many-body methods in chemistry and physics: MBPT and coupled-cluster theory." (2009).

[18] K. Raghavachari, G. W. Trucks, J. A. Pople, and M. Head-Gordon. "A fifth-order perturbation comparison of electron correlation theories." *Chem. Phys. Lett.* **157**, 479 (1989).

[19] R. J. Bartlett, J. D. Watts, S. A. Kucharski, and J. Noga. "Non-iterative fifth-order triple and quadruple excitation energy corrections in correlated methods." *Chem. Phys. Lett.* **165**, 513 (1990).

[20] J. F. Stanton. "Why CCSD(T) works: a different perspective." *Chem. Phys. Lett.* **281**, 130 (1997).

[21] B. O. Roos, P. R. Taylor, and P. E. M. Siegbahn. "A complete active space SCF method (CASSCF) using a density matrix formulated super-CI approach." *Chem. Phys.* **48**, 157 (1980).

[22] B. O. Roos, P. R. Taylor, and P. E. M. Siegbahn. "A complete active space SCF method (CASSCF) using a density matrix formulated super-CI approach." *Chem. Phys.* **48**, 157 (1980).

[23] P.-Å. Malmqvist and B. O. Roos. "The CASSCF state interaction method." *Chem. Phys. Lett.* **155**, 189 (1989).

[24] M. Bendikov, H. M. Duong, K. Starkey, K. N. Houk, E. A. Carter, and F. Wudl. "Oligoacenes: theoretical prediction of open-shell singlet diradical ground states." *JACS* **126**, 7416 (2004).

[25] Y. Kurashige, G. K.-L. Chan, and T. Yanai. "Entangled quantum electronic wavefunctions of the Mn4CaO5 cluster in photosystem II." *Nature Chem.* **5**, 660 (2013).

[26] J. M. Montgomery and D. A. Mazziotti. "Strong Electron Correlation in Nitrogenase Cofactor, FeMoco." *J. Phys. Chem. A* **122**, 4988 (2018).

[27] J. Ivanic. "Direct configuration interaction and multiconfigurational self-consistent-field method for multiple active spaces with variable occupations. I. Method." *J. Chem. Phys.* **119**, 9364 (2003).

[28] D. Ma, G. Li Manni, and L. Gagliardi. "The generalized active space concept in multiconfigurational self-consistent field methods." **135**, 044128 (2011).

[29] K. D. Vogiatzis, G. Li Manni, S. J. Stoneburner, D. Ma, and L. Gagliardi. "Systematic Expansion of Active Spaces beyond the CASSCF Limit: A GASSCF/SplitGAS Benchmark Study." *J. Chem. Theor. Comput.* **11**, 3010 (2015).

[30] S. Ghosh, C. J. Cramer, D. G. Truhlar, and L. Gagliardi. "Generalized-active-space pair-density functional theory: an efficient method to study large, strongly correlated, conjugated systems." *Chemical Science* **8**, 2741 (2017).

[31] S. R. White. "Density matrix formulation for quantum renormalization groups." *Phys. Rev. Lett.* **69**, 2863 (1992).

[32] S. R. White and R. L. Martin. "Ab initio quantum chemistry using the density matrix renormalization group." *J. Chem. Phys.* **110**, 4127 (1999).

[33] G. K.-L. Chan and M. Head-Gordon. "Highly correlated calculations with a polynomial cost algorithm: A study of the density matrix renormalization group." **116**, 4462 (2002).

[34] G. K.-L. Chan and S. Sharma. "The density matrix renormalization group in quantum chemistry." *Annu. Rev. Phys. Chem.* **62**, 465 (2011).

[35] G. Moritz, B. A. Hess, and M. Reiher. "Convergence behavior of the density-matrix renormalization group algorithm for optimized orbital orderings." *J. Chem. Phys.* **122**, 024107 (2005).

[36] Y. Ma and H. Ma. "Assessment of various natural orbitals as the basis of large active space density-matrix renormalization group calculations." *J. Chem. Phys.* **138**, 224105 (2013).

[37] J. Hachmann, J. J. Dorando, M. Avilés, and G. K.-L. Chan. "The radical character of the acenes: a density matrix renormalization group study." *J. Chem. Phys.* **127**, 134309 (2007).

[38] R. Olivares-Amaya, W. Hu, N. Nakatani, S. Sharma, J. Yang, and G. K.-L. Chan. "The ab-initio density matrix renormalization group in practice." *J. Chem. Phys.* **142**, 034102 (2015).

[39] N. Nakatani and S. Guo. "Density matrix renormalization group (DMRG) method as a common tool for large active-space CASSCF/CASPT2 calculations." *J. Chem. Phys.* (2017).

[40] W. Purwanto, S. Zhang, and H. Krakauer. "Excited state calculations using phaseless auxiliary-field quantum Monte Carlo: Potential energy curves of low-lying C2 singlet states." *J. Chem. Phys.* **130**, 094107 (2009).

[41] E. Giner, A. Scemama, and M. Caffarel. "Using perturbatively selected configuration interaction in quantum Monte Carlo calculations." *Can. J. Chem.* **91**, 879 (2013).

[42] F. R. Petruzielo, A. A. Holmes, H. J. Changlani, M. P. Nightingale, and C. J. Umrigar. "Semistochastic projector Monte Carlo method." *Phys. Rev. Lett.* **109**, 230201 (2012).

[43] S. Ten-no. "Stochastic determination of effective Hamiltonian for the full configuration interaction solution of quasi-degenerate electronic states." *J. Chem. Phys.* **138**, 164126 (2013).

[44] N. S. Blunt, A. Alavi, and G. H. Booth. "Krylov-projected quantum Monte Carlo method." *Phys. Rev. Lett.* **115**, 050603 (2015).

[45] G. Li Manni, S. D. Smart, and A. Alavi. "Combining the complete active space self-consistent field method and the full configuration interaction quantum monte carlo within a super-CI framework, with application to challenging metal-porphyrins." *J. Chem. Theor. Comput.* **12**, 1245 (2016).

[46] E. Giner, R. Assaraf, and J. Toulouse. "Quantum Monte Carlo with reoptimised perturbatively selected configuration-interaction wave functions." *Mol. Phys.* **114**, 910 (2016).

[47] G. H. Booth, A. J. Thom, and A. Alavi. "Fermion Monte Carlo without fixed nodes: A game of life, death, and annihilation in Slater determinant space." *J. Chem. Phys.* **131**, 054106 (2009).

[48] D. Cleland, G. H. Booth, and A. Alavi. "Communications: Survival of the fittest: Accelerating convergence in full configuration-interaction quantum Monte Carlo." *J. Chem. Phys.* **132**, 041103 (2010).

[49] G. H. Booth and A. Alavi. "Approaching chemical accuracy using full configuration-interaction quantum monte carlo: a study of ionization potentials." *J. Chem. Phys.* **132**, 174104 (2010).

[50] G. H. Booth, D. Cleland, A. J. Thom, and A. Alavi. "Breaking the carbon dimer: the challenges of multiple bond dissociation with full configuration interaction quantum Monte Carlo methods." *J. Chem. Phys.* **135**, 084104 (2011).

[51] G. H. Booth and G. K.-L. Chan. "Communication: Excited states, dynamic correlation functions and spectral properties from full configuration interaction quantum Monte Carlo." *J. Chem. Phys.* **137**, 191102 (2012).

[52] N. S. Blunt, S. D. Smart, G. H. Booth, and A. Alavi. "An excited-state approach within full configuration interaction quantum Monte Carlo." *J. Chem. Phys.* **143**, 134117 (2015).

[53] N. S. Blunt, G. H. Booth, and A. Alavi. "Density matrices in full configuration interaction quantum Monte Carlo: Excited states, transition dipole moments, and parallel distribution." **146**, 244105 (2017).

[54] D. M. Cleland, G. H. Booth, and A. Alavi. "A study of electron affinities using the initiator approach to full configuration interaction quantum Monte Carlo." *J. Chem. Phys.* **134**, 024112 (2011).

[55] R. E. Thomas, Q. Sun, A. Alavi, and G. H. Booth. "Stochastic multiconfigurational self-consistent field theory." *J. Chem. Theor. Comput.* **11**, 5316 (2015).

[56] D. A. Mazziotti. "First-order semidefinite programming for the direct determination of two-electron reduced density matrices with application to many-electron atoms and molecules." **121**, 10957 (2004).

[57] D. A. Mazziotti. "Variational reduced-density-matrix method using three-particle N-representability conditions with application to many-electron molecules." *Phys. Rev. A* **74**, 032501 (2006).

[58] D. A. Mazziotti. "Parametrization of the two-electron reduced density matrix for its direct calculation without the many-electron wave function." *Phys. Rev. Lett.* **101**, 253002 (2008).

[59] D. A. Mazziotti. "Large-scale semidefinite programming for many-electron quantum mechanics." *Phys. Rev. Lett.* **106**, 083001 (2011).

[60] G. Gidofalvi and D. A. Mazziotti. "Active-space two-electron reduced-density-matrix method: complete active-space calculations without diagonalization of the N-electron Hamiltonian." *J. Chem. Phys.* **129**, 134108 (2008).

[61] A. E. DePrince III. "Variational optimization of the two-electron reduced-density matrix under pure-state N-representability conditions." *J. Chem. Phys.* **145**, 164109 (2016).

[62] J. Fosso-Tande, D. R. Nascimento, and I. A Eugene DePrince. "Accuracy of two-particle N-representability conditions for describing different spin states and the singlet–triplet gap in the linear acene series." *Mol. Phys.* **114**, 423 (2016).

[63] J. Fosso-Tande, T.-S. Nguyen, G. Gidofalvi, and I. A Eugene DePrince. "Large-Scale Variational Two-Electron Reduced-Density-Matrix-Driven Complete Active Space Self-Consistent Field Methods." *J. Chem. Theor. Comput.* **12**, 2260 (2016).

[64] M. Mostafanejad and A. E. DePrince. "Combining pair-density functional theory and variational two-electron reduced-density matrix methods." *J. Chem. Theor. Comput.* **15**, 290 (2018).

[65] H.-J. Werner and P. J. Knowles. "An efficient internally contracted multiconfiguration–reference configuration interaction method." *J. Chem. Phys.* **89**, 5803 (1988).

[66] P. J. Knowles and H.-J. Werner. "Internally contracted multiconfiguration-reference configuration interaction calculations for excited states." *Theor. Chim. Acta* **84**, 95 (1992).

[67] H. Lischka, D. Nachtigallová, A. J. A. Aquino, P. G. Szalay, F. Plasser, F. B. C. Machado, and M. Barbatti. "Multireference Approaches for Excited States of Molecules." *Chem. Rev.* **118**, 7293 (2018).

[68] D. Datta, L. Kong, and M. Nooijen. "A state-specific partially internally contracted multireference coupled cluster approach." *J. Chem. Phys.* **134**, 214116 (2011).

[69] F. A. Evangelista and J. Gauss. "An orbital-invariant internally contracted multireference coupled cluster approach." **134**, 114102 (2011).

[70] M. Hanauer and A. Köhn. "Communication: Restoring full size extensivity in internally contracted multireference coupled cluster theory." *J. Chem. Phys.* **137**, 131103 (2012).

[71] B. Jeziorski and H. J. Monkhorst. "Coupled-cluster method for multideterminantal reference states." *Phys. Rev. A* **24**, 1668 (1981).

[72] U. S. Mahapatra, B. Datta, D. M. M. Physics, and 1998. "A state-specific multi-reference coupled cluster formalism with molecular applications." *Taylor & Francis* (1998).

[73] U. S. Mahapatra, B. Datta, and D. Mukherjee. "A size-consistent state-specific multireference coupled cluster theory: Formal developments and molecular applications." *J. Chem. Phys.* **110**, 6171 (1999).

[74] R. Maitra, D. Sinha, and D. Mukherjee. "Unitary group adapted state-specific multi-reference coupled cluster theory: Formulation and pilot numerical applications." *J. Chem. Phys.* **137**, 024105 (2012).

[75] F. A. Evangelista. "Alternative single-reference coupled cluster approaches for multireference problems: The simpler, the better." *J. Chem. Phys.* **134**, 224102 (2011).

[76] J. P. Malrieu, J.-L. Heully, and A. Zaitsevskii. "Multiconfigurational second-order perturbative methods: Overview and comparison of basic properties." *Theoret. Chim. Acta* **90**, 167 (1995).

[77] B. O. Roos, K. Andersson, M. P. Fülscher, P.-Å. Malmqvist, L. S. Andrés, K. Pierloot, and M. Merchán. *Multiconfigurational Perturbation Theory: Applications in Electronic Spectroscopy*, volume 162 of *New Methods in Computational Quantum Mechanics*. John Wiley & Sons, Ltd, Hoboken, NJ, USA (2007).

[78] D. R. Sanjuán, F. Aquilante, and R. Lindh. "Multiconfiguration second-order perturbation theory approach to strong electron correlation in chemistry and photochemistry." *WIREs Comput Mol Sci* **2**, 585 (2012).

[79] K. Andersson, P. A. Malmqvist, and B. O. Roos. "Second-order perturbation theory with a CASSCF reference function." *J. Phys. Chem.* **94**, 5483 (1990).

[80] K. Andersson, P.-Å. Malmqvist, and B. O. Roos. "Second-order perturbation theory with a complete active space self-consistent field reference function." *J. Chem. Phys.* **96**, 1218 (1998).

[81] J. Finley, P.-Å. Malmqvist, B. O. Roos, and L. Serrano-Andrés. "The multi-state CASPT2 method." *Chem. Phys. Lett.* **288**, 299 (1998).

[82] C. Angeli, R. Cimiraglia, S. Evangelisti, T. Leininger, and J. P. Malrieu. "Introduction of n-electron valence states for multireference perturbation theory." *J. Chem. Phys.* **114**, 10252 (2001).

[83] D. Zgid, D. Ghosh, E. Neuscamman, and G. K.-L. Chan. "A study of cumulant approximations to n-electron valence multireference perturbation theory." *J. Chem. Phys.* **130**, 194107 (2009).

[84] Q. M. Phung, S. Wouters, and K. Pierloot. "Cumulant approximated second-order perturbation theory based on the density matrix renormalization group for transition metal complexes: a benchmark study." *J. Chem. Theor. Comput.* **12**, 4352 (2016).

[85] Y. Kurashige and T. Yanai. "Theoretical study of the π π* excited states of oligoacenes: A full π-valence DMRG-CASPT2 study." *Bull. Chem. Soc. Japan* **87**, 1071 (2014).

[86] B. O. Roos and K. Andersson. "Multiconfigurational perturbation theory with level shift — the Cr_2 potential revisited." *Chem. Phys. Lett.* **245**, 215 (1995).

[87] S. D. Głazek and K. G. Wilson. "Renormalization of hamiltonians." *Phys. Rev. D* **48**, 5863 (1993).

[88] S. D. Glazek and K. G. Wilson. "Perturbative renormalization group for Hamiltonians." *Phys. Rev. D: Part. Fields* **49**, 4214 (1994).

[89] F. Wegner. "Flow-equations for Hamiltonians." *Ann. Phys.* **506**, 77 (1994).

[90] F. Wegner. "Flow equations and normal ordering: a survey." *J. Phys. A: Math. Gen.* **39**, 8221 (2006).

[91] F. A. Evangelista. "A driven similarity renormalization group approach to quantum many-body problems." **141**, 054109 (2014).

[92] C. Li and F. A. Evangelista. "Multireference driven similarity renormalization group: a second-order perturbative analysis." *J. Chem. Theor. Comput.* **11**, 2097 (2015).

[93] C. Li and F. A. Evangelista. "Towards numerically robust multireference theories: The driven similarity renormalization group truncated to one- and two-body operators." **144**, 164114 (2016).

[94] M. J. M. Bernal and S. F. Boys. "Electronic Wave Functions. VIII. A Calculation of the Ground States NaFormula, Ne and FFormula." *Philosophical Transactions of the Royal Society A: Mathematical, Physical and Engineering Sciences* **245**, 139 (1952).

[95] P. Claverie, S. Diner, and J. P. Malrieu. "The Use of Perturbation Methods for the Study of the Effects of Configuration Interaction." *Int. J. Quant. Chem.* **1**, 751 (1967).

[96] C. F. Bunge. "Electronic Wave Functions for Atoms. I. Ground State of Be." *Phys. Rev.* **168**, 92 (1968).

[97] Z. Gershgorn and I. Shavitt. "An application of perturbation theory ideas in configuration interaction calculations." *Int. J. Quant. Chem.* **2**, 751 (1968).

[98] A. Pipano and I. Shavitt. "Convergence studies in configuration interaction calculations." *Int. J. Quant. Chem.* **2**, 741 (1968).

[99] C. F. Bender and E. R. Davidson. "Studies in Configuration Interaction: The First-Row Diatomic Hydrides." *Phys. Rev.* **183**, 23 (1969).

[100] J. L. Whitten and M. Hackmeyer. "Configuration Interaction Studies of Ground and Excited States of Polyatomic Molecules. I. The CI Formulation and Studies of Formaldehyde." *J. Chem. Phys.* **51**, 5584 (1969).

[101] B. Huron, J. P. Malrieu, and P. Rancurel. "Iterative perturbation calculations of ground and excited state energies from multiconfigurational zeroth-order wavefunctions." *J. Chem. Phys.* **58**, 5745 (1973).

[102] R. J. Buenker and S. D. Peyerimhoff. "Individualized configuration selection in CI calculations with subsequent energy extrapolation." *Theoret. Chim. Acta* **35**, 33.

[103] R. J. Buenker and S. D. Peyerimhoff. "Energy extrapolation in CI calculations." *Theoret. Chim. Acta* **39**, 217 (1975).

[104] S. Evangelisti, J.-P. Daudey, and J. P. Malrieu. "Convergence of an improved CIPSI algorithm." *Chem. Phys.* **75**, 91 (1983).

[105] R. Cimiraglia. "Second order perturbation correction to CI energies by use of diagrammatic techniques: An improvement to the CIPSI algorithm." *J. Chem. Phys.* **83**, 1746 (1985).

[106] P. J. Knowles and N. C. Handy. "A new determinant-based full configuration interaction method." *Chem. Phys. Lett.* **111**, 315 (1984).

[107] P. J. Knowles. "Very large full configuration interaction calculations." *Chem. Phys. Lett.* **155**, 513 (1989).

[108] P. J. Knowles and N. C. Handy. "A determinant based full configuration interaction program." *Comput. Phys. Commun.* **54**, 75 (1989).

[109] A. O. Mitrushenkov. "Passing the several billions limit in FCI calculations on a mini-computer." *Chem. Phys. Lett.* **217**, 559 (1994).

[110] A. O. Mitrushenkov and Y. Y. Dmitriev. "Passing the several billion limit in FCI calculations on a mini-computer. A norm-consistent zero CI threshold estimate within the dynamic CI approach." *Chem. Phys. Lett.* **235**, 410 (1995).

[111] A. L. Wulfov. "Passing the one-quadrillion limit in FCl extrapolations on a personal computer." *Chem. Phys. Lett.* (1996).

[112] R. Caballol and J. P. Malrieu. "Direct selected configuration interaction using a hole-particle formalism." *Chem. Phys. Lett.* **188**, 543 (1992).

[113] À. Povill and J. Rubio. "An efficient improvement of the string-based direct selected CI algorithm." *Theoret. Chim. Acta* **92**, 305 (1995).

[114] M. Hanrath and B. Engels. "New algorithms for an individually selecting MR-CI program." *Chem. Phys.* (1997).

[115] P. Stampfuß, K. Hamacher, and W. Wenzel. "Massively parallel individually selecting configuration interaction." *J. Mol. Struct.:THEOCHEM* **506**, 99 (2000).

[116] J. Ivanic, K. R. T. C. Accounts, and 2001. "Identification of deadwood in configuration spaces through general direct configuration interaction." *Springer* **106**, 339 (2001).

[117] P. Stampfuß and W. Wenzel. "Improved implementation and application of the individually selecting configuration interaction method." *J. Chem. Phys.* **122**, 024110 (2005).

[118] L. Bytautas and K. Ruedenberg. "A priori identification of configurational deadwood." *Chem. Phys.* **356**, 64 (2009).

[119] R. J. Harrison. "Approximating full configuration interaction with selected configuration interaction and perturbation theory." **94**, 5021 (1991).

[120] J. Meller, J. L. Heully, and J. P. Malrieu. "Size-consistent self-consistent combination of selected CI and perturbation theory." *Chem. Phys. Lett.* **218**, 276 (1994).

[121] J. Miralles, O. Castell, R. Caballol, and J. P. Malrieu. "Specific CI calculation of energy differences: Transition energies and bond energies." *Chem. Phys.* **172**, 33 (1993).

[122] V. M. García, O. Castell, R. Caballol, and J. P. Malrieu. "An iterative difference-dedicated configuration interaction. Proposal and test studies." *Chem. Phys. Lett.* **238**, 222 (1995).

[123] F. Neese. "A spectroscopy oriented configuration interaction procedure." *J. Chem. Phys.* **119**, 9428 (2003).

[124] J. C. Greer. "Estimating full configuration interaction limits from a Monte Carlo selection of the expansion space." *J. Chem. Phys.* **103**, 1821 (1995).

[125] J. C. Greer. "Monte Carlo Configuration Interaction." *Journal of Computational Physics* **146**, 181 (1998).

[126] J. P. Coe and M. J. Paterson. "Development of Monte Carlo configuration interaction: natural orbitals and second-order perturbation theory." *J. Chem. Phys.* **137**, 204108 (2012).

[127] J. P. Coe and M. J. Paterson. "State-averaged Monte Carlo configuration interaction applied to electronically excited states." *J. Chem. Phys.* **139**, 154103 (2013).

[128] J. P. Coe, P. Murphy, and M. J. Paterson. "Applying Monte Carlo configuration interaction to transition metal dimers: Exploring the balance between static and dynamic correlation." *Chem. Phys. Lett.* (2014).

[129] T. P. Kelly, A. Perera, R. J. Bartlett, and J. C. Greer. "Monte Carlo configuration interaction with perturbation corrections for dissociation energies of first row diatomic molecules: C2, N2, O2, CO, and NO." *J. Chem. Phys.* **140**, 084114 (2014).

[130] J. P. Coe and M. J. Paterson. "Open-shell systems investigated with Monte Carlo configuration interaction." *Int. J. Quant. Chem.* n/a–n/a (2016).

[131] J. P. Coe, N. M. S. Almeida, and M. J. Paterson. "Investigation of challenging spin systems using Monte Carlo configuration interaction and the density matrix renormalization group." *J. Comp. Chem.* **38**, 2701 (2017).

[132] P. J. Knowles. "Compressive sampling in configuration interaction wavefunctions." *Mol. Phys.* **113**, 1655 (2015).

[133] J. R. McClean and A. Aspuru-Guzik. "Compact wavefunctions from compressed imaginary time evolution." *RSC Advances* (2015).

[134] M. L. Abrams and C. D. Sherrill. "Important configurations in configuration interaction and coupled-cluster wave functions." *Chem. Phys. Lett.* **412**, 121 (2005).

[135] C. F. Bunge. "Selected configuration interaction with truncation energy error and application to the Ne atom." *J. Chem. Phys.* **125**, 014107 (2006).

[136] F. A. Evangelista. "Adaptive multiconfigurational wave functions." **140**, 054109 (2014).

[137] N. M. Tubman, J. Lee, T. Y. Takeshita, M. Head-Gordon, and K. B. Whaley. "A deterministic alternative to the full configuration interaction quantum Monte Carlo method." *J. Chem. Phys.* **145**, 044112 (2016).

[138] N. M. Tubman, C. D. Freeman, D. S. Levine, D. Hait, M. Head-Gordon, and K. B. Whaley. "Modern Approaches to Exact Diagonalization and Selected Configuration Interaction with the Adaptive Sampling CI Method." *arXiv* https:—-arxiv.org–abs–1807.00821 (2018).

[139] Y. Ohtsuka and J.-y. Hasegawa. "Selected configuration interaction method using sampled first-order corrections to wave functions." *J. Chem. Phys.* **147**, 034102 (2017).

[140] E. Giner, A. Scemama, and M. Caffarel. "Fixed-node diffusion Monte Carlo potential energy curve of the fluorine molecule F2 using selected configuration interaction trial wavefunctions." *J. Chem. Phys.* **142**, 044115 (2015).

[141] P.-F. Loos, A. Scemama, A. Blondel, Y. Garniron, M. Caffarel, and D. Jacquemin. "A Mountaineering Strategy to Excited States: Highly Accurate Reference Energies and Benchmarks." *J. Chem. Theor. Comput.* **14**, 4360 (2018).

[142] A. Scemama, T. Applencourt, E. Giner, and M. Caffarel. "Accurate nonrelativistic ground-state energies of 3d transition metal atoms." **141**, 244110 (2014).

[143] A. Scemama, A. Benali, D. Jacquemin, M. Caffarel, and P.-F. Loos. "Excitation energies from diffusion Monte Carlo using selected configuration interaction nodes." *J. Chem. Phys.* **149**, 034108 (2018).

[144] A. A. Holmes, N. M. Tubman, and C. J. Umrigar. "Heat-Bath Configuration Interaction: An Efficient Selected Configuration Interaction Algorithm Inspired by Heat-Bath Sampling." *J. Chem. Theor. Comput.* **12**, 3674 (2016).

[145] S. Sharma, A. A. Holmes, G. Jeanmairet, A. Alavi, and C. J. Umrigar. "Semistochastic heat-bath configuration interaction method: Selected configuration interaction with semistochastic perturbation theory." *J. Chem. Theor. Comput.* **13**, 1595 (2017).

[146] A. A. Holmes, C. J. Umrigar, and S. Sharma. "Excited states using semistochastic heat-bath configuration interaction." *J. Chem. Phys.* **147**, 164111 (2017).

[147] V. A. Neufeld and A. J. W. Thom. "Exciting determinants in Quantum Monte Carlo: Loading the dice with fast, low memory weights." *J. Chem. Theor. Comput.* **15**, 127 (2018).

[148] J. Li, M. Otten, A. A. Holmes, S. Sharma, and C. J. Umrigar. "Fast semistochastic heat-bath configuration interaction." *J. Chem. Phys.* **149**, 214110 (2018).

[149] A. D. Chien, A. A. Holmes, M. Otten, C. J. Umrigar, S. Sharma, and P. M. Zimmerman. "Excited States of Methylene, Polyenes, and Ozone from Heat-Bath Configuration Interaction." *J. Phys. Chem. A* **122**, 2714 (2018).

[150] J. E. T. Smith, B. Mussard, A. A. Holmes, and S. Sharma. "Cheap and Near Exact CASSCF with Large Active Spaces." *J. Chem. Theor. Comput.* **13**, 5468 (2017).

[151] J. B. Schriber, K. P. Hannon, C. Li, and F. A. Evangelista. "A Combined Selected Configuration Interaction and Many-Body Treatment of Static and Dynamical Correlation in Oligoacenes." *J. Chem. Theor. Comput.* **14**, 6295 (2018).

[152] S. Shirai, Y. Kurashige, and T. Yanai. "Computational evidence of inversion of 1La and 1Lb-derived excited states in naphthalene excimer formation from ab initio multireference theory with large active space: DMRG-CASPT2 study." *Journal of chemical theory and computation* (2016).

[153] S. Guo, M. A. Watson, W. Hu, Q. Sun, and G. K.-L. Chan. "N-Electron Valence State Perturbation Theory Based on a Density Matrix Renormalization Group Reference Function, with Applications to the Chromium Dimer and a Trimer Model of Poly(p-Phenylenevinylene)." *J. Chem. Theor. Comput.* **12**, 1583 (2016).

[154] M. Roemelt, S. Guo, and G. K.-L. Chan. "A projected approximation to strongly contracted N-electron valence perturbation theory for DMRG wavefunctions." **144**, 204113 (2016).

[155] Z. Luo, Y. Ma, X. Wang, and H. Ma. "Externally-Contracted Multireference Configuration Interaction Method Using a DMRG Reference Wave Function." *J. Chem. Theor. Comput.* (2018).

Chapter 2

The Adaptive Configuration Interaction Method

2.1 Introduction

Most popular methods in electronic structure theory by some means attempt to exploit the sparsity of full configuration interaction (FCI) wave functions.[1] The exponential scaling of the number of determinants with respect to the number of orbitals required for FCI calculations prevents its use for all but trivially small systems, or for active space calculations no larger than 18 electrons in 18 orbitals. Recently, wave function factorization techniques such as the density matrix renormalization group,[2–6] and stochastic CI approaches such as Monte Carlo CI (MCCI)[7–10] and FCI Quantum Monte Carlo (FCIQMC)[11–14] have risen as promising alternatives to FCI and complete active space CI (CASCI), allowing for the description of chemically interesting systems.[15,16]

In this study, we propose a new adaptive configuration interaction (ACI) method that produces compact wave functions with tunable accuracy. The ACI is based on the framework of selected CI,[17–20] which recently has received renewed attention.[21–30] It uses two parameters to control the treatment of electron correlation. As will be shown, a remarkable property of the ACI is its ability to compute electronic energies with almost perfect control over the energy error. Additionally, we demonstrate that the ACI is a viable alternative to traditional complete active space (CAS) methods by performing ACI computations on active spaces that are outside the reach of CASCI.

2.2 The Adaptive Configuration Interaction Method

Given a set of orthonormalized one-electron molecular orbitals, $\{\phi_p\}$, the ACI requires the user to specify the number of electrons, the spin multiplicity, and two orbital subsets: doubly occupied orbitals and active orbitals. The latter are partially occupied in all determinants generated by the ACI. The ACI procedure is illustrated in Fig. 2.1 and consists of the following steps:

i) At each iteration k we define the space of reference determinants $[P^{(k)}]$:

$$P^{(k)} = \{\Phi_\mu \ : \mu = 1, 2, \ldots, d_k\}, \tag{2.1}$$

where d_k is the dimension of the $P^{(k)}$ space. To this space, we associate the configuration interaction wave function $\Psi_P^{(k)}$, defined as:

$$|\Psi_P^{(k)}\rangle = \sum_{\mu=1}^{d_k} C_\mu \, |\Phi_\mu\rangle \,, \tag{2.2}$$

where the coefficients C_μ are determined by diagonalizing the Hamiltonian in the space $P^{(k)}$. In most cases, we begin the ACI process with an initial reference space, $P^{(0)}$, that contains a single determinant, though a set of determinants can be used to speed convergence.

ii) From the reference space $P^{(k)}$, all singly and doubly excited determinants are gener-

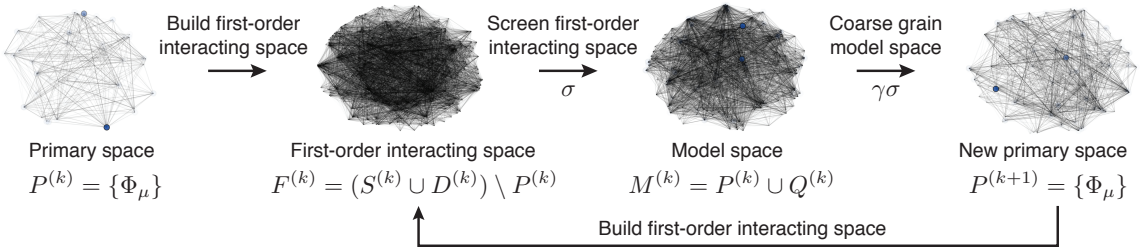

Figure 2.1: Evolution of determinant spaces in the ACI algorithm. Each node represents a determinant, and the edges represent coupling through the Hamiltonian between two nodes. The edges are weighted by the magnitude of this coupling, and the nodes are weighted proportionally to the square modulus of the determinant coefficient ($|C_\mu|^2$).

ated. For a given $P^{(k)}$ space, we define the usual first-order interacting space (FOIS), $F^{(k)}$, as the union of all unique singly [$S^{(k)}$] and doubly [$D^{(k)}$] excited determinants out of the reference space:

$$F^{(k)} = (S^{(k)} \cup D^{(k)}) \setminus P^{(k)}. \tag{2.3}$$

Denoting the occupied (virtual) orbitals of determinant $\Phi_\mu \in P^{(k)}$ as $i, j, \ldots$ $(a, b, \ldots)$, then $S^{(k)}$ and $D^{(k)}$ may be written compactly as $S^{(k)} = \{\hat{a}_a^\dagger \hat{a}_i \Phi_\mu \ : \forall \Phi_\mu \in P^{(k)}\}$ and $D^{(k)} = \{\hat{a}_a^\dagger \hat{a}_b^\dagger \hat{a}_j \hat{a}_i \Phi_\mu \ : \forall \Phi_\mu \in P^{(k)}\}$.

iii) To each determinant in $F^{(k)}$ we associate an estimate of the energy contribution. Following degeneracy-corrected perturbation theory,[31] we consider the two-by-two Hamiltonian for a determinant $\Phi_I \in F^{(k)}$ interacting with a the P-space wave function $\Psi_P^{(k)}$:

$$\mathbf{H} = \begin{pmatrix} \langle \Psi_P^{(k)} | \hat{H} | \Psi_P^{(k)} \rangle & \langle \Psi_P^{(k)} | \hat{H} | \Phi_I \rangle \\ \langle \Phi_I | \hat{H} | \Psi_P^{(k)} \rangle & \langle \Phi_I | \hat{H} | \Phi_I \rangle \end{pmatrix} = \begin{pmatrix} E_P & V \\ V^* & E_I \end{pmatrix}. \tag{2.4}$$

Diagonalization of $\mathbf{H}$ yields two real eigenvalues (λ_1, λ_2, $\lambda_1 \leq \lambda_2$), the lower of which differs from the energy of $\Psi_P^{(k)}$ (E_P) by:

$$\varepsilon(\Phi_I) = \lambda_1 - E_P = \frac{\Delta}{2} - \sqrt{\frac{\Delta^2}{4} + |V|^2}, \tag{2.5}$$

where $\Delta = E_I - E_P$. Eq. (2.5) defines the energy importance criterion used in ACI to screen the first-order interacting space.

iv) Using the energy importance criterion we define the *secondary space* $Q^{(k)}$, the set of the most important determinants in $F^{(k)}$. To build $Q^{(k)}$, we use an aimed selection scheme.[32] Firstly, we sort the set $F^{(k)}$ in decreasing order according to $|\varepsilon(\Phi_I)|$, the absolute value of the energy importance criterion. Secondly, starting from the determinant with the lowest $|\varepsilon(\Phi_I)|$, we exclude all those elements of $F^{(k)}$ such that the cumulative energy error is less than a user-specified threshold σ expressed in units of

mE_h:

$$\sum_{\Phi_I \in F^{(k)} \setminus Q^{(k)}} |\varepsilon(\Phi_I)| \leq \sigma. \tag{2.6}$$

The determinants that are not discarded from $F^{(k)}$ form the set $Q^{(k)}$.

v) With the $Q^{(k)}$ space built, we can define the *total model space* at iteration k [$M^{(k)}$] as the union between the reference space and the secondary space:

$$M^{(k)} = P^{(k)} \cup Q^{(k)}, \tag{2.7}$$

and diagonalize the Hamiltonian in the space $M^{(k)}$ to obtain the model space wave function:

$$|\Psi_M^{(k)}\rangle = \sum_{\Phi_I \in M^{(k)}} C_I |\Phi_I\rangle, \tag{2.8}$$

and the associated energy $E_M^{(k)}$. The model space energy may be corrected for the contributions of the determinants excluded from the secondary space [$\Phi_I \in F^{(k)} \setminus Q^{(k)}$] using the second-order perturbative estimate:

$$E_F^{(k)} \approx E_M^{(k)} + \sum_{\Phi_I \in F^{(k)} \setminus Q^{(k)}} \varepsilon(\Phi_I). \tag{2.9}$$

In the limit of V that goes to zero, the contribution of a single determinant to the second-order perturbative correction is approximately $\varepsilon(\Phi_I) \approx -|V|^2/\Delta$. Therefore, Eq. (2.9) may be viewed as a state-specific second-order correction based on the Epstein–Nesbet partitioning of the Hamiltonian.[18]

vi) Rather than directly augmenting the total model space as the iterations proceed, as is traditionally done in selected CI methods, we coarse grain the space $M^{(k)}$ to form an updated reference space $P^{(k+1)}$. Specifically, the $M^{(k)}$-space determinants are sorted according to the square of the CI coefficients ($|C_I|^2$) in decreasing order. Determinants are progressively included in $P^{(k+1)}$ until the sum of the squared coefficients is less

than $1-\gamma\sigma$, where γ is a constant that has units of (energy)$^{-1}$:

$$\sum_{\Phi_\mu \in P^{(k+1)}} |C_\mu|^2 < 1-\gamma\sigma. \tag{2.10}$$

vii) Steps i–vi are repeated until the energy of the $M^{(k)}$ space is converged. This convergence of the energy coincides with the convergence of $P^{(k)}$ and $M^{(k)}$ with respect to the determinants included.

ACI improves upon previous selected CI methods like CIPSI[18] and CI+PT[20] in a number of important ways. Firstly, the aimed selection procedure gives the user *a priori* control over the absolute error in a computation. Additionally, the coarse-graining step (vi) increases the efficiency of the selection process (analogous to the initiator approximation of FCIQMC)[12] and decreases the dependence on the starting wave function guess.

2.3 Numerical Tests and Applications

For all ACI calculations, the parameters σ and γ are directly related to the desired energy accuracy. We found it convenient to assume a constant value of γ, and in this work all results were obtained using $\gamma = 1$ mE_h^{-1}. Accordingly, ACI results will be denoted as ACI(σ), while the ACI energy corrected for the determinant excluded from the secondary space [Eq. (2.9)] will instead be indicated as ACI(σ)+PT2.

2.3.1 The Dissociation of N_2

To illustrate the ability of ACI to determine molecular energies with nearly constant accuracy along a potential energy surface, we examine the dissociation of N_2. To maximize efficiency, ACI works in the basis of Slater determinants rather than configuration state functions. Consequently, $P^{(k)}$ and $M^{(k)}$ may not form spin complete sets. To bypass this issue, in certain cases we have enforced spin completeness by appropriately augmenting $P^{(k)}$ and $M^{(k)}$. In practice, correcting for spin incompleteness is only necessary to describe near-degenerate states of different spin. Therefore, in this work this procedure is only

applied to our N_2 computations to recover the correct asymptotic dissociation limit. Figure 2.2 shows the error with respect to FCI for the ground-state potential energy curve of N_2 computed with ACI using canonical restricted Hartree–Fock (RHF) orbitals. In addition, we plot results for the internally-contracted multireference CISD (MR-CISD),[33] and MR-CISD with Davidson's correction (MR-CISD+Q)[34] based on a CAS self-consistent-field reference with six electrons in six orbitals [CASSCF(6,6)]. MR-CISD and MR-CISD+Q data from Ref 35 was used. Figure 2.2A illustrates a distinguishing factor of the ACI: the absolute error at each point along the curve is reliably estimated by the energy threshold σ. Moreover, while the ACI(10) curve displays noticeable microscopic discontinuity, the ACI(5) and ACI(1) curves are progressively smoother. The inclusion of the second-order perturbative correction (see Fig. 2.2B) leads to curves that are approximately within 1 mE_h from the FCI energy. In comparison, MR-CISD shows fairly constant error throughout the dissociation, but with a noticeable increase near 1.6 Å. With the $+Q$ correction, the error is fairly constant across the potential, though with a slight decrease in accuracy towards dissociation. Additionally, these energies are not variational.

Table 2.1 compares the energy error with respect to FCI (ΔE) and the size of the ACI determinant space for N_2 at the bond distances 1.1 and 3 Å. In both cases, ACI energy errors with respect to FCI show very good correlation with the value of σ. For a given value of σ, the energy difference $|\Delta E(r = 3) - \Delta E(r = 1.1)|$ is only a fraction of the absolute error, showing the ability of the ACI method to describe both static and dynamic correlation in a balanced way. With the perturbative correction, the absolute energy errors are further reduced but the NPEs remain virtually unchanged. When we use natural orbitals from second-order Møller–Plesset perturbation theory or CASSCF (see Table 2.1), the ACI(1) gives a more compact model space, with improved energy error with respect to RHF orbitals. This result suggests that the parameter σ effectively controls the ACI error regardless of the molecular orbital basis.

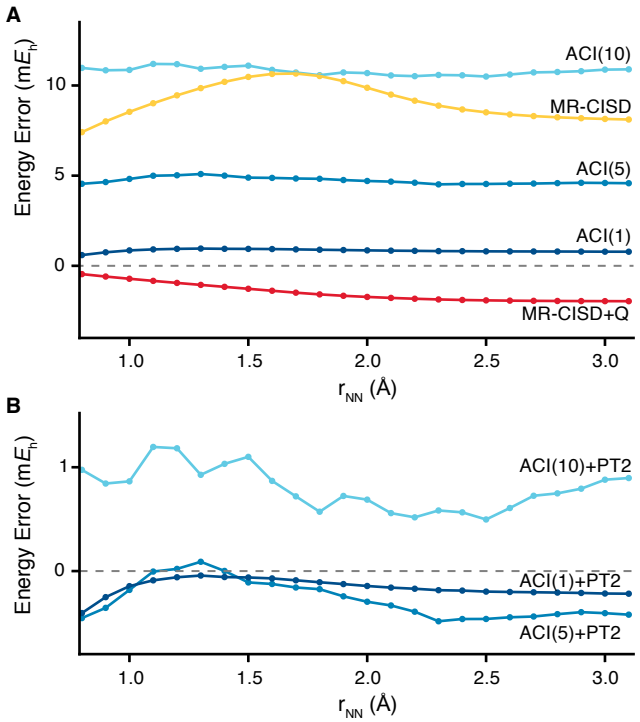

Figure 2.2: Ground-state potential energy curve of N_2 computed with the cc-pVDZ basis set. (A) Energy errors with respect to FCI for the ACI, MR-CISD, and MR-CISD+Q. (B) Energy errors with respect to FCI for the ACI plus the second-order energy correction [Eq. (2.9)]. ACI results used restricted Hartree–Fock orbitals while MR-CISD and MR-CISD+Q results are based on a CASSCF(6,6) reference. The 1s-like orbitals of nitrogen were frozen in all correlated computations.

2.3.2 Singlet-Triplet Splittings in Oligoacenes

To demonstrate the ability of ACI in accurately exploiting the sparsity of CASCI spaces, we turn to the polyacene series.[36–42] The polyacene geometries from Ref. 36 were used in our calculations, and only the π bonding and antibonding pairs included in the STO-3G basis were correlated. This corresponds to a CAS($4n+2$,$4n+2$) wave function, where n is the number of fused benzene rings. Such a problem is intractable with CASCI for $n \geq 4$, but it is well suited for DMRG[36] and the two-electron reduced density matrix (v-2RDM) method.[42–44] To directly compare with previous results,[36,42] all ACI computations use canonical RHF orbitals.

Table 2.2 shows the vertical singlet-triplet splittings ($\Delta E_{\mathrm{ST}} = E^{S=1} - E^{S=0}$) for various values of σ, in addition to comparison with DMRG[36] and v-2RDM[42] results. We also re-

Table 2.1: Errors with respect to FCI (ΔE, in mE_h), number of variational parameters (N_par), and non-parallelism error (NPE = $|\Delta E(r=3) - \Delta E(r=1.1)|$) for the ground state of N_2 at r = 1.1 and 3 Å computed with the cc-pVDZ basis set. ACI and MR-CI computations used restricted Hartree–Fock and CASSCF(6,6) orbitals, respectively. The 1s-like orbitals of nitrogen were frozen in all correlated computations. For $\sigma = 1$, we also report ACI results computed using MP2 natural orbitals (NO) and CASSCF(6,6) orbitals (CAS).

	$r = 1.1$ Å		$r = 3$ Å		NPE
	ΔE	N_par[a]	ΔE	N_par	
MR-CISD	9.02	5352/28030	8.14	5352/28030	0.88
MR-CISD+Q	−0.83	5352/28030	−1.96	5352/28030	1.13
ACI(50)	50.73	963	54.02	8044	3.29
ACI(10)	11.20	23940	10.88	54008	0.32
ACI(5)	5.00	104398	4.59	308804	0.41
ACI(1)	0.91	613198	0.78	1727993	0.13
ACI(1) (CAS)	0.90	369562	0.69	1338097	0.11
ACI(1) (NO)	0.87	348789	0.78	1494181	0.09
ACI(50)+PT2	0.73	963	4.03	8044	3.30
ACI(10)+PT2	1.20	23940	0.88	54008	0.32
ACI(5)+PT2	−0.01	104398	−0.41	308804	0.40
ACI(1)+PT2	−0.09	613198	−0.22	1727993	0.13
FCI		540924024		540924024	

[a] For MR-CISD and MR-CISD+Q we report the total number of contracted/uncontracted configuration state functions.

Table 2.2: Singlet-triplet splittings of the acene series computed with the ACI , DMRG, and v-2RDM methods using the STO-3G basis set. All carbon π orbitals were correlated.

		ΔE_ST (kcal mol^{-1})				
n	CAS	ACI(100)	ACI(50)	ACI(10)	v-2RDM	DMRG
2	(10,10)	67.4	66.3	62.4	63.8	61.5
3	(14,14)	51.8	51.0	46.8	45.2	46.0
4	(18,18)	38.4	38.3	35.5	32.8	34.7
5	(22,22)	30.5	29.4	27.4	24.5	26.7
6	(26,26)	25.3	22.4	21.0	19.7	21.0
8	(34,34)	13.0	15.3		15.4	14.2
10	(42,42)	9.1			13.0	11.6

port the corresponding numbers of determinants required in each computation in Table 2.3. Note that to guarantee sub-kcal mol^{-1} accuracy, a σ value less than 1.6 mE_h is in principle required. However, already for $\sigma = 10$ mE_h, the ACI error with respect to DMRG is consistently less that 1 kcal mol^{-1} through hexacene. For $\sigma = 50$ mE_h, we see the maximum error at anthracene, and in general the errors in the singlet-triplet splitting decrease with increasing n. A similar trend is seen with the v-2RDM data, where the maximum in error is at $n = 5$. The singlet-triplet splittings were also computed with ACI+PT2, and

Table 2.3: Number of determinants required for the ACI wave functions used for the oligoacenes in this work.

		Singlet			Triplet		
n	CAS	ACI(100)	ACI(50)	ACI(10)	ACI(100)	ACI(50)	ACI(10)
2	(10,10)	14	41	332	16	43	376
3	(14,14)	76	230	8325	73	249	8600
4	(18,18)	278	930	136190	280	1097	146814
5	(22,22)	821	3444	1260702	849	4990	1495276
6	(26,26)	2174	31294	2770391	2220	40774	3352196
8	(34,34)	10580	1677179		11140	1496690	
10	(42,42)	82403			81034		

they on average deviated from the corresponding ACI values on the order of 0.01 kcal mol^{-1} with a maximum of 0.4 kcal mol^{-1} for the $\sigma = 100$ calculation of naphthalene. Our current pilot ACI code can be used to perform computations with up to about 5×10^6 determinants, which currently limits the ACI(10) to hexacene and the ACI(100) to decacene. However, we anticipate that a production-level implementation of the ACI method that can take advantage of distributed memory architectures will be able to routinely target 10^7–10^8 determinants.[45] Furthermore, we anticipate that like in the case of the DMRG,[3,46] in the context of the ACI a localized molecular orbital basis will be crucial to significantly compress the number of variational parameters, and in turn, expand the applicability of this method to larger active spaces.

2.4 Conclusions

In summary, the major benefits of the ACI method are that: i) electron correlation can be treated in a balanced way without *a priori* knowledge of a system's electronic structure and ii) that the energy error is precisely controlled by one user-specified parameter. The most promising application of ACI is as a replacement for prohibitively large CASCI reference wave functions used in perturbative and non-perturbative treatments of electron correlation. However, to overcome the deficiencies of CASCI, ACI can be coupled with orbital optimization schemes to produce CASSCF-like references for active spaces much larger than the CAS(18,18) limit. The straightforward computation of ACI reduced density matrices enables these extensions. Given that the ACI: i) is a variational deterministic

procedure, ii) does not require orbital ordering, iii) can be straightforwardly extended to excited states, and iv) can be easily implemented on distributed memory architectures, it is an interesting alternative to DMRG, MCCI, FCIQMC, and v-2RDM methods.

All ACI results were obtained using our pilot code (FORTE),[47] which is a suite of multireference methods written as a plugin to the open-source quantum chemistry package PSI4.[48]

Bibliography

[1] C. D. Sherrill and H. F. Schaefer III. "The configuration interaction method: Advances in highly correlated approaches." *Adv. Quant. Chem.* **34**, 143 (1999).

[2] S. R. White. "Density matrix formulation for quantum renormalization groups." *Phys. Rev. Lett.* **69**, 2863 (1992).

[3] G. K.-L. Chan and M. Head-Gordon. "Highly correlated calculations with a polynomial cost algorithm: A study of the density matrix renormalization group." *J. Chem. Phys.* **116**, 4462 (2002).

[4] G. Moritz, A. Wolf, and M. Reiher. "Relativistic DMRG calculations on the curve crossing of cesium hydride." *J. Chem. Phys.* **123**, 184105 (2005).

[5] Y. Kurashige and T. Yanai. "High-performance ab initio density matrix renormalization group method: Applicability to large-scale multireference problems for metal compounds." *J. Chem. Phys.* **130**, 234114 (2009).

[6] R. Olivares-Amaya, W. Hu, N. Nakatani, S. Sharma, J. Yang, and G. K.-L. Chan. "The ab-initio density matrix renormalization group in practice." *J. Chem. Phys.* **142**, 034102 (2015).

[7] J. Greer. "Estimating full configuration interaction limits from a Monte Carlo selection of the expansion space." *J. Chem. Phys.* **103**, 1821 (1995).

[8] T. P. Kelly, A. Perera, R. J. Bartlett, and J. C. Greer. "Monte Carlo configuration interaction with perturbation corrections for dissociation energies of first row diatomic molecules: C2, N2, O2, CO, and NO." *J. Chem. Phys.* **140**, 084114 (2014).

[9] J. Coe and M. Paterson. "Development of Monte Carlo configuration interaction: Natural orbitals and second-order perturbation theory." *J. Chem. Phys.* **137**, 204108 (2012).

[10] J. Coe, P. Murphy, and M. Paterson. "Applying Monte Carlo configuration interaction to transition metal dimers: exploring the balance between static and dynamic correlation." *Chem. Phys. Lett.* **604**, 46 (2014).

[11] G. H. Booth, A. J. Thom, and A. Alavi. "Fermion Monte Carlo without fixed nodes: A game of life, death, and annihilation in Slater determinant space." *J. Chem. Phys.* **131**, 054106 (2009).

[12] D. Cleland, G. H. Booth, and A. Alavi. "Communications: Survival of the fittest: Accelerating convergence in full configuration-interaction quantum Monte Carlo." *J. Chem. Phys.* **132**, 041103 (2010).

[13] F. R. Petruzielo, A. A. Holmes, H. J. Changlani, M. P. Nightingale, and C. J. Umrigar. "Semistochastic Projector Monte Carlo Method." *Phys. Rev. Lett.* **109**, 230201 (2012).

[14] S. Ten-no. "Stochastic determination of effective Hamiltonian for the full configuration interaction solution of quasi-degenerate electronic states." *J. Chem. Phys.* **138**, 164126 (2013).

[15] Y. Kurashige, G. K.-L. Chan, and T. Yanai. "Entangled quantum electronic wavefunctions of the Mn4CaO5 cluster in photosystem II." *Nature Chem.* **5**, 660 (2013).

[16] G. H. Booth, A. Grüneis, G. Kresse, and A. Alavi. "Towards an exact description of electronic wavefunctions in real solids." *Nature* **493**, 365 (2013).

[17] C. F. Bender and E. R. Davidson. "Studies in configuration interaction: The first-row diatomic hydrides." *Phys. Rev.* **183**, 23 (1969).

[18] B. Huron, J. P. Malrieu, and P. Rancurel. "Iterative perturbation calculations of ground and excited state energies from multiconfigurational zeroth-order wavefunctions." *J. Chem. Phys.* **58**, 5745 (1973).

[19] R. J. Buenker and S. D. Peyerimhoff. "Individualized configuration selection in CI calculations with subsequent energy extrapolation." *Theor. Chim. Acta* **35**, 33 (1974).

[20] R. J. Harrison. "Approximating full configuration interaction with selected configuration interaction and perturbation theory." *J. Chem. Phys.* **94**, 5021 (1991).

[21] V. García, O. Castell, R. Caballol, and J. Malrieu. "An iterative difference-dedicated configuration interaction. Proposal and test studies." *Chem. Phys. Lett.* **238**, 222 (1995).

[22] F. Neese. "A spectroscopy oriented configuration interaction procedure." *J. Chem. Phys.* **119**, 9428 (2003).

[23] H. Nakatsuji and M. Ehara. "Iterative CI general singles and doubles (ICIGSD) method for calculating the exact wave functions of the ground and excited states of molecules." *J. Chem. Phys.* **122**, 194108 (2005).

[24] M. L. Abrams and C. D. Sherrill. "Important configurations in configuration interaction and coupled-cluster wave functions." *Chem. Phys. Lett.* **412**, 121 (2005).

[25] L. Bytautas and K. Ruedenberg. "A priori identification of configurational deadwood." *Chem. Phys.* **356**, 64 (2009).

[26] R. Roth. "Importance truncation for large-scale configuration interaction approaches." *Phys. Rev. C* **79**, 064324 (2009).

[27] F. A. Evangelista. "Adaptive multiconfigurational wave functions." *J. Chem. Phys.* **140**, 054109 (2014).

[28] P. J. Knowles. "Compressive sampling in configuration interaction wavefunctions." *Mol. Phys.* **113**, 1655 (2015).

[29] W. Liu and M. R. Hoffmann. "iCI: iterative CI toward full CI." *J. Chem. Theory Comput.* (2016).

[30] N. M. Tubman, J. Lee, T. Y. Takeshita, M. Head-Gordon, and K. B. Whaley. "A deterministic alternative to the full configuration interaction quantum Monte Carl o method." (2016).

[31] X. Assfeld, J. E. Almlöf, and D. G. Truhlar. "Degeneracy-corrected perturbation theory for electronic structure calculations." *Chem. Phys. Lett.* **241**, 438 (1995).

[32] C. Angeli and M. Persico. "Multireference perturbation CI II. Selection of the zero-order space." *Theor. Chem. Acc.* **98**, 117 (1997).

[33] H.-J. Werner and P. J. Knowles. "An efficient internally contracted multiconfiguration–reference configuration interaction method." *J. Chem. Phys.* **89**, 5803 (1988).

[34] S. R. Langhoff and E. R. Davidson. "Configuration interaction calculations on the nitrogen molecule." *Int. J. Quant. Chem.* **8**, 61 (1974).

[35] C. Li and F. A. Evangelista. "Towards numerically robust multireference theories: The driven similarity renormalization group truncated to one-and two-body operators." *arXiv preprint arXiv:1602.05667* (2016).

[36] J. Hachmann, J. J. Dorando, M. Avilés, and G. K.-L. Chan. "The radical character of the acenes: A density matrix renormalization group study." *J. Chem. Phys.* **127**, 134309 (2007).

[37] B. Hajgató, D. Szieberth, P. Geerlings, F. De Proft, and M. Deleuze. "A benchmark theoretical study of the electronic ground state and of the singlet-triplet split of benzene and linear acenes." *J. Chem. Phys.* **131**, 224321 (2009).

[38] B. Hajgató, M. Huzak, and M. S. Deleuze. "Focal point analysis of the singlet–triplet energy gap of octacene and larger acenes." *J. Phys. Chem. A* **115**, 9282 (2011).

[39] W. Mizukami, Y. Kurashige, and T. Yanai. "More π electrons make a difference: Emergence of many radicals on graphene nanoribbons studied by ab initio DMRG theory." *J. Chem. Theory Comput.* **9**, 401 (2012).

[40] P. Rivero, C. A. Jiménez-Hoyos, and G. E. Scuseria. "Entanglement and polyradical character of polycyclic aromatic hydrocarbons predicted by projected Hartree–Fock theory." *J. Phys. Chem. B* **117**, 12750 (2013).

[41] C. U. Ibeji and D. Ghosh. "Singlet–triplet gaps in polyacenes: a delicate balance between dynamic and static correlations investigated by spin–flip methods." *Phys. Chem. Chem. Phys.* **17**, 9849 (2015).

[42] J. Fosso-Tande, D. R. Nascimento, and A. E. DePrince III. "Accuracy of two-particle N-representability conditions for describing different spin states and the singlet–triplet gap in the linear acene series." *Mol. Phys.* **114**, 1 (2015).

[43] G. Gidofalvi and D. A. Mazziotti. "Active-space two-electron reduced-density-matrix method: Complete active-space calculations without diagonalization of the N-electron Hamiltonian." *J. Chem. Phys.* **129**, 134108 (2008).

[44] D. A. Mazziotti. "Large-scale semidefinite programming for many-electron quantum mechanics." *Phys. Rev. Lett.* **106**, 083001 (2011).

[45] P. Stampfuß and W. Wenzel. "Improved implementation and application of the individually selecting configuration interaction method." *J. Chem. Phys.* **122**, 024110 (2005).

[46] G. Moritz, B. A. Hess, and M. Reiher. "Convergence behavior of the density-matrix renormalization group algorithm for optimized orbital orderings." *J. Chem. Phys.* **122**, 024107 (2005).

[47] Forte, a suite of quantum chemistry methods for strongly correlated electrons. For the current version, see https://github.com/evangelistalab/forte (2015).

[48] J. M. Turney, A. C. Simmonett, R. M. Parrish, E. G. Hohenstein, F. A. Evangelista, J. T. Fermann, B. J. Mintz, L. A. Burns, J. J. Wilke, M. L. Abrams, *et al.*. "Psi4: an open-source ab initio electronic structure program." *WIREs: Comp. Mol. Sci.* **2**, 556 (2012).

Chapter 3

ACI for Computing Challenging Excited States

3.1 Introduction

Perhaps the biggest difficulty in modeling electronic excited states is in quantifying varying degrees of dynamic and static electron correlation equally well among states of different character. This challenge is exacerbated, for example, in multielectron excited states, which frequently occur in chemically relevant systems containing transition metals or highly conjugated hydrocarbons.[1–3] Conventional excited-state electronic structure methods, including time-dependent density functional theory (TD-DFT)[4,5] and the equation-of-motion coupled cluster hierarchy,[6,7] often cannot efficiently compute multielectron excited states due to their considerable multireference character in which double or higher excitations dominate. Another example of challenging excited states are avoided crossings and conical intersections, which play a fundamental role in non-radiative processes.[8–10] In these cases, two or more electronic states with potentially different character become degenerate or near-degenerate, a situation that is difficult to describe with single-reference methods and state-specific multireference approaches, especially when the states involved are the ground- and first-excited state. In this work, we generalize our previously developed adaptive configuration interaction (ACI),[11] which is very well-suited for treating large numbers of strongly correlated electrons, to the general description of excited states, including multielectron and near-degenerate states.

In order to describe electronic states in which static correlation plays a dominant role, a multireference method is typically required. The most common choice is to build a multideterminantal reference wave function by permuting a chosen number of electrons in a set of selected active orbitals. While these complete active space (CAS) wave functions, with (CASSCF) or without (CASCI) orbital optimization, are good references for excited state computations, the number of variational parameters in CASCI wave functions grows combinatorially with the number of electrons and orbitals and quickly becomes prohibitive. Therefore, efficient alternatives to CASCI are required to describe the excitations of large, chemically-relevant molecular systems.

Wave function factorization techniques,[12–18] stochastic approaches,[19–28] symmetry projection schemes,[29–35] and various truncated configuration interaction (CI) methods[11,36–56] have risen as the most economical, near-exact representations of compressed full CI (FCI) or CASCI wave functions. Moreover, these techniques have allowed accurate descriptions of unprecedentedly large systems with significant multireference character by finding an efficient, sub-combinatorial scaling of the number of parameters with respect to the size of the active space. The density matrix renormalization group (DMRG)[12–18] and full CI quantum Monte Carlo (FCIQMC)[20,22] have been particularly successful in describing the ground states of large systems by correlating to near exactness active spaces beyond the conventional CAS limit of 18 electrons in 18 orbitals [CAS(18e,18o)].

In general, effective FCI and CASCI alternatives achieve sub-exponential scaling of the number of variational parameters with respect to the active space by neglecting or approximating the typically large number of unimportant terms in the full determinantal expansion. For molecular systems characterized by weakly and strongly correlated electrons alike, ground state wave functions can often be constructed using orders of magnitude fewer determinants than in FCI, a point rigorously demonstrated in decades of selected CI research,[36–44,57–60] including a recent revival of those techniques.[11,24,46–56,61,62] In order for selected CI methods to be viable for excited state computations, a similar sparsity must

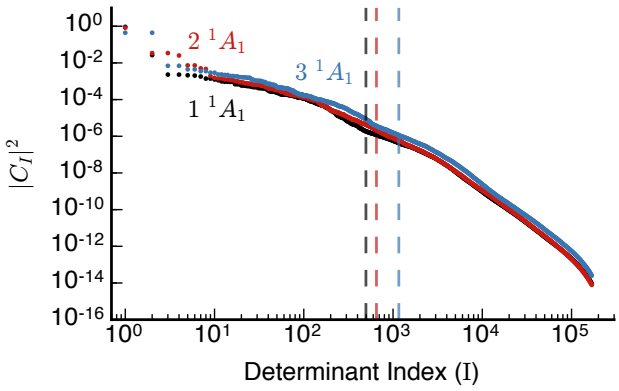

Figure 3.1: Squared expansion coefficients computed from full CI wave functions of the three lowest singlets of methylene. The DZ basis was used without freezing orbitals, resulting in a CAS(8e,14o) and 239,259 determinants. The squared coefficients are sorted by magnitude, and vertical lines represent where the accumulation of squared coefficients reaches 0.999 for each state.

be present in excited state wave functions, and we believe this to be generally true.

In Figure 3.1, we plot the square of the CI expansion coefficients, sorted, for all $239,259$ determinants in the FCI wave function for the three lowest singlet A_1 states of methylene. Additionally, we show vertical lines representing the number of determinants needed to capture 99.9% of the exact wave function for each state. While the excited state wave functions are slightly less sparse, even for the 3^1A_1 state less than 0.5% of the determinants are required to reach the 99.9% threshold.

Even with sparsity in excited state wave functions, the application of DMRG, FCIQMC, and selected CI to excited states is not straightforward, however.[18,21,26,37,45,63–69] For these methods, excited states can be computed either *sequentially* or *simultaneously*. For states computed sequentially, orthogonalization between individually computed states needs to be addressed. In DMRG, for example, the renormalized basis states are in general not optimal for multiple roots, and can be sequentially optimized for each root in a state-specific scheme. Recently introduced alternatives include derivations of Tamm-Dancoff (TDA) or random phase approximations (RPA) from a DMRG matrix product state reference,[65] in addition to time-dependent formalisms.[70] For FCIQMC, state-specific algorithms can

be achieved by using a Gaussian projector shifted near the energy of the desired root,[66] or by projecting out all previously computed lower roots from the solution of the current root.[68,71,72] However, near-degenerate electronic states can pose a significant challenge for state-specific methods, and typically an excited state method that computes states simultaneously is required.

Alternatively, methods that compute states simultaneously usually incorporate some form of state-averaging, in which a common basis is used to describe multiple states. In DMRG, this averaging is realized by renormalizing basis states with respect to multiple roots, though this procedure generally requires more basis states to achieve accuracy comparable with ground state DMRG calculations.[63] Coe and Patterson introduced a modified Monte Carlo CI (MCCI), which stochastically samples Hilbert space by selecting determinants based on a criterion averaged over roots of interests, and then forms and diagonalizes a matrix within the selected space.[73] Blunt *et al.* recently proposed a modified FCIQMC method in which all states are computed simultaneously, and orthogonalized with a Graham-Schmidt procedure at each iteration.[68] Finally, Rodríguez-Guzmán and coworkers presented a method in which ground and excited states are expanded in terms of nonorthogonal variationally-optimized symmetry-projected configurations.[74]

Another method well-suited to accurately describe very large excited states is the variational 2RDM (v-2RDM) method,[75–80] which forgoes wave functions entirely and directly optimizes the one and two-particle reduced density matrices subjected to N-representability conditions. The v-2RDM method can treat the lowest energy state of a given symmetry and total spin with high accuracy,[80,81] and its ability to compute excited states of the same symmetry based on the equations of motion of the 1-RDM has also been recently reported.[82]

Two of the most commonly used selected CI methods, CIPSI[37] and MRD-CI,[38,83] both have been modified to compute excited states using a single space of selected determinants.[39,60,84,85] Though the definition of the selection importance criterion is different for each method, both add determinants to the model space based on the maximum value of

the selection criterion with respect to all electronic states. This approach is equivalent to adding determinants to the model space that are important to at least one state being studied. While the success of both methods has prompted numerous excited state studies,[86–92] [See Ref. 93 and references therein] there has been a lack of comparison of numerical results to determine the most effective way to compute excited states with selected CI methods.

In this work, we provide a detailed analysis of both simultaneous and sequential ACI methods for computing excited state wave functions. Although our analysis is focused on ACI, our comparisons of various excited state methods is applicable to selected CI methods in general. One of the hallmark features of ACI is its ability to compute ground state energies to a user-defined accuracy.[11] Similar in spirit to the recently proposed variance-matching variational Monte Carlo method of Robinson and Neuscamman,[94] which computes all states to a similar quality as monitored by the wave function's energy variance, we seek an adaptation of ACI such that any excited state energy can be efficiently computed with a specifiable error. As shown in this work, ACI can be generalized to compute excitation energies with state-specific error control and near perfect error cancellation.

3.2 Theory

3.2.1 Brief review of ground-state ACI

We begin with a brief overview of ACI.[11] ACI is an iterative selected CI method which generates and optimal space of Slater determinants such that the total error in the ground state energy approximately matches a user defined parameter, σ:

$$|E_0^{\mathrm{FCI}} - E_0^{\mathrm{ACI}}(\sigma)| \approx \sigma, \tag{3.1}$$

where E_0^{FCI} and E_0^{ACI} are the FCI and ACI ground state energies, respectively. The procedure is as follows:

1. At iteration k, we define a reference space, $P^{(k)} = \{\Phi_\mu\}$, and associated reference

wave function,

$$\Psi_P^{(k)} = \sum_{\mu \in P^{(k)}} c_\mu^{(k)} \Phi_\mu, \tag{3.2}$$

where expansion coefficients $c_\mu^{(k)}$ are obtained by diagonalizing the Hamiltonian in the $P^{(k)}$ space. The procedure is started with a reference space, $P^{(0)}$, comprised of all determinants in a small CASCI (< 1000 determinants).

2. All singly and doubly excited determinants are generated from $P^{(k)}$ to form the first order interacting space, $F^{(k)}$. An estimate of the energy contribution to the reference space, $\varepsilon(\Phi_I)$, is computed for each determinant $\Phi_I \in F^{(k)}$. This energy importance measure is defined as the variational correlation energy of a two-state system involving $\Psi_P^{(k)}$ and Φ_I, and takes the form,[95]

$$\varepsilon(\Phi_I) = \frac{1}{2}\left(\Delta_I - \sqrt{\Delta_I^2 + 4V_I^2}\right), \tag{3.3}$$

where the Epstein–Nesbet denominator (Δ_I) and coupling (V_I) are defined as

$$\Delta_I = \langle \Psi_P^{(k)} | \hat{H} | \Psi_P^{(k)} \rangle - \langle \Phi_I | \hat{H} | \Phi_I \rangle, \tag{3.4}$$

$$V_I = \langle \Psi_P^{(k)} | \hat{H} | \Phi_I \rangle. \tag{3.5}$$

The generation of all singles and doubles has a computational cost that scales as $|F^{(k)}| \approx |P^{(k)}| N_\mathrm{O}^2 N_\mathrm{V}^2$, where $|P^{(k)}|$ is the number of determinants in the set $P^{(k)}$, while N_O and N_V are the number of occupied and virtual orbitals, respectively. The quantity V_I is computed as

$$V_I = \sum_{\mu \in P^{(k)}} c_\mu^{(k)} \langle \Phi_\mu | \hat{H} | \Phi_I \rangle, \tag{3.6}$$

by an algorithm that generates all single and double excitations out of the determinants in $P^{(k)}$. To reduce the memory necessary to store the vector V_I, we apply screening and store only those elements for which one of the contributions $|c_\mu^{(k)} \langle \Phi_\mu | \hat{H} | \Phi_I \rangle| > \tau_V$, where τ_V is a user-specified screening threshold. Unless otherwise noted, calculations reported in this work use a screening threshold $\tau_V = 10^{-12}\ E_\mathrm{h}$.

3. We define the secondary space, $Q^{(k)}$, as the smallest possible subset of $F^{(k)}$ such that the accumulation of error estimates for sampled determinants not in $Q^{(k)}$ is approximately equal to σ, the energy selection parameter. In practice, this truncation of $F^{(k)}$ is performed by accumulating the $\varepsilon(\Phi_I)$ estimates in increasing order until σ is reached,

$$\sum_{\Phi_I \in F^{(k)} \setminus Q^{(k)}} |\varepsilon(\Phi_I)| \leq \sigma. \tag{3.7}$$

The total model space $M^{(k)}$ is then defined as the union of the secondary space and the reference,

$$M^{(k)} = Q^{(k)} \cup P^{(k)}. \tag{3.8}$$

In our current implementation, this step has a computational cost that scales as $|F^{(k)}| \ln |F^{(k)}|$ due to sorting of the error estimates $|\varepsilon(\Phi_I)|$. In principle, sorting can be avoided by using an optimization algorithm that identifies an error threshold η such that the difference between σ and the sum of the error estimates $|\varepsilon(\Phi_I)|$ for the determinants with $|\varepsilon(\Phi_I)| < \eta$ is zero. This can be achieved by introducing a function $f(\eta)$,

$$f(\eta) = \sum_{\Phi_I \in F^{(k)}} |\varepsilon(\Phi_I)| \theta(\eta - |\varepsilon(\Phi_I)|) - \sigma, \tag{3.9}$$

and seeking the largest η such that $f(\eta) \leq 0$. The function $f(\eta)$ is monotonous (albeit not continuous) and has one zero if $\sigma \leq \sum_{\Phi_I \in F^{(k)}} |\varepsilon(\Phi_I)|$ (otherwise, all determinants should be included). Therefore, η may be found by using the bisection method with cost proportional to $|F^{(k)}|$.

4. The Hamiltonian is formed and diagonalized in the model space, $M^{(k)}$, yielding a total energy $E_M^{(k)}$ and wave function,

$$|\Psi_M^{(k)}\rangle = \sum_{\Phi_I \in M^{(k)}} C_I^{(k)} |\Phi_I\rangle . \tag{3.10}$$

The procedure ends when $E_M^{(k)}$ converges, which occurs when the determinantal

makeup of $M^{(k)}$ is identical between iterations [$M^{(k)} = M^{(k+1)}$]. This diagonalization is usually the most expensive step in the ACI procedure and has a cost between $|M^{(k)}|$ and $|M^{(k)}|N_O^2 N_V^2$.

5. If the energy is not converged, the updated reference $P^{(k+1)}$ space is generated from the most important subset of the $M^{(k)}$ space. Specifically, $P^{(k+1)}$ is formed by storing determinants in $M^{(k)}$ with the largest $|C_I^{(k)}|^2$ values, until the accumulation of the $|C_I^{(k)}|^2$ values of determinants kept reaches a second user-defined value,

$$\sum_{\Phi_\mu \in P^{(k+1)}} |C_\mu^{(k)}|^2 \leq 1 - \gamma\sigma, \tag{3.11}$$

where γ is a user-specified constant with units (energy)$^{-1}$. Following our previous work,[11] we set $\gamma = 1\ E_\mathrm{h}^{-1}$. This step requires sorting of the determinant coefficients and scales as $|M^{(k)}| \ln |M^{(k)}|$. However, as noted above, sorting may also be avoided in this step. Analogous to the initiator approximation in FCIQMC,[22] this step greatly increases the efficiency of ACI by only allowing determinants important in the model space to generate candidate determinants in $F^{(k)}$.

The aimed selection strategy gives the user nearly perfect control over the error for ground state calculations. This control is achieved in step 3 by accurately identifying determinants that need to be explicitly treated in the diagonalization procedure and ignoring those determinants whose cumulative energy contribution is smaller than the desired error. Another recently proposed selected CI method, heat-bath CI (HCI),[52,62] uses a very similar algorithm to ACI with the important exception that its generation of the model space is done without sampling any unselected determinants. Specifically, it selects determinants individually using a threshold ε_1, only adding a determinant Φ_I to the model space for which the inequality,

$$|H_{IJ} c_J| > \varepsilon_1 \quad \forall \Phi_J \in P^{(k)}, \tag{3.12}$$

holds. Sorting of the integrals allows the selection of determinants to be done with perfect efficiency, meaning that no determinants are sampled that are not added to the model space. Additionally, HCI continually grows the model space, so that at iteration $k+1$ all the model space determinants are retained,

$$P^{(k+1)} = M^{(k)}, \tag{3.13}$$

rather than truncating it as is done with ACI. The resulting method is extremely efficient, but does not provide an inherent means of estimating the total energy error. The predictive control over the error in ACI relies on a fairly complete sampling of unselected determinants, and a potentially fruitful development in ACI would be to somehow adopt the heat-bath sampling method while still preserving the predictive power of the current method. In the following section, we generalize the ground state ACI method to determinant spaces capable of describing excited state wave functions.

3.2.2 Excited State Methods in ACI

In principle, excited state wave functions can be obtained nearly automatically by solving for the lowest eigenvalues of the Hamiltonian in the ground state determinant space (M_0) optimized by ACI. However, the determinant set M_0 is biased towards the ground state and provides no way to control the accuracy of higher eigenvalues. One solution is a state-averaged (SA) approach in which the definition of the selection importance criterion, $\varepsilon(\Phi_I)$, is modified to reflect importance with respect to multiple roots, resulting in a single space of determinants capable of describing all roots of interest. Alternatively, an algorithm may be preferred wherein determinant selection is done separately for each root, allowing each state to be described by potentially unique determinant spaces. We expand upon both approaches below.

For all methods considered, we generalize our definition of the energy importance criterion, $\varepsilon(\Phi_I)$, to apply to any arbitrary state n,

$$\varepsilon(\Phi_I, n) = \frac{1}{2}\left(\Delta_{I,n} - \sqrt{\Delta_{I,n}^2 + 4V_{I,n}^2}\right), \tag{3.14}$$

where,

$$\Delta_{I,n} = \langle \Psi^{(k)}_{P,n} | \hat{H} | \Psi^{(k)}_{P,n} \rangle - \langle \Phi_I | \hat{H} | \Phi_I \rangle , \tag{3.15}$$

$$V_{I,n} = \langle \Psi^{(k)}_{P,n} | \hat{H} | \Phi_I \rangle , \tag{3.16}$$

and $|\Psi^{(k)}_{P,n}\rangle$ refers to the n-th eigenstate of the $P^{(k)}$ space. For converged wave functions, the (k) superscript will be dropped.

By combining different definitions of selection criteria and model spaces, it is possible to formulate several excited state methods. In this work we consider five excited state ACI methods, which, for convenience are summarized in Table 3.1. We separate these approaches into two categories: methods that use a single model space for all states, and methods that use or combine different model spaces. What follows is a detailed description of each excited state method.

State-averaged methods based on a single model space

The goal of a state-averaged ACI (SA-ACI) procedure is to obtain a single compact space of determinants capable of describing multiple electronic states with controlled accuracy. Algorithmically, the only difference in SA-ACI compared to the ground state algorithm is the definition of the energy importance criterion, $\varepsilon(\Phi_I, n)$, where we propose two ways to define a determinant's importance in lowering the energy of multiple states. One option is to simply take the average importance of a determinant ($|\varepsilon(\Phi_I, n)|$) among N roots of interest,

$$\bar{\varepsilon}(\Phi_I) = \frac{1}{N} \sum_{n=0}^{N-1} |\varepsilon(\Phi_I, n)|. \tag{3.17}$$

In addition, the reference space is updated by selecting determinants based on an average of the expansion coefficient,

$$\sum_{\Phi_\mu \in P^{(k+1)}} \left(\frac{1}{N} \sum_{n=0}^{N-1} |C_{\mu,n}|^2 \right) \leq 1 - \gamma\sigma, \tag{3.18}$$

where $C_{\mu,n}$ is the CI coefficient from root n corresponding to the reference space determinant Φ_μ.

This averaged procedure, denoted SA-ACI$_{\text{avg}}$, only requires one optimization to obtain multiple roots, which are rigorously orthogonal as they are eigenvectors of a common Hamiltonian. However, the near-exact energy control in ground state ACI is exchanged for a control over the average error among roots.

The loss of state-specific error control may become potentially hazardous if one state has a significantly different determinantal makeup with respect to the other computed roots, where the optimized space will become biased towards those roots described by similar determinants. This biasing can be remedied either by adding user-specified weights to each state, or by defining the selection importance criterion as a maximum function rather than an average. Specifically, we can redefine $\bar{\varepsilon}(\Phi_I)$ as,

$$\bar{\varepsilon}(\Phi_I) = \max_{0 \leq n \leq N-1} |\varepsilon(\Phi_I, n)|, \tag{3.19}$$

and similarly the maximum of the expansion coefficient among roots is then used to truncate the model space M to update the reference. This procedure, denoted as SA-ACI$_{\text{max}}$, will build a final model space of determinants which are important to *at least* one root of interest rather than all to roots of interest in averaged way.

Methods based on state-specific model spaces

Perhaps the most attractive feature of ground state ACI is that the error is predicted by σ to remarkable accuracy. SA-ACI methods achieve this in an averaged way because all states are computed with the same set of determinants. To better preserve error prediction in higher roots, we propose a second class of ACI methods which form separate model spaces M_n with corresponding wave functions Ψ_{M_n} for each root n of interest, a procedure we define as unconstrained ACI. Unfortunately, the model space wave functions, Ψ_{M_n}, are in general not mutually orthogonal when optimized separately. In fact, the degree of nonorthogonality between states can be viewed as a measure of the inaccuracy of individually optimized wave functions, since all states become orthogonal in the FCI limit ($\sigma \to 0$). We propose three methods which attempt to preserve state-wise energy control

while maintaining orthogonality among roots.

Two of the following methods begin with an unconstrained ACI calculation, yielding separate determinant spaces for each root. In order to correctly converge each state to the right solution, a reasonable initial guess is required. To achieve correct convergence to each root, we start each computation with three or four warmup iterations of SA-ACI, select the desired root, and then optimize it individually. To avoid the possibility of root flipping, we do all optimizations within a root-following scheme

State Combined ACI. The N non-orthogonal states are first optimized separately with unconstrained ACI to produce a set of converged model spaces $\{M_n\}$, with which we can define a final model space M_{SC} as the union of all individually selected spaces,

$$M_{\mathrm{SC}} = M_0 \cup M_1 \cup \cdots \cup M_{N-1}. \tag{3.20}$$

Finally, the matrix representation of the Hamiltonian in the M_{SC} space can be diagonalized to yield orthogonal eigenstates for the N roots. This state-combined procedure (SC-ACI) can also be viewed as a more rigorous way to remove any determinant space biasing in SA-ACI$_{\mathrm{avg}}$. While the energy errors derived from the individually converged model subspaces $\{M_n\}$ are well controlled by σ, the final energies computed from the final model space M_{SC} may not be. Since this final model space will have more determinants than any individually optimized space (unless all spaces M_n are identical), then the energies of the final model space will be lower than their individually optimized counterparts. This energy lowering effect should not be considered entirely a good consequence, as the lowering may be inconsistent among roots, resulting in poorer error cancellation. Nonetheless, σ remains an approximate upper bound to the expected error for each state.

Multistate ACI. Another approach to overcome the nonorthogonality problem in unconstrained ACI is to simply recouple the nonorthogonal solutions to yield a multistate ACI (MS-ACI). Specifically, we form the multi-state Hamiltonian in the basis of individually optimized states, and then solve the resulting generalized eigenvalue problem for N

Table 3.1: Comparison of excited state ACI methods.

Method	Energy importance criterion	Model space
SA-ACI$_{\text{avg}}$	$\frac{1}{N+1}\sum_{n=0}^{N}\varepsilon(\Phi_I,n)$	Single average space (M_{avg})
SA-ACI$_{\text{max}}$	$\max_{0\le n\le N}\varepsilon(\Phi_I,n)$	Single average space (M_{max})
SC-ACI	$\varepsilon(\Phi_I,n)$	Union of individual model spaces ($M_{\text{SC}}=\bigcup_n M_n$)
MS-ACI	$\varepsilon(\Phi_I,n)$	Union of individual model spaces ($M_{\text{MS}}=\bigcup_n M_n$)
OC-ACI	$\varepsilon(\Phi_I,n)$	Different spaces per state ($M_0\subseteq M_1\subseteq M_2\ldots$)

roots,

$$\mathbf{HC}=\mathbf{SCE}, \tag{3.21}$$

where the Hamiltonian ($\mathbf{H}$) and overlap ($\mathbf{S}$) matrices are defined as

$$(\mathbf{H})_{mn}=\langle\Psi_{M_m}|\hat{H}|\Psi_{M_n}\rangle \quad m,n=0,\ldots,N-1, \tag{3.22}$$

and

$$(\mathbf{S})_{mn}=\langle\Psi_{M_m}|\Psi_{M_n}\rangle \quad m,n=0,\ldots,N-1, \tag{3.23}$$

while $\mathbf{E}=\text{diag}(E_0,\ldots,E_{N-1})$ is a diagonal matrix. Though simple, this approach is vulnerable to numerical instability when the eigenvalues of the overlap matrix, $\mathbf{S}$, are nearly zero, corresponding to near linear-dependencies in the basis of individually optimized states. Near-degenerate electronic states may also pose a significant challenge for the initial computation of nonorthogonal wave functions, however, and issues in correctly identifying the root to be optimized and root-flipping could preclude the use of an ACI method. Additionally, nonorthogonal wave functions create difficulties for certain properties and computations that require multiple wave functions, such as transition dipole moments.

Orthogonality-constrained ACI. The final excited state method, orthogonality constrained ACI (OC-ACI), sequentially optimizes determinant spaces M_n in the orthogonal complement of the space spanned by the previous roots. This strategy has been success-

fully applied in the context of density functional theory to obtain both valence[96] and core-excited states.[97] In this procedure, the selection and screening for $P^{(k)}$ and $M^{(k)}$ spaces is identical to the unconstrained ACI, but the computation of the energies and wave functions for these spaces differs.

Specifically, in the optimization of the n-th root, we define the projector onto the space complementary to the first $n-1$ roots ($\hat{\mathscr{Q}}_{M,n}$)

$$\hat{\mathscr{Q}}_{M,n} = 1 - \sum_{m=0}^{n-1} |\Psi_{M,m}\rangle \langle \Psi_{M,m}| , \tag{3.24}$$

where $|\Psi_{M,m}\rangle$ is the optimized wave function for root m computed from the M_m model space. Thus, this projector makes the n-th root orthogonal to all $n-1$ roots in the intersection of their subspaces.

At each iteration, the $P^{(k)}$ and $M^{(k)}$ space wave functions are computed by projecting out the converged wave functions of the previous roots,

$$\hat{\mathscr{Q}}_{M,n}\hat{H}\hat{\mathscr{Q}}_{M,n} |\Psi_{P^{(k)},n}\rangle = E_{P,n} |\Psi_{P^{(k)},n}\rangle \tag{3.25}$$

$$\hat{\mathscr{Q}}_{M,n}\hat{H}\hat{\mathscr{Q}}_{M,n} |\Psi_{M^{(k)},n}\rangle = E_{M,n} |\Psi_{M^{(k)},n}\rangle , \tag{3.26}$$

where the lowest eigenstate of this projected Hamiltonian yields the desired excited state wave function. Note that this procedure is equivalent to the Gram-Schmidt orthogonalization of an excited state wave function with respect to lower roots, with the requirement that the Gram-Schmidt orthogonalized remains variationally optimal. In practice, Eqs. (3.25)-(3.26) are implemented by projecting out eigenvectors for the first $n-1$ roots from the trial vectors in the Davidson–Liu algorithm.[98,99]

The excited state ACI methods are all developed in the freely available open-source software, FORTE,[100] written as a plugin to PSI4.[101,102]

3.3 Results and Discussion

3.3.1 Methylene

We compare all ACI excited state methods using benchmark data on the three lowest singlet A_1 states of methylene. These states provide a rigorous test for the various ACI excited state methods due to their different determinantal character.[103–108] The 1 $^1A_1$ state is closed-shell with a single dominant configuration, while the 2 $^1A_1$ state has considerable double excitation character and the 3 $^1A_1$ is a multi-configurational open-shell singlet biradical. The geometries used were taken from Ref. 105 and are of C_{2v} symmetry. The cc-pVDZ basis was used,[109] augmented with additional *s* functions for both the carbon and hydrogen atoms, as outlined in Ref. 105, and no orbitals were frozen, resulting in a FCI space equivalent to a CAS(8e,27o).

In the limit $\sigma \to 0$, all ACI methods are equivalent to FCI. However, the rates at which each method converges to FCI as σ is reduced will likely be different, as each method uses a different selection algorithm. Table 3.2 shows the error in excitation energy for the two excited states studied computed with conventional CI truncated to double (SD), triple (SDT), and quadruple (SDTQ) excitations, equation of motion coupled cluster with singles and doubles (EOM-CCSD),[110] approximate coupled cluster with triples (CC3),[111] and excited-state ACI methods. For CI and CC methods, the computed 2 $^1A_1$ excitation energy converges to the correct result much faster than for the 2 $^1A_1$ vertical excitation energy. This result is well understood considering that the 3 $^1A_1$ state, though a multireference open-shell singlet, is most significantly composed of determinants with excitation rank up to triples. For the 2 $^1A_1$ state, however, higher excitations are required, and the inclusion of triples in CC methods is required even to achieve sub-eV accuracy.

For the ACI methods, this trend does not hold—the 2 $^1A_1$ state is more easily described than is the 3 $^1A_1$ state, and only slightly. Regardless of excitation rank, the 2 $^1A_1$ state is largely dominated by a single determinant, so the ACI methods converge very quickly to

Table 3.2: Methylene vertical excitation energies (eV) obtained with truncated CI, EOM-CCSD, CC3, and ACI methods. All computations use restricted Hartree–Fock orbitals and the modified cc-pVDZ basis described in Ref. 105 with no frozen orbitals, resulting in a CAS(8e,27o).

All values shown are errors with respect to FCI, for which the excitation energy is instead shown.

	Number of variational	Excitation Energy Error (eV)	
Method	parameters (N_p)	$2\ ^1A_1$	$3\ ^1A_1$
CISD	3,607	2.639	1.990
CISDT	83,689	1.113	0.035
CISDTQ	1,020,759	0.046	0.032
EOM-CCSD	3,607	1.456	−0.005
CC3	83,689	0.471	−0.004
	$\sigma = 0.25$ eV		
SA-ACI$_{avg}$	6279	0.056	0.220
SA-ACI$_{max}$	12684	0.021	0.095
SC-ACI	8871	0.028	0.063
MS-ACI	1513/2525/6250	−0.016	0.026
OC-ACI	1513/2059/6282	−0.007	0.008
	$\sigma = 0.054$ eV		
SA-ACI$_{avg}$	54,575	0.003	0.027
SA-ACI$_{max}$	112,563	0.002	0.015
SC-ACI	70,253	0.003	0.013
MS-ACI	23,563/24,401/47,049	< 0.001	0.008
OC-ACI	23,563/24,094/47,875	< 0.001	< 0.001
FCI	77,145,700	4.655	6.514

the FCI result for this typically challenging case. With a threshold of $\sigma = 0.054$ eV, all ACI methods produce excitation energy errors on the order of 1 *m*eV or better for the $2\ ^1A_1$ state. The $3\ ^1A_1$ excitation energy is more challenging since it is multideterminantal, and for the OC-ACI and MS-ACI methods it requires additional determinants to achieve the same level of accuracy. Among the ACI methods, the OC-ACI shows the best performance for methylene as it gives ∼1-8 meV accuracy while requiring much fewer determinants than the other methods. Even for the modest σ values shown, we see that ACI, particularly

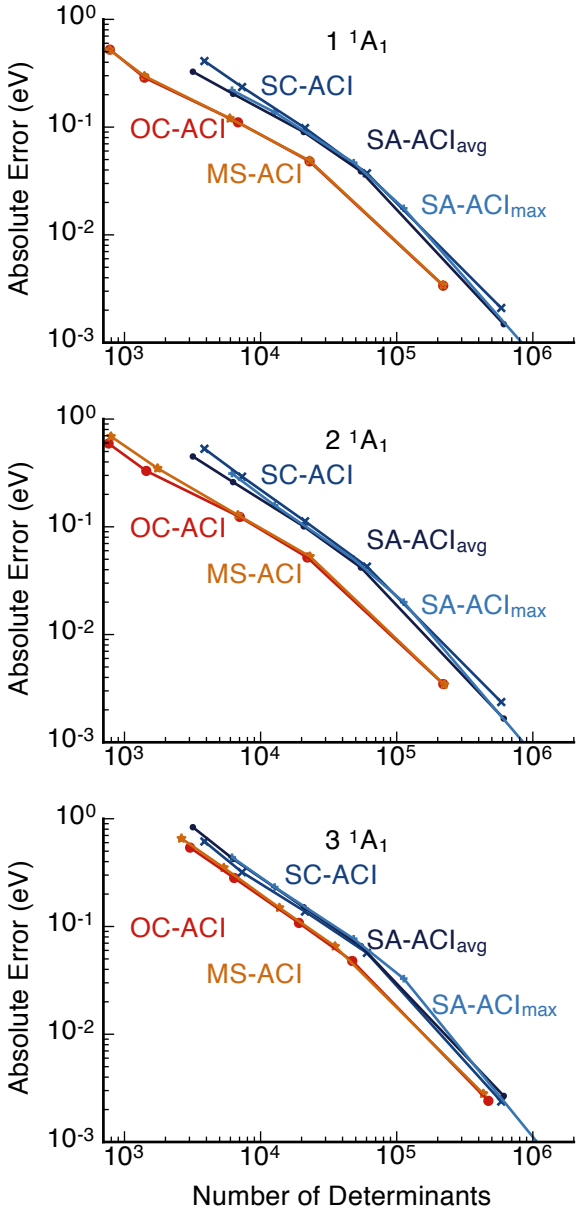

Figure 3.2: Comparison of ACI excited state methods for three electronic states of methylene. The points shown are computed for $\sigma = 0.5$, 0.25, 0.1, 0.05, and 0.005 eV. All computations used the modified cc-pVDZ basis set as described in Ref. 105 with no frozen orbitals.

OC-ACI, can compute excited state energies more accurately and efficiently than the CI and CC methods in our example.

To further understand the varying efficiencies of each ACI method, we can analyze the

absolute error of each state with respect to the required number of determinants, shown in Figure 3.2. Note that the efficiencies of SA-ACI$_{\text{avg}}$, SA-ACI$_{\text{max}}$, and SC-ACI are very similar for all three states, meaning that they produce comparable absolute errors with a similar number of determinants. In contrast, OC-ACI and MS-ACI show an improved efficiency for the 1 $^1A_1$ and 2 $^1A_1$ states. These lowest two states can be treated with fewer determinants than the 3 $^1A_1$ state to achieve a similar absolute error, but this property cannot be exploited by SA-ACI and SC-ACI as they employ a single set of determinants for all states. In general, the efficiencies of ACI methods which use a single determinant space for all states are spoiled if one of the states studied shows high multiconfigurational character. OC-ACI and MS-ACI, in contrast, optimize each state individually with as few determinants as possible, maximizing efficiency.

3.3.2 LiF avoided crossing

The avoided crossing in the dissociation potential of the two lowest $^1\Sigma^+$ states of LiF is a well-studied benchmark for excited state methods due to the presence of near-degenerate electronic states.[112–114] Near equilibrium, the ground state wave function is qualitatively single-determinantal with ionic character, and the first excited state is an open-shell biradical singlet dominated by low-weighted pairs of covalent configurations, requiring a multireference treatment. At the avoided crossing point, the ionic and covalent character swaps between these two states, thus requiring a balanced treatment of strong and weak correlation to achieve good accuracy for both states.[115,116]

All LiF computations used the Li (9s 5p)/[4s 2p]; F (9s 6p 1d)/[4s 3p 1d] basis defined in Ref. 112 and restricted Hartree–Fock orbitals with the 1s-like molecular orbitals frozen on each atom, resulting in the explicit treatment of 8 electrons in 27 orbitals. To ensure proper convergence, we use a γ value of 0.1 mE_{h}^{-1}. The FCI solution requires 7.7×10^7 determinants and predicts the avoided crossing point to be around 11.5 bohr. We compare our ACI methods to SA-MCCI,[73] which is very similar to the SA-ACI$_{\text{avg}}$ except that it

Table 3.3: Comparison of LiF avoided crossing curves. We report the average error for the lowest two Σ^+ states, the non paralellism error (NPE)[a], the standard deviation ($\sigma_{\Delta E}$) with respect to FCI, and the average number of variational parameters (N_p) required for each computation. For OC-ACI computations, the two numbers represent the average number of determinants required for ground and excited states, respectively. All values are reported in mE_h, and computed from seven bond distances from 8.5 a.u. to 14.5 a.u. incremented by 1 a.u. in order to enable comparison with PMC-SD and SA-MCCI. We do not show data for MS-ACI and SC-ACI as they diverge near the avoided crossing. All ACI computations used restricted Hartree–Fock orbitals and the custom basis set defined in Ref. 112, with the two 1s-like molecular orbitals frozen on each atom resulting in a CAS(8,27).

	Average Error (mE_h)		NPE (mE_h)			
Method	$X\ ^1\Sigma^+$	$2\ ^1\Sigma^+$	$X\ ^1\Sigma^+$	$2\ ^1\Sigma^+$	$\sigma_{\Delta E}$	N_p
CISDT	14.075	15.584	9.825	10.231	4.400	76,365
CISDTQ	1.295	1.273	1.275	1.378	0.593	978,423
SA-ACI$_{\mathrm{avg}}$(50)	42.853	48.873	13.896	21.110	7.368	488
SA-ACI$_{\mathrm{avg}}$(10)	10.243	10.052	1.262	1.314	0.437	3,341
SA-ACI$_{\mathrm{avg}}$(1)	0.891	0.830	0.089	0.109	0.047	57,798
SA-ACI$_{\mathrm{avg}}$(0.5)	0.448	0.410	0.055	0.071	0.029	95,711
OC-ACI(50)	46.185	46.150	2.845	11.205	2.234	246/261
OC-ACI(10)	10.721	9.685	1.043	1.593	0.721	1576/1929
OC-ACI(1)	0.963	0.871	0.102	0.077	0.055	37,986/38,675
OC-ACI(0.5)	0.471	0.442	0.038	0.041	0.020	65,144/67,980
[b]SA-MCCI	–	–	–	–	0.586	2734
[c]PMC-SD	1.571	1.143	1.000	2.000	0.497	5×10^6

[a] NPE is computed as the minimum error along the curve subtracted from the maximum error along the curve.
[b] Values taken from Ref. 73, N_p refers to configuration state functions.
[c] Values computed from data in Ref. 71, N_p refers to the approximate number of walkers in projector Monte Carlo simulation.

instead selects configuration state functions (CSFs) individually and stochastically. With only 2,734 CSFs, SA-MCCI yields an avoided crossing curve with a shape very similar to FCI, though shifted by roughly 5 mE_h. We also compare our results with the projector Monte Carlo method (PMC-SD), which computes excited states sequentially by projecting out lower roots in the imaginary time propagator.[71] However, they report only three decimal places for the seven points they compute, so direct comparisons we make to their results are only approximate.

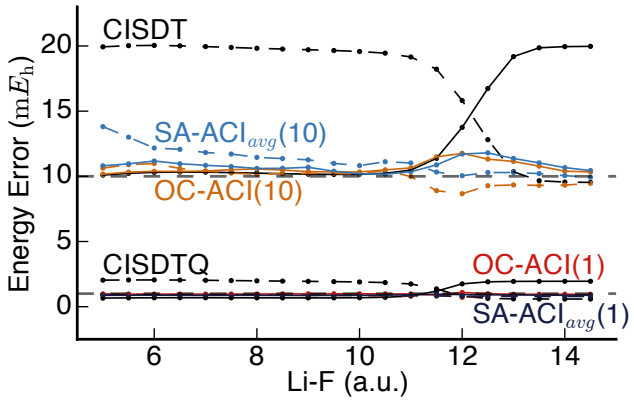

Figure 3.3: Absolute energy errors (mE_h) for the avoided crossing of LiF computed with various methods. For all ACI methods, values of $\sigma = 10$ and 1.0 mE_h are used and plotted as grey dashed lines. Solid lines represent errors in the ground $X\ ^1\Sigma^+$ state, while dashed lines represent errors in the $2\ ^1\Sigma^+$ excited state. The custom basis from Ref. 112 was used with two 1s-like molecular orbitals frozen.

As noted, the MS-ACI and SC-ACI methods require first a state-specific optimization of each root of interest. While these states are ultimately made orthogonal in both methods, the degree of nonorthogonality prior to this step can spoil the computation in a number of ways. The convergence in the state-specific optimization can lead roots to either collapse into lower ones or to form spurious admixtures of several near-degenerate roots, even if their optimization uses root-following. For SC-ACI, both issues effectively do not guarantee that a given root is properly represented in the final combined Hamiltonian. For MS-ACI, root collapse causes incurable linear dependencies in the multi-state Hamiltonian, and states with significant overlap can lead to meaningless solutions in the multi-state solution. These problems typically arise for small determinant spaces, and their threat diminishes as the individually optimized states approach the exact solution. As a result, these two methods fail in the avoided crossing region. In the following we focus only on the OC-ACI and SA-ACI$_{\text{avg}}$ methods. As shown in the previous example, the SA-ACI$_{\text{max}}$ method has an efficiency that is comparable or smaller than that of the SA-ACI$_{\text{avg}}$ scheme, therefore, we do not report results for it.

SA-ACI$_{\text{max}}$ results are not reported since this In Figure 3.3, we report absolute en-

ergy errors in mE_h for CISDT, CISDTQ, OC-ACI, and SA-ACI$_{avg}$ for $\sigma = 10$ and 1 mE_h. CISDT and CISDTQ fail to describe the multireference character of the covalent state with the same accuracy as the ionic state, while both states are described to similar accuracy in the ACI methods. For $\sigma = 10$ mE_h, the OC-ACI(10) and SA-ACI$_{avg}$(10) produce errors near 10 mE_h throughout the curve, with deviations up to about 2 mE_h near the avoided crossing point. Decreasing σ to 1 mE_h gives nearly identical results for the two ACI methods, which both consistently yield an error near the preselected value without noticeable deviations at this scale.

In Table 3.3 we report the number of variational parameters in each computation in addition to the average error of each state, the non-parallelism error (NPE) and the standard deviation ($\sigma_{\Delta E}$) of each curve with respect to FCI. The OC-ACI(10) and SA-MCCI produce an avoided crossing curve of similarly good quality using a modest number of parameters. To achieve a comparably accurate PES, PMC-SD requires each state to be computed to within 1 mE_h, while all ACI methods can produce a given $\sigma_{\Delta E}$ value by computing each state with an order of magnitude less accuracy. The systematic improvability allows the ACI methods to compute the avoided crossing with NPEs on the order of 40 μE_h.

The OC-ACI and SA-ACI$_{avg}$ give reasonably similar energy errors for all chosen σ values, but with OC-ACI requiring fewer determinants without exception. Furthermore, the OC-ACI shows consistently better NPEs for all σ values shown. This result is somewhat surprising in that the SA-ACI$_{avg}$ is very well suited for this particular problem. While the determinantal character for each state is different and swaps at the avoided crossing point, the total determinantal makeup of both states in combination remains fairly unchanged throughout dissociation. Despite the determinantal basis for the SA-ACI$_{avg}$ Hamiltonian remaining fairly constant, it still shows greater NPEs with respect to OC-ACI because it lacks the direct state-specific error control of OC-ACI.

3.3.3 Extended polyenes

The *trans*-polyene series (C_nH_{n+2}) is a set of nearly one-dimensional conjugated carbon chains, which contain numerous low-lying π-π^*excited states often with double excitation character. As the chain length increases, the energies of π bonding and anti bonding orbital pairs converge, which further enhances the strong correlation effects present in these low-lying excited states.[117–119]

In the following sections, we first compare all ACI methods with available FCI benchmarks on octatetraene to establish the capacity of each method to describe these low-lying transitions. Next, we apply the OC-ACI to a series of extended polyenes.

Comparison of Methods

To investigate the performance of each ACI method on large numbers of dense states, we studied the eight lowest singlets of octatetraene, the all-*trans* polyene with eight carbon atoms and four double bonds. The geometry was obtained from a DFT optimization at the B3LYP/cc-pVDZ level of theory using C_{2h} symmetry.[120] The ACI and CASCI computations employed a CAS(8,16) π-double active space in which all eight π electrons were correlated in sixteen π bonding and anti bonding orbitals, all within the cc-pVDZ basis. To achieve fast convergence in ACI computations, we use Pipek-Mezey split-localized orbitals[121,122] in which the active π orbitals occupied in the initial RHF reference wave function are localized separately from the active π orbitals unoccupied in the reference. Additionally, the ACI computations were performed without symmetry for better localization, though we report the results using C_{2h} labels.

The CAS(8,16) is within the scope of CASCI calculations, allowing direct comparison of absolute and excitation energies computed with ACI. Table 3.4 shows the absolute and excitation energy errors with respect to CASCI of the lowest 8 states of octatetraene for all ACI methods computed with $\sigma = 10$ and 1 mE_h. Similarly with the LiF example, the unconstrained ACI computation required for MS-ACI and SC-ACI suffered from incurable variational collapse for $\sigma = 10$ mE_h. In this case, the 2 ^1B_u state collapses into the 1 ^1B_u

Table 3.4: Comparison of excited state ACI methods for the lowest eight singlet electronic states of octatetraene (C_8H_{10}) computed with $\sigma = 1$ and 10 mE_h. All computations use split-localized orbitals, with an active space including all sixteen π orbitals defined in the cc-pVDZ basis. We report both the excitation energy errors (ΔE_{ex}) and absolute energy errors (ΔE_{abs}) with respect to FCI in mE_h.

	State								Average
	$X\ ^1A_g$	$2\ ^1A_g$	$1\ ^1B_u$	$2\ ^1B_u$	$3\ ^1A_g$	$4\ ^1A_g$	$3\ ^1B_u$	$5\ ^1A_g$	$\lvert\Delta E\rvert$
				$\Delta E_{ex}(\sigma = 10\ \text{m}E_h)$					
SA-ACI$_{avg}$		11.97	9.41	6.75	9.40	12.06	8.99	7.43	9.43
SA-ACI$_{max}$		12.96	12.13	6.12	12.69	12.52	11.76	9.93	11.16
SC-ACI		4.95	4.27	3.45	4.49	4.32	3.76	4.10	4.19
OC-ACI		−2.53	−1.85	−0.51	−0.62	−2.15	−2.20	−0.22	1.44
				$\Delta E_{ex}(\sigma = 1\ \text{m}E_h)$					
SA-ACI$_{avg}$		0.85	0.71	0.68	0.73	0.91	0.75	0.77	0.77
SA-ACI$_{max}$		0.60	0.57	0.50	0.54	0.56	0.56	0.59	0.56
SC-ACI		0.40	0.37	0.35	0.37	0.38	0.36	0.38	0.37
MS-ACI		−0.22	−0.20	−0.18	−0.18	−0.22	−0.23	−0.14	0.20
OC-ACI		−0.30	−0.24	−0.20	−0.23	−0.26	−0.27	−0.19	0.24
				$\Delta E_{abs}(\sigma = 10\ \text{m}E_h)$					
SA-ACI$_{avg}$	3.34	15.30	12.75	10.09	12.74	15.39	12.33	10.76	11.59
SA-ACI$_{max}$	3.67	16.63	15.81	9.79	16.36	16.20	15.45	13.61	13.44
SC-ACI	3.65	8.61	7.92	7.10	8.14	7.97	7.41	7.76	7.32
OC-ACI	12.66	10.13	10.81	12.15	12.04	10.51	10.46	12.44	11.40
				$\Delta E_{abs}(\sigma = 1\ \text{m}E_h)$					
SA-ACI$_{avg}$	0.26	1.12	0.98	0.95	0.99	1.17	1.02	1.04	0.94
SA-ACI$_{max}$	0.21	0.81	0.78	0.70	0.75	0.77	0.77	0.79	0.70
SC-ACI	0.19	0.59	0.56	0.54	0.56	0.57	0.55	0.57	0.52
MS-ACI	1.14	0.92	0.95	0.96	0.96	0.93	0.91	1.00	0.97
OC-ACI	1.18	0.88	0.94	0.99	0.96	0.93	0.91	1.00	0.97

state, so MS-ACI is not feasible, but we do report SC-ACI values determined from the seven roots the unconstrained ACI did converge. For $\sigma = 1$ mE_h, all correct roots were found in the unconstrained ACI.

In Table 3.4, we see that OC-ACI and MS-ACI consistently give the lowest errors in excitation energy, 0.24 and 0.20 mE_h respectively, compared to SC-ACI (0.37 mE_h), SA-ACI$_{avg}$ (0.77 mE_h) , and SA-ACI$_{max}$ (0.56 mE_h) for $\sigma = 1$ mE_h. However, SC-ACI con-

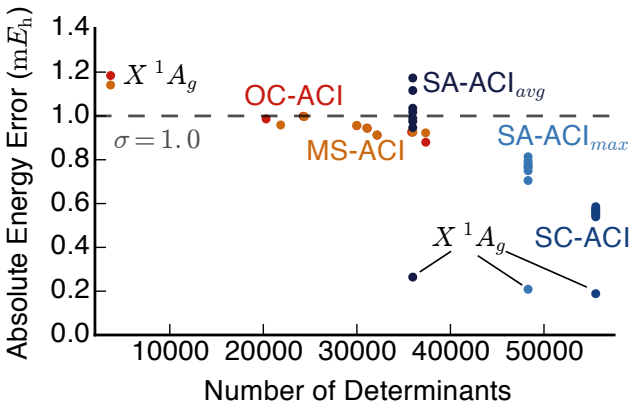

Figure 3.4: Absolute energy errors (mE_h) and number of determinants required for the lowest eight singlets of octatetraene computed with all excited state ACI methods with $\sigma = 1.0$. The ground electronic state is labeled in each calculation, while all excited states are unlabeled.

sistently gives the lowest absolute error for each state, and for many states the SA-ACI methods give lower absolute errors than do the state-specific ACI methods. Most notably, the ground state absolute energy errors for SC-ACI (0.19 mE_h), SA-ACI$_{avg}$ (0.26 mE_h), and SA-ACI$_{max}$ (0.21 mE_h) are significantly lower than the corresponding error of OC-ACI (1.18 mE_h) and MS-ACI (1.14 mE_h), which are much closer to the value predicted by σ. It is this over-stabilization of the ground state in SC-ACI and SA-ACI methods which causes the large errors in the excitation energies. In fact, OC-ACI and MS-ACI both give an average absolute energy error of 0.97 mE_h, close to $\sigma = 1.0$ mE_h, with little deviation from each state, resulting in very accurate excitation energies.

As mentioned with the previous methylene example, the state-specific ACI methods perform better for relative energies as they allow each state to be described by a different number of determinants. Figure 3.4 shows the absolute error with respect to CASCI of each of the eight states computed with all ACI excited state methods for $\sigma = 1.0$ mE_h, plotted against the required number of determinants. Note that SC-ACI, SA-ACI$_{avg}$, and SA-ACI$_{max}$ use the same number of determinants for all states, while OC-ACI and MS-ACI do not. The determinantal contributions of higher roots in the SC-ACI, SA-ACI$_{avg}$, and SA-ACI$_{max}$ methods cause the observed energy lowering in the $X\ ^1A_g^1$ ground state, while

the state-specific ACI methods give errors close to $\sigma = 1$ for all states considered, though differences in excitation energy errors are less than 1.0 mE_h at this scale. Furthermore, the state-specific ACI methods require much fewer determinants to achieve the desired accuracy and ultimately give superior tunability and error control in comparison to the state-averaged schemes.

The n-polyene series

Extended polyenes ($C_{2n}H_{2n+2}$) and their excited states serve as good models for many interesting materials and various biological chromophores, including carotenoids, due to their complex $\pi - \pi^*$ excitations. As the polyene chain length increases, excitation energies systematically decrease as doubly excited determinants become increasingly important in ground and excited state wave functions, which necessitates explicit treatment of strong correlation for their correct description.[65,119,123–128]

We use OC-ACI to describe the lowest four singlets of ($C_{2n}H_{2n+2}$) where n = 4, 6, 8, 10, and 12, with n representing the number of double bonds in the polyene. Our OC-ACI calculations are run in a π valence space, corresponding to CAS($2n, 2n$), with split-localized orbitals and $\sigma = 10$ mE_h. Optimized geometries were obtained at the B3LYP/cc-pVDZ level of theory with C_{2h} symmetry. For $n = 12$, we use a prescreening threshold value of $\tau_V = 10^{-8}$ in building the external space $F^{(k)}$ which introduces an error negligible with respect to the chosen value of $\sigma = 10$ mE_h. For these polyenes, we report the excited states with C_{2h} symmetry labels in addition to the particle/hole symmetry label in order to distinguish states characterized by ionic (+) or covalent (−) valence structures, as is done conventionally (see Ref.64 for more details). Moreover, this labeling distinguishes the $1\ ^1B_u^-$ state, which we compute, from the $1\ ^1B_u^+$ state, which we do not compute, despite being the second excited state in experimental results. We do not compute the $1\ ^1B_u^+$ state because it is largely described by $\pi - \sigma$ excitations outside of our selected active space.

Table 3.1 shows vertical excitation energies for the $2\ ^1A_g^-$, $1\ ^1B_u^-$, and $3\ ^1A_g^-$ states as computed with CASCI, OC-ACI(10), DMRG with a projected atomic orbital basis

Table 3.5: Vertical excitation energies (eV) for the polyene series ($C_{2n}H_{2n+2}$) computed with various methods. All ACI, CASCI, and DRMG methods use a CAS($2n$,$2n$), and the NOCI calculation was performed with 10 nonorthogonal determinants as described in Ref 129. The OC-ACI computation uses σ = 10 mE_h.

n	CAS	State	CASCI	OC-ACI	DMRG PAO-CASCI[64]	DMRG CASSCF[64]	NOCI[129]	CASCI-MRMP[118]
4	(8,8)	$2\,^1A_g^-$	4.97	4.96	6.33	4.69	5.09	4.26
		$1\,^1B_u^-$	6.13	6.12	7.49	5.88		5.30
		$3\,^1A_g^-$	6.82	6.86	7.95	6.60		7.20
6	(12,12)	$2\,^1A_g^-$	3.97	3.97	5.40	3.76	4.10	3.19
		$1\,^1B_u^-$	4.94	4.95	6.30	4.74		3.98
		$3\,^1A_g^-$	5.77	5.82	7.01	5.59		5.12
8	(16,16)	$2\,^1A_g^-$	3.42	3.43	4.90	3.25	3.46	2.50
		$1\,^1B_u^-$	4.18	4.18	5.60	4.03		3.10
		$3\,^1A_g^-$	4.81	4.85	6.28	4.78		3.99
10	(20,20)	$2\,^1A_g^-$		3.12	4.60	2.93	2.94	2.04
		$1\,^1B_u^-$		3.71	5.15	3.57		2.51
		$3\,^1A_g^-$		4.31	5.71	4.20		3.11
12	(24,24)	$2\,^1A_g^-$		3.04	4.42	2.73		1.70
		$1\,^1B_u^-$		3.45	4.85	3.25		2.05
		$3\,^1A_g^-$		3.89	5.31	3.78		2.45

(DMRG-PAO-CASCI),[64] DMRG with orbital opitmization (DMRG-CASSCF),[64] non-orthogonal CI (NOCI),[129] and the multireferece Møller–Plesset method with a CASCI reference (CASCI-MRMP).[118] The DMRG methods used the same active space as the OC-ACI, and CASCI-MRMP used a subset of the π valence space in a CAS(10,10) for all polyenes and subsequently correlated the remaining orbitals perturbatively.[118] Finally, the NOCI results were obtained from ten nonorthogonal basis states, the selection of which is detailed in Ref. 129. The CASCI and OC-ACI were run with identical geometries and a cc-pVDZ basis, while comparison to the DMRG methods is complicated by slightly differing geometries despite using the same basis set and geometry optimization procedure. The CASCI-MRMP and NOCI correlate orbitals outside the CAS($2n, 2n$) active space, so any agreement with those values is a direct result of the extent of active-virtual correlation.

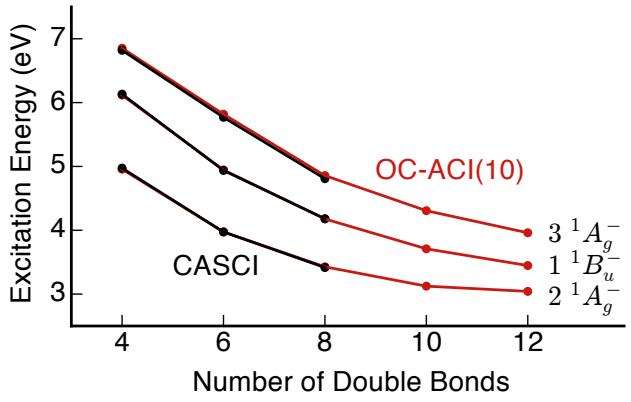

Figure 3.5: Vertical excitation energies (eV) for five polyenes computed with OC-ACI(10) and with CASCI for the first three polyenes.

For the available CASCI values, the OC-ACI(10) vertical excitations are accurate to less that 0.01 eV on average. OC-ACI(10) and DMRG-CASSCF consistently differ by about 0.2 eV, suggesting some systematic error between the two as a result of slightly different geometries. The effect of different geometries is also supported by the similar error seen between DMRG-CASSCF and CASCI, where normally it is assumed that these two methods give the same quality of result for the active spaces used. As expected, the NOCI and CASCI-MRMP vertical excitation energies are consistently smaller that ACI and DMRG results, further indicating that additional treatment of external orbitals is required—particularly for larger polyenes. Fig. 3.5 shows the decreasing excitation energies with increasing polyene length as computed by OC-ACI(10) and CASCI. Furthermore, the excellent agreement demonstrates the ability of OC-ACI to replace CASCI for computing ground and excited states with large active spaces.

3.4 Conclusions

In this study, we have detailed five methods for computing challenging excited states using the ACI formalism. These excited state methods iteratively optimize either a single space of determinants or separate determinant spaces in describing multiple electronic

states. We rigorously compared each method using challenging excited-state benchmarks characterized by strong correlation and double excitation character, including methylene excited states, the LiF avoided crossing, and many excited states of large polyenes. In these comparisons, we find that the OC-ACI method is generally the most effective and widely applicable because it shows the best error prediction and tunability while still maintaining orthogonality among solutions. We attribute its success to its flexibility; by allowing separate determinant spaces to describe each electronic state, the method can use the appropriate determinants for each state such that their preselected errors are the same. We demonstrate the ability of OC-ACI to compute large polyenes, with up to a CAS(24,24), with remarkable error cancellation, in addition to computing excited states with accuracy competitive with DMRG.

In its current form, OC-ACI is well-suited to compute excitation energies of small molecules to high accuracy. Despite its remarkable error cancellation, computations in larger basis sets including extrapolations to the complete basis limit are required for experimental predictability. For small systems, OC-ACI could be a very valuable tool in the benchmarking of excited states, where single-reference methods like CC3 currently represent the highest applied level of theory. In application to larger systems (>100 orbitals), OC-ACI and SA-ACI are most useful in generating reference wave functions which then need to be connected to theories of dynamical correlation to enable comparison to experiment. We are actively working on these extensions.

While this article was in revision, we noticed a similar study posted to the arXiv[130] in which the aforementioned HCI is adapted for excited states. This work employs an algorithm similar to SA-ACI in addition to a semi-stochastic multireference perturbation theory, all which allow the authors to accurately compute excitation energies using large basis sets.

Bibliography

[1] L. González, D. Escudero, and L. S. Andrés. "Progress and challenges in the calculation of electronic excited states." *ChemPhysChem* **13**, 28 (2012).

[2] C. Daniel. "Photochemistry and photophysics of transition metal complexes: quantum chemistry." *Coord. Chem. Rev.* **282-283**, 19 (2015).

[3] A. Dreuw and M. Head-Gordon. "Single-reference ab initio methods for the calculation of excited states of large molecules." *Chem. Rev.* **105**, 4009 (2005).

[4] E. Runge and E. K. U. Gross. "Density-functional theory for time-dependent systems." *Phys. Rev. Lett.* **52**, 997 (1984).

[5] K. Burke, J. Werschnik, and E. K. U. Gross. "Time-dependent density functional theory: Past, present, and future." *J. Chem. Phys.* **123**, 062206 (2005).

[6] J. F. Stanton and R. J. Bartlett. "The equation of motion coupled-cluster method. A systematic biorthogonal approach to molecular excitation energies, transition probabilities, and excited state properties." *J. Chem. Phys.* **98**, 7029 (1993).

[7] O. Christiansen, H. Koch, and P. Jørgensen. "The second-order approximate coupled cluster singles and doubles model CC2." *Chem. Phys. Lett.* **243**, 409 (1995).

[8] S. Matsika and P. Krause. "Nonadiabatic events and conical intersections." *Ann. Rev. Phys. Chem.* **62**, 621 (2011).

[9] L. Blancafort. "Photochemistry and photophysics at extended seams of conical intersection." *ChemPhysChem* **15**, 3166 (2014).

[10] J. P. Zobel, J. J. Nogueira, and L. González. "The IPEA dilemma in CASPT2." *Chemical Science* **8**, 1482 (2017).

[11] J. B. Schriber and F. A. Evangelista. "Communication: An adaptive configuration interaction approach for strongly correlated electrons with tunable accuracy." *J. Chem. Phys.* **144**, 161106 (2016).

[12] S. R. White and R. L. Martin. "Ab initio quantum chemistry using the density matrix renormalization group." *J. Chem. Phys.* **110**, 4127 (1999).

[13] G. K.-L. Chan and M. Head-Gordon. "Highly correlated calculations with a polynomial cost algorithm: A study of the density matrix renormalization group." *J. Chem. Phys.* **116**, 4462 (2002).

[14] G. K.-L. Chan, J. J. Dorando, D. Ghosh, J. Hachmann, E. Neuscamman, H. Wang, and T. Yanai. "An Introduction to the Density Matrix Renormalization Group Ansatz in Quantum Chemistry." In S. Wilson, P. Grout, J. Maruani, G. Delgado-Barrio, and P. Piecuch, editors, "Frontiers in Quantum Systems in Chemistry and Physics," 49–65. Springer Netherlands (2008).

[15] G. K.-L. Chan and S. Sharma. "The density matrix renormalization group in quantum chemistry." *Annu. Rev. Phys. Chem.* **62**, 465 (2011).

[16] S. Sharma and G. K.-L. Chan. "Spin-adapted density matrix renormalization group algorithms for quantum chemistry." *J. Chem. Phys.* **136**, 124121 (2012).

[17] R. Olivares-Amaya, W. Hu, N. Nakatani, S. Sharma, J. Yang, and G. K.-L. Chan. "The ab-initio density matrix renormalization group in practice." *J. Chem. Phys.* **142**, 034102 (2015).

[18] S. Sharma. "A general non-Abelian density matrix renormalization group algorithm with application to the C_2 dimer." *J. Chem. Phys.* **142**, 024107 (2015).

[19] J. C. Greer. "Estimating full configuration interaction limits from a Monte Carlo selection of the expansion space." *J. Chem. Phys.* **103**, 1821 (1995).

[20] G. H. Booth, A. J. Thom, and A. Alavi. "Fermion Monte Carlo without fixed nodes: A game of life, death, and annihilation in Slater determinant space." *J. Chem. Phys.* **131**, 054106 (2009).

[21] W. Purwanto, S. Zhang, and H. Krakauer. "Excited state calculations using phaseless auxiliary-field quantum Monte Carlo: Potential energy curves of low-lying C_2 singlet states." *J. Chem. Phys.* **130**, 094107 (2009).

[22] D. Cleland, G. H. Booth, and A. Alavi. "Communications: Survival of the fittest: Accelerating convergence in full configuration-interaction quantum Monte Carlo." *J. Chem. Phys.* **132**, 041103 (2010).

[23] J. P. Coe and M. J. Paterson. "Development of Monte Carlo configuration interaction: natural orbitals and second-order perturbation theory." *J. Chem. Phys.* **137**, 204108 (2012).

[24] E. Giner, A. Scemama, and M. Caffarel. "Using perturbatively selected configuration interaction in quantum Monte Carlo calculations." *Can. J. Chem.* **91**, 879 (2013).

[25] F. R. Petruzielo, A. A. Holmes, H. J. Changlani, M. P. Nightingale, and C. J. Umrigar. "Semistochastic projector Monte Carlo method." *Phys. Rev. Lett.* **109**, 230201 (2012).

[26] S. Ten-no. "Stochastic determination of effective Hamiltonian for the full configuration interaction solution of quasi-degenerate electronic states." *J. Chem. Phys.* **138**, 164126 (2013).

[27] G. Li Manni, S. D. Smart, and A. Alavi. "Combining the complete active space self-consistent field method and the full configuration interaction quantum monte carlo within a super-CI framework, with application to challenging metal-porphyrins." *J. Chem. Theor. Comput.* **12**, 1245 (2016).

[28] E. Giner, R. Assaraf, and J. Toulouse. "Quantum Monte Carlo with reoptimised perturbatively selected configuration-interaction wave functions." *Mol. Phys.* **114**, 910 (2016).

[29] C. A. Jiménez-Hoyos, T. M. Henderson, T. Tsuchimochi, and G. E. Scuseria. "Projected Hartree–Fock theory." *J. Chem. Phys.* **136**, 164109 (2012).

[30] C. A. Jiménez-Hoyos, R. Rodríguez-Guzmán, and G. E. Scuseria. "Multi-component symmetry-projected approach for molecular ground state correlations." *J. Chem. Phys.* **139**, 204102 (2013).

[31] K. Samanta, C. A. Jiménez-Hoyos, and G. E. Scuseria. "Exploring copper oxide cores using the projected Hartree–Fock method." *J. Chem. Theory Comput.* **8**, 4944 (2012).

[32] P. Rivero, C. A. Jiménez-Hoyos, and G. E. Scuseria. "Entanglement and polyradical character of polycyclic aromatic hydrocarbons predicted by projected Hartree–Fock theory." *J. Phys. Chem. B* **117**, 12750 (2013).

[33] M. Degroote, T. M. Henderson, J. Zhao, J. Dukelsky, and G. E. Scuseria. "Polynomial similarity transformation theory: A smooth interpolation between coupled cluster doubles and projected BCS applied to the reduced BCS Hamiltonian." *Phys. Rev. B* **93**, 125124 (2016).

[34] Y. Qiu, T. M. Henderson, and G. E. Scuseria. "Communication: Projected Hartree–Fock theory as a polynomial similarity transformation theory of single excitations." *J. Chem. Phys.* **145**, 111102 (2016).

[35] J. M. Wahlen-Strothman, T. M. Henderson, M. R. Hermes, M. Degroote, Y. Qiu, J. Zhao, J. Dukelsky, and G. E. Scuseria. "Merging symmetry projection methods with coupled cluster theory: Lessons from the Lipkin model Hamiltonian." *J. Chem. Phys.* **146**, 054110 (2017).

[36] C. F. Bender and E. R. Davidson. "Studies in configuration interaction: The first-row diatomic hydrides." *Phys. Rev.* **183**, 23 (1969).

[37] B. Huron, J. P. Malrieu, and P. Rancurel. "Iterative perturbation calculations of ground and excited state energies from multiconfigurational zeroth-order wavefunctions." *J. Chem. Phys.* **58**, 5745 (1973).

[38] R. J. Buenker and S. D. Peyerimhoff. "Individualized configuration selection in CI calculations with subsequent energy extrapolation." *Theor. Chim. Acta* **35**, 33 (1974).

[39] S. Evangelisti, J.-P. Daudey, and J. P. Malrieu. "Convergence of an improved CIPSI algorithm." *Chem. Phys.* **75**, 91 (1983).

[40] R. J. Harrison. "Approximating full configuration interaction with selected configuration interaction and perturbation theory." *J. Chem. Phys.* **94**, 5021 (1991).

[41] V. M. García, O. Castell, R. Caballol, and J. P. Malrieu. "An iterative difference-dedicated configuration interaction. Proposal and test studies." *Chem. Phys. Lett.* **238**, 222 (1995).

[42] F. Neese. "A spectroscopy oriented configuration interaction procedure." *J. Chem. Phys.* **119**, 9428 (2003).

[43] H. Nakatsuji and M. Ehara. "Iterative CI general singles and doubles (ICIGSD) method for calculating the exact wave functions of the ground and excited states of molecules." *J. Chem. Phys.* **122**, 194108 (2005).

[44] M. L. Abrams and C. D. Sherrill. "Important configurations in configuration interaction and coupled-cluster wave functions." *Chem. Phys. Lett.* **412**, 121 (2005).

[45] W. Hu and G. Chan. "Excited-state geometry optimization with the density matrix renormalization group, as applied to polyenes." *J. Chem. Theor. Comput.* **11**, 3000 (2015).

[46] L. Bytautas and K. Ruedenberg. "A priori identification of configurational deadwood." *Chem. Phys.* **356**, 64 (2009).

[47] R. Roth. "Importance truncation for large-scale configuration interaction approaches." *Phys. Rev. C* **79**, 064324 (2009).

[48] F. A. Evangelista. "Adaptive multiconfigurational wave functions." *J. Chem. Phys.* **140**, 054109 (2014).

[49] P. J. Knowles. "Compressive sampling in configuration interaction wavefunctions." *Mol. Phys.* **113**, 1655 (2015).

[50] W. Liu and M. R. Hoffmann. "iCI: Iterative CI toward full CI." *J. Chem. Theor. Comput.* **12**, 1169 (2016).

[51] N. M. Tubman, J. Lee, T. Y. Takeshita, M. Head-Gordon, and K. B. Whaley. "A deterministic alternative to the full configuration interaction quantum Monte Carlo method." *J. Chem. Phys.* **145**, 044112 (2016).

[52] A. Holmes, N. Tubman, and C. J. Umrigar. "Heat-bath configuration interaction: An efficient selected CI algorithm inspired by heat-bath sampling." *J. Chem. Theor. Comput.* **12**, 3674 (2016).

[53] T. Zhang and F. A. Evangelista. "A deterministic projector configuration interaction approach for the ground state of quantum many-body systems." *J. Chem. Theor. Comput.* **12**, 4326 (2016).

[54] J. S. Boschen, D. Theis, K. Ruedenberg, and T. L. Windus. "Correlation energy extrapolation by many-body expansion." *J. Phys. Chem. A* **121**, 836 (2017).

[55] A. D. Chien and P. M. Zimmerman. "Recovering dynamic correlation in spin flip configuration interaction through a difference dedicated approach." *J. Chem. Phys.* **146**, 014103 (2017).

[56] J. P. Coe and M. J. Paterson. "Open-shell systems investigated with Monte Carlo configuration interaction." *Int. J. Quant. Chem.* **116**, 1772 (2016).

[57] R. Cimiraglia. "Second order perturbation correction to CI energies by use of diagrammatic techniques: An improvement to the CIPSI algorithm." *J. Chem. Phys.* **83**, 1746 (1985).

[58] R. Caballol and J. P. Malrieu. "Direct selected configuration interaction using a hole-particle formalism." *Chem. Phys. Lett.* **188**, 543 (1992).

[59] M. Hanrath and B. Engels. "New algorithms for an individually selecting MR-CI program." *Chem. Phys.* **225**, 197 (1997).

[60] C. Angeli and M. Persico. "Multireference perturbation CI II. Selection of the zero-order space." *Theor. Chem. Acc.* **98**, 117 (1997).

[61] J. R. McClean and A. Aspuru-Guzik. "Compact wavefunctions from compressed imaginary time evolution." *RSC Advances* **5**, 102277 (2015).

[62] S. Sharma, A. A. Holmes, G. Jeanmairet, A. Alavi, and C. J. Umrigar. "Semistochastic heat-bath configuration interaction method: Selected configuration interaction with semistochastic perturbation theory." *J. Chem. Theory Comput.* **13**, 1595 (2017).

[63] J. J. Dorando, J. Hachmann, and G. K.-L. Chan. "Targeted excited state algorithms." *J. Chem. Phys.* **127**, 084109 (2007).

[64] D. Ghosh, J. Hachmann, T. Yanai, and G. K.-L. Chan. "Orbital optimization in the density matrix renormalization group, with applications to polyenes and β-carotene." *J. Chem. Phys.* **128**, 144117 (2008).

[65] N. Nakatani, S. Wouters, D. Van Neck, and G. K.-L. Chan. "Linear response theory for the density matrix renormalization group: Efficient algorithms for strongly correlated excited states." *J. Chem. Phys.* **140**, 024108 (2014).

[66] G. H. Booth and G. K.-L. Chan. "Communication: Excited states, dynamic correlation functions and spectral properties from full configuration interaction quantum Monte Carlo." *J. Chem. Phys.* **137**, 191102 (2012).

[67] A. Humeniuk and R. Mitrić. "Excited states from quantum Monte Carlo in the basis of Slater determinants." *J. Chem. Phys.* **141**, 194104 (2014).

[68] N. S. Blunt, S. D. Smart, G. H. Booth, and A. Alavi. "An excited-state approach within full configuration interaction quantum Monte Carlo." *J. Chem. Phys.* **143**, 134117 (2015).

[69] N. S. Blunt, A. Alavi, and G. H. Booth. "Krylov-projected quantum Monte Carlo method." *Phys. Rev. Lett.* **115**, 050603 (2015).

[70] E. Ronca, Z. Li, C. A. Jiménez-Hoyos, and G. K.-L. Chan. "Time-step targeting time-dependent and dynamical density matrix renormalization group algorithms with ab initio Hamiltonians." arXiv:1706.09537 (2017).

[71] Y. Ohtsuka and S. Nagase. "Projector Monte Carlo method based on Slater determinants: Test application to singlet excited states of H_2O and LiF." *Chem. Phys. Lett.* **485**, 367 (2010).

[72] N. S. Blunt, G. H. Booth, and A. Alavi. "Density matrices in full configuration interaction quantum Monte Carlo: Excited states, transition dipole moments, and parallel distribution." *J. Chem. Phys.* **146**, 244105 (2017).

[73] J. P. Coe and M. J. Paterson. "State-averaged Monte Carlo configuration interaction applied to electronically excited states." *J. Chem. Phys.* **139**, 154103 (2013).

[74] R. Rodríguez-Guzmán, C. A. Jiménez-Hoyos, R. Schutski, and G. E. Scuseria. "Multireference symmetry-projected variational approaches for ground and excited states of the one-dimensional Hubbard model." *Phys. Rev. B* **87**, 235129 (2013).

[75] D. A. Mazziotti. "Pursuit of n-representability for the contracted Schrödinger equation through density-matrix reconstruction." *Phys. Rev. A* **60**, 3618 (1999).

[76] D. A. Mazziotti. "First-order semidefinite programming for the direct determination of two-electron reduced density matrices with application to many-electron atoms and molecules." *J. Chem. Phys.* **121**, 10957 (2004).

[77] D. A. Mazziotti. "Variational reduced-density-matrix method using three-particle n-representability conditions with application to many-electron molecules." *Phys. Rev. A* **74**, 032501 (2006).

[78] D. A. Mazziotti. "Parametrization of the two-electron reduced density matrix for its direct calculation without the many-electron wave function." *Phys. Rev. Lett.* **101**, 253002 (2008).

[79] A. E. DePrince III and D. A. Mazziotti. "Open-shell molecular electronic states from the parametric two-electron reduced-density-matrix method." *J. Chem. Phys.* **130**, 164109 (2009).

[80] J. Fosso-Tande, D. R. Nascimento, and A. E. DePrince III. "Accuracy of two-particle n-representability conditions for describing different spin states and the singlet–triplet gap in the linear acene series." *Mol. Phys.* **114**, 423 (2016).

[81] J. Fosso-Tande, T.-S. Nguyen, G. Gidofalvi, and A. E. DePrince III. "Large-Scale Variational Two-Electron Reduced-Density-Matrix-Driven Complete Active Space Self-Consistent Field Methods." *J. Chem. Theor. Comput.* **12**, 2260 (2016).

[82] D. B. Jeffcoat and A. E. DePrince III. "N-representability-driven reconstruction of the two-electron reduced-density matrix for a real-time time-dependent electronic structure method." *J. Chem. Phys.* **141**, 214104 (2014).

[83] R. J. Buenker, R. A. Phillips, S. Krebs, H.-P. Liebermann, A. B. Alekseyev, and P. Funke. "The Wuppertal multireference configuration interaction (MRD-CI) program system." *Theor. Chem. Acc.* **133**, 1 (2014).

[84] C. Angeli, R. Cimiraglia, M. Persico, and A. Toniolo. "Multireference perturbation CI I. Extrapolation procedures with CAS or selected zero-order spaces." *Theor. Chem. Acc.* **98**, 57 (1997).

[85] S. Krebs and R. J. Buenker. "Multireference configuration interaction study of the mixed Valence–Rydberg character of the C_2H_4 1(π,π*)âĂL'V state." *J. Chem. Phys.* **106**, 7208 (1998).

[86] A. Banichevich and S. D. Peyerimhoff. "Theoretical study of the ground and excited states of ozone in its symmetric nuclear arrangement." *Chem. Phys.* **174**, 93 (1993).

[87] H. Hogreve. "The ground state geometry of the Ne^{+3} trimer." *Chem. Phys. Lett.* **215**, 72 (1993).

[88] R. C. Mawhinney, P. J. Bruna, and F. Grein. "Multireference configuration interaction studies on metastable states of the dication BN^{2+}." *J. Chem. Phys.* **103**, 8944 (1995).

[89] H. Hogreve. "Ab initio study of the dication carbon trimer C_3^{2+}." *J. Chem. Phys.* **102**, 3281 (1998).

[90] B. Mennucci, A. Toniolo, and J. Tomasi. "Ab initio study of the electronic excited states in 4-(n,n-dimethylamino) benzonitrile with inclusion of solvent effects:âĂL' the internal charge transfer process." *J. Am. Chem. Soc.* **122**, 10621 (2000).

[91] P. S. Żuchowski, R. Guerout, and O. Dulieu. "Ground- and excited-state properties of the polar and paramagnetic RbSr molecule: A comparative study." *Phys. Rev. A* **90**, 012507 (2014).

[92] M. Chaieb, H. Habli, L. Mejrissi, B. Oujia, and F. X. Gadéa. "Ab initio spectroscopic study for the NaRb molecule in ground and excited states." *Int. J. Quant. Chem.* **114**, 731 (2014).

[93] P. G. Szalay, T. Müller, G. Gidofalvi, H. Lischka, and R. Shepard. "Multiconfiguration self-consistent field and multireference configuration interaction methods and applications." *Chem. Rev.* **112**, 108 (2012).

[94] P. J. Robinson and E. Neuscamman. "Excitation variance matching with limited configuration interaction expansions in variational monte carlo." arXiv:1705.04856 (2017).

[95] X. Assfeld, J. E. Almlöf, and D. G. Truhlar. "Degeneracy-corrected perturbation theory for electronic structure calculations." *Chem. Phys. Lett.* **241**, 438 (1995).

[96] F. A. Evangelista, P. Shushkov, and J. C. Tully. "Orthogonality Constrained Density Functional Theory for Electronic Excited States." *J. Phys. Chem. A* **117**, 7378 (2013).

[97] W. D. Derricotte and F. A. Evangelista. "Simulation of X-ray absorption spectra with orthogonality constrained density functional theory." *Phys. Chem. Chem. Phys.* **17**, 14360 (2015).

[98] E. R. Davidson. "The iterative calculation of a few of the lowest eigenvalues and corresponding eigenvectors of large real-symmetric matrices." *J. Comp. Phys.* **17**, 87 (1975).

[99] B. Liu. *The simultaneous expansion for the solution of several of the lowest eigenvalues and corresponding eigenvectors of large real-symmetric matrices*. Numerical Algorithms in Chemistry: Algebraic Method (1978).

[100] Forte, a suite of quantum chemistry methods for strongly correlated electrons. For the current version, see https://github.com/evangelistalab/forte (2017).

[101] J. M. Turney, A. C. Simmonett, R. M. Parrish, E. G. Hohenstein, F. A. Evangelista, J. T. Fermann, B. J. Mintz, L. A. Burns, J. J. Wilke, M. L. Abrams, and others. "Psi4: an open-source ab initio electronic structure program." *WIREs: Comp. Mol. Sci.* **2**, 556 (2012).

[102] R. M. Parrish, L. A. Burns, D. G. A. Smith, A. C. Simmonett, A. E. DePrince III, E. G. Hohenstein, U. Bozkaya, A. Y. Sokolov, R. Di Remigio, R. M. Richard, J. F. Gonthier, A. M. James, H. R. McAlexander, A. Kumar, M. Saitow, X. Wang, B. P. Pritchard, P. Verma, H. F. Schaefer, K. Patkowski, R. A. King, E. F. Valeev, F. A. Evangelista, J. M. Turney, T. D. Crawford, and C. D. Sherrill. "Psi4 1.1: An Open-Source Electronic Structure Program Emphasizing Automation, Advanced Libraries, and Interoperability." *J. Chem. Theory Comput.* Article ASAP (2017).

[103] H. F. Schaefer. "Methylene: A paradigm for computational quantum chemistry." *Science* **231**, 1100 (1986).

[104] C. D. Sherrill, M. L. Leininger, T. J. Van Huis, and H. F. Schaefer. "Structures and vibrational frequencies in the full configuration interaction limit: Predictions for four electronic states of methylene using a triple-zeta plus double polarization (TZ2P) basis." *J. Chem. Phys.* **108**, 1040 (1998).

[105] H. Koch, O. Christiansen, P. Jørgensen, and J. Olsen. "Excitation energies of BH, CH 2 and Ne in full configuration interaction and the hierarchy CCS, CC2, CCSD and CC3 of coupled cluster models." *Chem. Phys. Lett.* **244**, 75 (1995).

[106] P. M. Zimmerman, J. Toulouse, Z. Zhang, C. B. Musgrave, and C. J. Umrigar. "Excited states of methylene from quantum Monte Carlo." *J. Chem. Phys.* **131**, 124103 (2009).

[107] P. J. Reynolds, M. Dupuis, and W. A. Lester Jr. "Quantum Monte Carlo calculation of the singlet–triplet splitting in methylene." *J. Chem. Phys.* **82**, 1983 (1985).

[108] C. D. Sherrill, T. J. Van Huis, Y. Yamaguchi, and H. F. Schaefer. "Full configuration interaction benchmarks for the X 3B1, $a\ ^1A_1$, $b\ ^1B_1$ and $c\ ^1A_1$ states of methylene." *J. Mol. Struct. (Theochem)* **400**, 139 (1997).

[109] T. H. Dunning Jr. "Gaussian basis sets for use in correlated molecular calculations. I. The atoms boron through neon and hydrogen." *J. Chem. Phys.* **90**, 1007 (1998).

[110] J. F. Stanton and R. J. Bartlett. "The equation of motion coupled-cluster method. A systematic biorthogonal approach to molecular excitation energies, transition probabilities, and excited state properties." *J. Chem. Phys.* **98**, 7029 (1998).

[111] O. Christiansen, H. Koch, and P. Jorgensen. "Response functions in the CC3 iterative triple excitation model." *J. Chem. Phys.* **103**, 7429 (1995).

[112] C. W. Bauschlicher Jr and S. R. Langhoff. "Full configuration-interaction study of the ionic–neutral curve crossing in LiF." *J. Chem. Phys.* **89**, 4246 (1988).

[113] M. Hanrath. "Multi-reference coupled-cluster study of the ionic-neutral curve crossing LiF." *Mol. Phys.* **106**, 1949 (2008).

[114] A. J. C. Varandas. "Accurate ab initio potential energy curves for the classic Li-F ionic-covalent interaction by extrapolation to the complete basis set limit and modeling of the radial nonadiabatic coupling." *J. Chem. Phys.* **131**, 124128 (2009).

[115] J. P. Malrieu, J.-L. Heully, and A. Zaitsevskii. "Multiconfigurational second-order perturbative methods: Overview and comparison of basic properties." *Theoret. Chim. Acta* **90**, 167 (1995).

[116] J. Finley, P.-Å. Malmqvist, B. O. Roos, and L. Serrano-Andrés. "The multi-state CASPT2 method." *Chem. Phys. Lett.* **288**, 299 (1998).

[117] W. Barford, R. J. Bursill, and M. Y. Lavrentiev. "Density-matrix renormalization-group calculations of excited states of linear polyenes." *Phys. Rev. B* **63**, 195108 (2001).

[118] Y. Kurashige, H. Nakano, Y. Nakao, and K. Hirao. "The π-π* excited states of long linear polyenes studied by the CASCI-MRMP method." *Chem. Phys. Lett.* **400**, 425 (2004).

[119] J. H. Starcke, M. Wormit, J. Schirmer, and A. Dreuw. "How much double excitation character do the lowest excited states of linear polyenes have?" *Chem. Phys.* **329**, 39 (2006).

[120] A. D. Becke. "Density-functional exchange-energy approximation with correct asymptotic behavior." *Phys. Rev. A* **38**, 3098 (1988).

[121] J. Pipek and P. G. Mezey. "A fast intrinsic localization procedure applicable for ab initio and semiempirical linear combination of atomic orbital wave functions." *J. Chem. Phys.* **90**, 4916 (1989).

[122] L. Bytautas, J. Ivanic, and K. Ruedenberg. "Split-localized orbitals can yield stronger configuration interaction convergence than natural orbitals." *J. Chem. Phys.* **119**, 8217 (2003).

[123] I. A. Mikhailov, S. Tafur, and A. E. Masunov. "Double excitations and state-to-state transition dipoles in π- π* excited singlet states of linear polyenes: Time-dependent density-functional theory versus multiconfigurational methods." *Phys. Rev. A* **77**, 012510 (2008).

[124] P. Tavan and K. Schulten. "Electronic excitations in finite and infinite polyenes." *Phys. Rev. B* **36**, 4337 (1987).

[125] M. Schmidt and P. Tavan. "Electronic excitations in long polyenes revisited." *J. Chem. Phys.* **136**, 124309 (2012).

[126] J. Hachmann, W. Cardoen, and G. K.-L. Chan. "Multireference correlation in long molecules with the quadratic scaling density matrix renormalization group." *J. Chem. Phys.* **125**, 144101 (2006).

[127] K. Boguslawski. "Targeting excited states in all-trans polyenes with electron-pair states." *J. Chem. Phys.* **145**, 234105 (2016).

[128] A. Y. Sokolov, S. Guo, E. Ronca, and G. K.-L. Chan. "Time-dependent N-electron valence perturbation theory with matrix product state reference wavefunctions for large active spaces and basis sets: Applications to the chromium dimer and all-transpolyenes." *J. Chem. Phys.* **146**, 244102 (2017).

[129] E. J. Sundstrom and M. Head-Gordon. "Non-orthogonal configuration interaction for the calculation of multielectron excited states." *J. Chem. Phys.* **140**, 114103 (2014).

[130] A. A. Holmes, C. J. Umrigar, and S. Sharma. "Excited states using semistochastic heat-bath configuration interaction." *arXiv preprint arXiv:1708.03456v1* (2017).

Chapter 4

Combining ACI with DSRG

4.1 Introduction

In order to make meaningful predictions about the electronic properties of molecules, theoretical computations need to satisfactorily converge both correlation and basis set effects. By correlation, we refer to its normal decomposition into a *static* component, defined by the strong mixing of electronic configurations typically resultant from degeneracies, and a *dynamical* component, which includes short-range Coulombic and long-range dispersion interactions.[1,2] Molecules with more than 2–4 strongly correlated electrons require a multireference method, wherein a specialized approach is adopted for both types of correlation. Static correlation is treated rigorously with a multiconfigurational reference wave function defined in a set of active orbitals, commonly from complete active space configuration interaction (CASCI) or CAS self consistent field (CASSCF),[3–5] while more affordable perturbative or non-perturbative many-body theories are invoked for dynamical correlation. Unfortunately, both correlation treatments will fail once the number of active orbitals becomes too large, usually around 18 active orbitals for CASCI, relegating applications of multireference methods to regimes in chemistry where static correlation is defined in just a few orbitals. In this article, we introduce a new strategy capable of treating static and dynamical correlation using large active spaces and basis sets to approach chemical accuracy (≤ 1 kcal mol^{-1} error).

The limitations of CASSCF and CASCI arise from the number of variational parameters growing combinatorially as the number of electrons and orbitals in the active space. New techniques can achieve a sub-combinatorial cost, or a significant reduction of the prefactor, by exploiting the sparse structure of CASCI wave functions, enabling reliable computations using significantly larger active spaces.[6–32] However, when augmenting any CAS method with a theory of dynamical correlation, numerical and practical concerns arise. Most multireference theories suffer from numerical instabilities known as "intruder states" which spoil computations with unphysical contributions difficult to systematically cure.[33] Additionally, theories of dynamical correlation require the computation of high-order density matrices and cumulants, causing methods like CAS second-order perturbation theory (CASPT2)[34] to scale as the ninth power of the number of active orbitals, limiting these methods to moderate active space sizes ($<$20–25). The development of approximate CAS techniques has as of yet outpaced the ability for dynamical correlation methods to make use of them.

Some recent work has connected large active space ($\geq$ 20 orbitals) wave functions with dynamical correlation treatments, including active space DFT approaches[35–39] and the combination of density matrix renormalization group with perturbative[40–42] and CI-based[43] theories. Recently, the adiabatic connection has been used to compute correlation energies from CAS wave functions and only requires two-body density matrices.[44,45] To our knowledge, none of these approaches have treated the coupling of static and dynamical correlation, which we refer to as the *relaxation* effect of the reference wave function in response to a dynamical correlation treatment, the importance of which is not fully understood.[46] For this reason, and other drawbacks related to cost, density functional dependence, and potential neglect of static correlations, the development of a systematically improvable, numerically stable, and computationally efficient multireference theory with dynamical correlation is still an open problem.

4.2 Theory

We seek a complete treatment of electron correlation by, for the first time, interfacing two of our recently developed theories, the adaptive CI (ACI)[22,23] and the second-order perturbative variant of the multireference driven similarity renormalization group (DSRG-MRPT2).[47–51]

4.2.1 Adaptive CI

The goal of the ACI procedure is to converge an approximate CASCI wave function,

$$|\Psi_M\rangle = \sum_{\Phi_\mu \in M} C_\mu |\Phi_\mu\rangle \tag{4.1}$$

in an iteratively selected determinantal model space, M, such that the variational energy error approximately matches a user defined parameter, σ, i.e.

$$|E_{\text{CASCI}} - E_M| \approx \sigma \tag{4.2}$$

where $E_M = \langle\Psi_M|\hat{H}|\Psi_M\rangle$ is the ACI energy. The ACI wave function is built by iteratively growing a set of reference determinants (P) and screening its first order interacting space (F) using perturbative energy estimates. To ensure error control, the screening is done by excluding determinants with the smallest energy estimates such that the accumulation of these perturbative corrections approximately equals the energy criterion, σ. Additional details of the algorithm are presented elsewhere,[22,23] but we emphasize that the iterative procedure rigorously samples the total CASCI wave function to very closely meet the condition of eq (4.2) and yield a compact wave function whose energy error is controlled *a priori* by the user. As a result, ACI wave functions for different electronic states can be made with near-equal accuracy to approach perfect error cancellation in relative properties, such as singlet-triplet splittings.[22,23] We have previously illustrated this error cancellation in systems using up to 42 active orbitals.[22]

In our previous implementation, all determinants Φ_I in F were stored simultaneously

during the screening step of the algorithm, which incurs a memory cost of $\mathcal{O}(|P|N_O^2N_V^2)$ where $|P|$ is the number of reference determinants in the set P, and N_O and N_V are the numbers of the occupied and virtual orbitals in the active space, respectively. In addition to being the storage bottleneck, screening is usually the most expensive step with a complexity of $\mathcal{O}(|P|N_O^2N_V^2\log(|P|N_O^2N_V^2))$ due to sorting of all energy estimates. This storage becomes prohibitive if low values of σ are used in large active space computations. We have now implemented a batched selection algorithm that can mitigate this memory bottleneck by sequentially screening subsets of F using a scaled σ value, summarized in Figure 4.1. The number of batches, N_B, is chosen to be the smallest value such that an approxi-

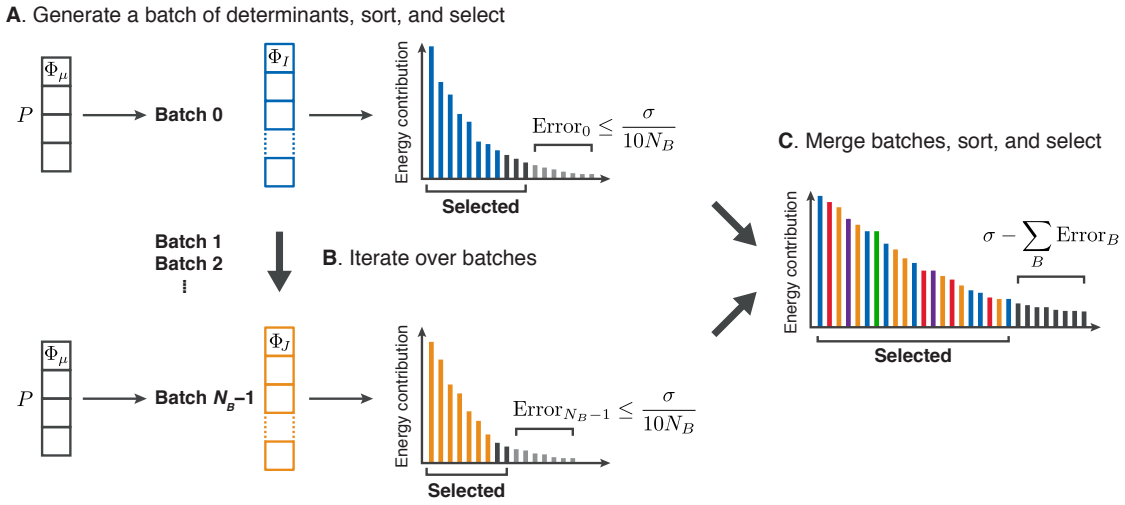

Figure 4.1: Summary of batched screening algorithm. (**A**) Determinants in the first batch are generated from a subset of the single and double excitations from the reference P space. The excited determinants in the batch are sorted and screened using a scaled σ value, with only selected ones being stored. (**B**) The procedure in **A** is repeated for all batches sequentially, with all selected determinants stored. (**C**) These selected determinants are merged and sorted, and a final screening is done to ensure that the total correlation energy ignored corresponds to the original σ value.

mate estimate of the memory requirement of $\frac{|F|}{N_B}$ can be handled by a single node. For each batch $B \in \{0, 1, \ldots, N_B - 1\}$, we iterate through all determinants in P, compute a hash value for each single and double excitation, $h(\Phi_I)$, and store this determinant with its associated energy estimate only if $h(\Phi_I) \mod B = 0$. With the resulting subset of F, we do our conventional screening described previously, but scaling σ by $\frac{1}{10N_B}$ to avoid over-truncation of

each batch, where the factor of $\frac{1}{10}$ is determined empirically. Once all batches have been screened, the surviving determinants are merged, and the accumulated energy estimates of determinants excluded are summed among batches to obtain an estimate of the total correlation being ignored. With the merged determinants, we do a final screening with σ shifted by the energy already screened from the batches. The remaining determinants merged with the reference P define the full model space M. Importantly, our hash function is evenly distributed among determinants so each batch contains fairly equally-weighted determinants and is thus able to exactly match results of the original algorithm. What results is memory storage of $\mathscr{O}(\frac{1}{N_B}|P|N_O^2N_V^2)$ and a reduced complexity of $\mathscr{O}(|P|N_O^2N_V^2\log(\frac{1}{N_B}|P|N_O^2N_V^2))$.

4.2.2 Implementation of RDMs

To connect ACI reference wave functions to the DSRG-MRPT2 perturbative treatment, the 1-, 2-, and 3- body reduced density matrices (RDMs) are required. Introducing second quantized creation ($\hat{a}^\dagger$) and annihilation ($\hat{a}$) operators, a generic k-particle RDM ($\gamma^{pq\cdots}_{rs\cdots}$) may be expressed as

$$\gamma^{pq\cdots}_{rs\cdots} = \sum_{\Phi_I,\Phi_J\in M} \langle\Phi_I|\,\hat{a}_p^\dagger\hat{a}_q^\dagger\ldots\hat{a}_s\hat{a}_r\,|\Phi_J\rangle\, C_I^* C_J \tag{4.3}$$

Storage and contraction of the 3-RDM scales only as $\mathscr{O}(N_A^6)$, where N_A is the number of active orbitals. This moderate scaling enables the use of large active spaces unreachable with conventional many-body dynamical correlation methods, for which active spaces beyond 20–24 active orbitals are impossible to treat without invoking approximations that can potentially introduce artificial numerical problems.[40]

Despite this reduced scaling, the construction of the 3-RDM from a selected CI (sCI) wave function is itself a formidable task. As is commonly done in sCI diagonalization procedures, intermediate residue lists, which map all Slater determinants in a set to all possible determinants with one or two fewer electrons,[52] can be used to predetermine all non-zero elements of the Hamiltonian matrix or of the RDMs. Our ACI implementation adopts this

strategy for the 1- and 2- RDMs and in directly building the sigma vector $\sigma = \mathbf{Hc}$ during diagonalization, as the storage scales at most as $\mathscr{O}(N_{\text{det}}N_{\text{el}}^2)$ for N_{det} determinants and N_{el} active electrons. For constructing the 3-RDM, storage of these lists become impractical since triple annihilations are required, increasing the memory scaling to $\mathscr{O}(N_{\text{det}}N_{\text{el}}^3)$. These lists also become prohibitive for the lower RDMs and for building σ for very large ($\geq 10^7$) determinant spaces. We have implemented a more memory efficient algorithm similar to the one described in ref 18, where we organize determinants by common occupation strings of α or β electrons. For components of the RDMs whose indices all correspond to the same spin, an element is easily computed by looping over determinants only with the same occupation in the opposite spin string, and performing a bitwise comparison to determine the appropriate creation/annihilation indices for evaluating equation (4.3). For mixed spin components, a loop over all α strings is required to determine which strings differ by the desired number of occupation differences. Then, a double loop only over determinants containing those α strings with the correct number of substitutions for the particular RDM component is performed to compute eq (4.3). Thus, the storage requirement changes only to twice the number of determinants, generally less than the 3-RDM itself, despite formally costing $\mathscr{O}(N_O^2N_V^2N_\alpha K_\alpha^2 + N_O^2N_V^2N_\beta K_\beta^2)$ in computational time, with N_α/N_β referring to the number of α/β strings, and K_α/K_β the average number of determinants per α/β string.

4.2.3 DSRG-MRPT2

All theories based on the MR-DSRG avoid intruder states by gradually block-diagonalizing the Hamiltonian ($\hat{H}$) using a unitary transformation dependent on a continuous flow parameter, s,

$$\hat{H} \to \bar{H}(s) = \hat{U}(s)\hat{H}\hat{U}^\dagger(s) \quad s \in [0,\infty) \tag{4.4}$$

The unitary operator is written in a connected form as $\hat{U}(s) = e^{\hat{A}(s)} = e^{\hat{T}(s) - \hat{T}^\dagger(s)}$, where the cluster operator $\hat{T}(s)$ is analogous to the coupled cluster operator.[53,54] In the DSRG, $\hat{T}(s)$

is determined implicitly by solving a set of nonlinear equations[47]

$$[\bar{H}(s)]_{\mathrm{N}} = \hat{R}(s) \tag{4.5}$$

where the source operator, $[\hat{R}(s)]$, drives the transformation, and the many-body condition expressed by eq (4.5) implies exclusive inclusion of nondiagonal (N) terms which couple the reference to its excited configurations. The DSRG total energy is then computed as,

$$E(s) = \langle \Psi_M | \bar{H}(s) | \Psi_M \rangle \tag{4.6}$$

Performing an order-by-order expansion of eqs (4.4)–(4.6), we can write the second-order MR-DSRG energy[48] as,

$$E^{(2)}(s) = \frac{1}{2} \langle \Psi_M | [\tilde{H}^{(1)}(s), \hat{A}^{(1)}(s)] | \Psi_M \rangle \tag{4.7}$$

where the modified first-order Hamiltonian, $\tilde{H}^{(1)}(s)$, is defined as $\tilde{H}^{(1)}(s) = \hat{H}^{(1)}(s) + [\hat{R}^{(1)}(s)]_{\mathrm{N}}$.

For our zeroth-order Hamiltonian, we use a spin-dependent Fock operator to compute $M_s = 0$ states of both singlets and triplets. We represent the Fock operator in a semicanonical basis so that core-core, active-active, and virtual-virtual blocks are diagonal, resulting in a diagonal zeroth-order Hamiltonian. Our choice of a spin-dependent Fock operator and the restriction to $M_s = 0$ states ensure that our dynamical correlation treatment will not introduce spin contamination nor yield an imbalanced treatment between states of different spins.[55,56]

We will report the DSRG-MRPT2 energy from two procedures. Firstly, we can compute the expectation value defined in eq (4.6) by coupling the reference, defined in a set of active orbitals, with the full set of non-frozen occupied and virtual orbitals using eq (4.7). This energy is the *unrelaxed* energy since the reference wave function is constant, and the corresponding approach can be classified as a diagonalize-then-perturb method. Alternatively, the second-order effective Hamiltonian, $\bar{H}^{(2)}(s)$, can be rediagonalized to yield the

relaxed energy and wave function in a diagonalize-perturb-diagonalize scheme, each diagonalization done with ACI. In principle, the relaxation of the wave function should be self-consistently converged in order to approach the FCI solution, absent of approximations in ACI and DSRG. We find that this convergence is fast, so in this work we report the partially relaxed solutions in which the relaxation procedure is done once. Due primarily to cost, reference relaxation is generally ignored in CASPT2 and fully internally-contracted multireference CI methods,[46] but the relaxation in DSRG-MRPT2 is done at the same cost as computing the reference wave function, similar to the state-specific MRPT2 developed by Mao *et al.*[57] and the CIPT2 of Celani and coworkers.[58]

Previous combinations of sCI with perturbation theory (sCI+PT) usually employ both the sCI and PT within the same set of orbitals, where contributions from determinants not selected in the CI wave function are computed with Epstein-Nesbet perturbation theory (ENPT) in either a deterministic, stochastic, or hybrid approach.[18,19,29,59–61] With highly optimized implementations, sCI+PT can essentially reproduce FCI energies for small molecules with around 30 electrons in up to 100 orbitals. Similar success has been demonstrated in combining full-basis sCI with fixed-node diffusion Monte Carlo methods.[62,63] The PT2 variants typically employed in sCI+PT are decontracted and scale with the complexity of the reference wave function. Our DSRG-MRPT2 approach requires only active space 1-, 2-, and 3-RDMs, involves simple contractions, and can take advantage of density fitting. By employing our dynamical correlation treatment in a different set of orbitals than the sCI, we are able to target molecules requiring treatment of up to 138 electrons in over 1000 orbitals. Furthermore, the active space formalism we adopt allows us to easily connect ACI to higher-orders of perturbative and non-perturbative DSRG variants.

Similar to sCI+PT methods, we can use second-order ENPT (ENPT2) to correct for unselected determinants in the diagonalization of either the original or DSRG-MRTP2 transformed Hamiltonian to improved unrelaxed and relaxed energies, respectively. As reported in previous work, this procedure does not incur any additional cost because the energy con-

tributions are already computed during the screening procedure in ACI. The application of an *a posteriori* ENPT2 correction will reduce errors associated with using an incomplete determinant basis during diagonalization. We expect this correction to cancel nearly exactly when computing energy differences between states containing the same number of electrons but to be important in obtaining accurate absolute energies and in computing relative quantities between systems with different numbers of electrons. In this work, we report ACI-DSRG-MRPT2 with this correction by default unless noted otherwise.

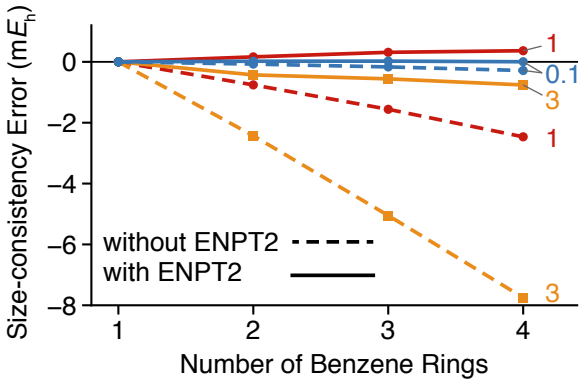

Figure 4.2: Size consistency errors $[E_n(\sigma) - n \times E_1(\sigma)]$ for n non-interacting benzene molecules computed with relaxed ACI-DSRG-MRPT2 using CAS($6n$,$6n$) active spaces and a cc-pVDZ basis set. Each curve is labeled by its σ value in mE_h.

An additional advantage to the DSRG-MRPT2 approach is that its equations contain only connected terms. This feature ensures size extensivity for unrelaxed, partially relaxed, and fully relaxed procedures when the reference wave function itself is multiplicatively separable, and its size consistency with exact references has been previously demonstrated numerically.[48] However, ACI references with $\sigma > 0$ are not multiplicatively separable and break size extensivity in both relaxed and unrelaxed DSRG-MRPT2. We investigate size consistency errors of relaxed ACI-DSRG-MRPT2 with and without the ENPT2 correction during the relaxation procedure for n noninteracting benzene molecules in Figure 4.2. Without the ENPT2 correction, we see that the size consistency error can be as large as about -8 mE_h when $\sigma = 3.0$ mE_h which uses 19 determinants for $n = 1$ (CASCI = 400), and 1461 determinants for $n = 4$ (CASCI = 7.3×10^{12}). The determinantal space for

$n = 1$ is too small a dimension for ACI to reliably target an error of σ, causing negative values for the unperturbed size consistency errors due to the higher accuracy for larger n. Decreasing σ to 0.1 mE_h leads to errors less than 0.3 mE_h and requires 61 determinants for $n = 1$ and 49,349 for $n = 4$. As expected, the ENPT2 correction significantly reduces the size-consistency error by a factor of 10 on average. For the $\sigma = 0.1$ mE_h case with $n = 4$, the error is reduced to around 3 μE_h. Generally, the size consistency errors in relaxed ACI-DSRG-MRPT2 are well-controlled by the cumulative selection of the ACI and nearly eliminated with application of the perturbative correction during relaxation. We do not expect size-consistency errors to affect the accuracy of the singlet-triplet gaps reported in this work because of i) our inclusion of the ENPT2 correction and 2) the expected cancellation of size-consistency error for states with the same number of electrons.

The combination of ACI and DSRG represents one of the few viable options for accurately studying large molecules with complex electronic structures. ACI allows us to use large active spaces while the DSRG provides an efficient, systematically improvable, and intruder-free formalism to recover dynamical correlation. Beyond energies, the relaxation procedure computes reference wave functions in response to dynamical correlation effects, a feature neglected with MRPT2 and DFT approaches. These relaxed wave functions allow us to probe electronic properties without inherent bias towards effects of static correlation.

4.3 The Oligoacenes

This balanced treatment of static and dynamical correlation is particularly important in our application to the oligoacenes, or n-acenes for n linearly fused benzene rings. The oligoacenes have long been of fundamental interest to chemists due to their semiconducting and optical properties,[64–74] and theoreticians have been studying their singlet-triplet splittings and ground state electronic structures with particular attention to the disputed emergence of a stable, open-shell singlet ground state with increasing acene size.[12,22,64,75–86] In characterizing the ground state, qualitatively different interpretations can arise depending

on the degree of dynamical correlation included, with recent studies suggesting that pure active-space methods tend to overestimate the radical character in these ground states.[84–87] An accurate theoretical characterization of the oligoacenes is complicated, however, by (*i*) strong correlation in the π/π^* manifold, (*ii*) their size, prohibitive for many *ab initio* methods, and (*iii*) the large basis sets required for experimental comparisons. For these reasons, a chemically accurate prediction of the singlet-triplet splittings and precise descriptions of ground states have remained elusive to theoretical techniques. The application of ACI-DSRG represents an important step in understanding fundamental electronic properties of oligoacenes.

4.3.1 Computational Details

Singlet and triplet state geometries for the oligoacenes, reported in the supplemental information, were optimized at the UB3LYP/6-31G(*d*) level of theory and are generally the same as those reported by Hachmann and co-workers.[76] Analytic Hessians were computed with ORCA[88] to ensure stability of our geometries and to compute zero-point vibrational energy corrections (ZPVEs). The ACI-DSRG-MRPT2 approach was implemented in FORTE, our freely available software, which is run as a plugin to PSI4.[89] All ACI-DSRG-MRPT2 computations use restricted Hartree-Fock (RHF) and restricted open-shell HF (ROHF) orbitals for singlet and triplet computations, respectively, and the full π/π^* manifold in the active space, resulting in a CAS($4n+2, 4n+2$), for n fused benzene rings. We use the conventional notation of CAS(*e*,*o*), for *e* active electrons and *o* active orbitals. To further compress CI expansions, we separately localize doubly occupied, singly occupied, and virtual active orbitals,[90] which requires the use of C_1 symmetry. The ACI computations of the reference use a prescreening threshold of $\tau_V = 10^{-12}\ E_\mathrm{h}$ (see ref 23) for all acenes except heptacene which required $\tau_V = 10^{-7}\ E_\mathrm{h}$, which is still safely above the corresponding value of σ. Our ACI-DSRG-MRPT2 computations are run in the cc-pV*X*Z, (*X* = D, T, Q) basis sets,[91,92] with all 1*s*-like orbitals on carbon atoms treated

with the frozen core approximation. For all computations, we use density fitted integrals and a DSRG-MRPT2 implementation specialized for three-index integrals.[50] We use the corresponding cc-pVXZ-JKFIT auxiliary basis[93] for RHF/ROHF computations, and the cc-pVXZ-RI auxiliary basis sets[94,95] for DSRG-MRPT2 computations of the correlation energy.

In running ACI-DSRG-MRPT2, two user-specified parameters need to be considered. The first is the energy importance criterion in ACI, σ, which we choose to be as small as practically possible. We will show that our reported energies are converged with respect to σ. The second parameter we need to select is the flow parameter, s, of the DSRG-MRPT2. Guided by our previous work with the DSRG,[48,50] we use $s = 0.5\ E_\mathrm{h}^{-2}$ for all computations in order to recover sufficient correlation without becoming vulnerable to intruders. Figure 4.3 shows the absolute energies of singlet and triplet states, the corresponding singlet-triplet splittings, and the norm of the T_1 amplitudes as a function of s for pentacene using $\sigma = 5\ mE_\mathrm{h}$ and the cc-pVDZ basis computed without a PT2 correction. While increasing s in principle recovers increasingly more correlation, we observe minima in the total energies for both the singlet and triplet states around $s = 1\ E_\mathrm{h}^{-2}$. Interestingly, the singlet-triplet splittings are not particularly stable in this region and do not stabilize with derivatives approaching zero until about $s = 4\ E_\mathrm{h}^{-2}$. Finally, the norm of the triplet T_1 amplitudes increases rapidly, particularly compared to those of the singlet, signaling a potential imbalance in the expected stability of the total energy for each state. The value $s = 0.5\ E_\mathrm{h}^{-2}$ we use in this work is safely away from potential divergences in the energy, while still being close to the energy minima we compute in this test. It is important to note that, despite having favorable stability and being fairly well converged in the absolute energy, the singlet-triplet splittings are susceptible to 1–2 kcal mol^{-1} changes for deviations of 0.1–0.2 E_h^{-2} in s. Preliminary results for naphthalene show that a composite MR-DSRG scheme that combines perturbative and nonperturbative (i.e., CCSD-like) approximations reduces the s-dependence of the singlet-triplet splitting and yields values that are within

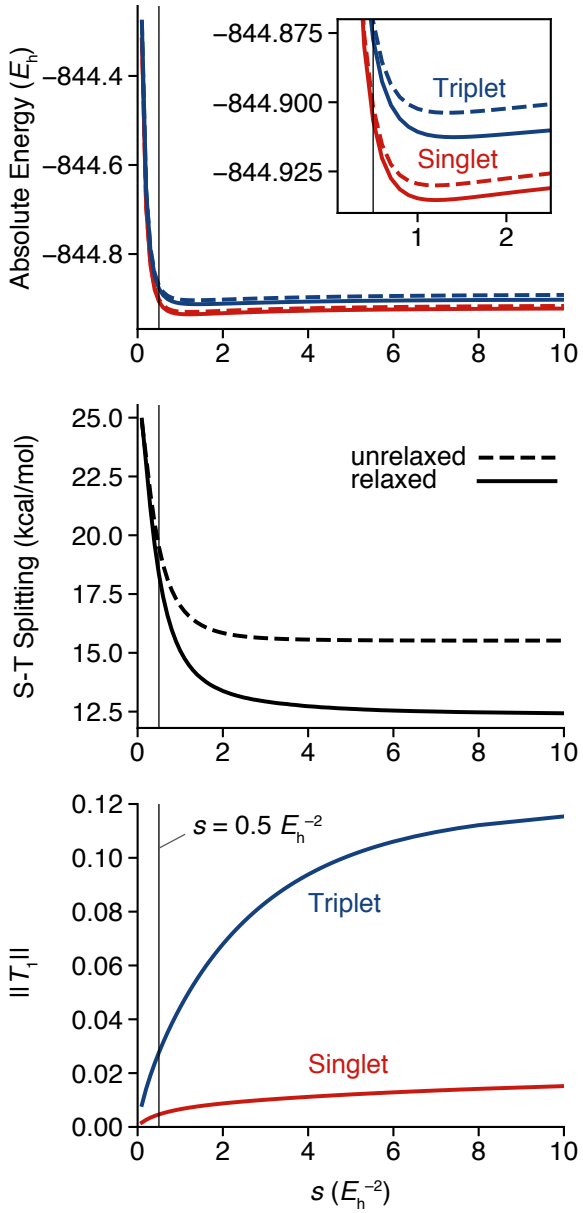

Figure 4.3: Absolute energy, singlet-triplet splitting, and norm of the T_1 amplitudes as a function of s, computed for pentacene with ACI-DSRG-MRPT2 using a CAS(22,22) and $\sigma = 5\ mE_h$. Red and dark blue curves represent singlet and triplet states, respectively, and solid (dashed) lines represent relaxed (unrelaxed) energies. The vertical black line indicates the $s = 0.5\ E_h^{-2}$ value used in the remainder of this work.

1–2 kcal mol^{-1} from the DSRG-MRPT2 values reported in this work. These composite MR-DSRG schemes are a promising direction to improve the accuracy of the dynamical correlation treatment even for large system.

4.3.2 Singlet-Triplet Splittings

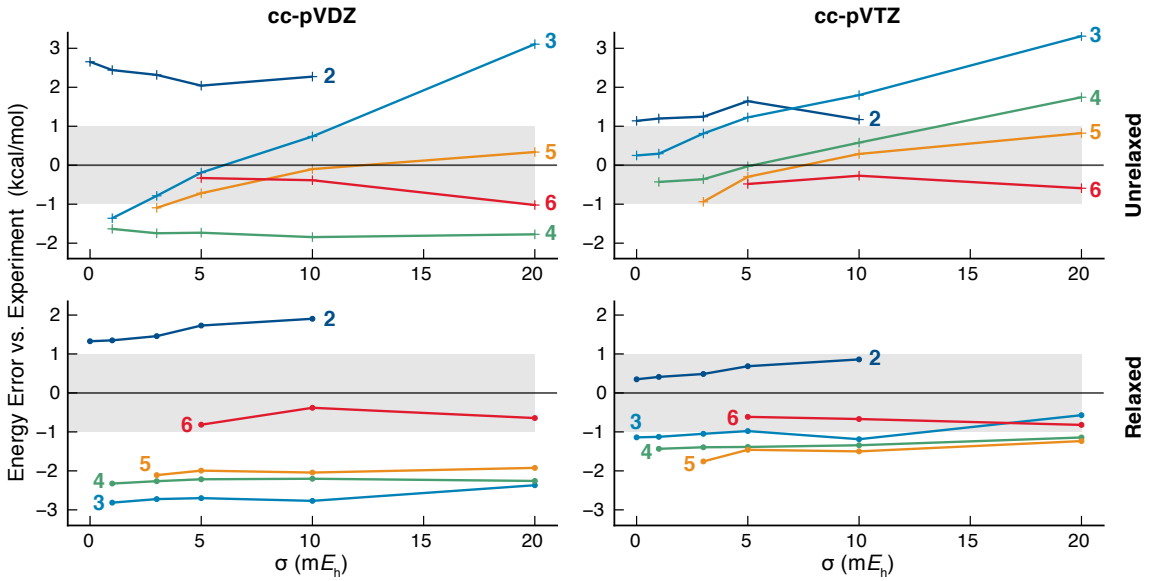

Figure 4.4: ACI-DSRG-MRPT2 error in adiabatic singlet-triplet splitting of n-acenes ($2 \leq n \leq 6$) with respect to experiment using cc-pVDZ (left) and cc-pVTZ (right) basis sets and unrelaxed (top) and relaxed (bottom) references. The shaded area indicates a ± 1 kcal mol^{-1} error window, and no zero-point vibrational energy correction is included.

To understand the behavior of ACI-DSRG-MRPT2, we first analyze the errors in the adiabatic singlet-triplet splittings ($\Delta E_{\mathrm{ST}} = E_{\mathrm{T}} - E_{\mathrm{S}}$) of n-acenes ($n = 2-6$) with both relaxed and unrelaxed references built with varying σ, using the cc-pVDZ and cc-pVTZ basis sets. These computations use optimized geometries for both singlet and triplet states, and we show the errors with respect to experimental adiabatic ΔE_{ST}[96–100] in Figure 4.4. For unrelaxed references, the convergence of the error with respect to decreasing σ is slow and at times erratic, particularly for naphthalene computed with cc-pVDZ. Upon relaxation of the reference, we see that the errors become very stable, even for large σ (10 mE_{h}). This effect suggests that the reference relaxation can help alleviate inaccuracies from an overly-truncated reference wave function. Even for small σ values, relaxation effects can be large and tend to be larger for smaller acenes. Using the cc-pVTZ basis, the errors in the relaxed energies for all acenes converge with decreasing σ and seem to loosely agree with the experimental values despite neglect of vibrational effects and the non-exact geometries we

employ. The most important result from Figure 4.4 is that, using a large basis set and a relaxation procedure, we can use highly-truncated wave functions without incurring serious energetic errors.

The stability of the relaxed singlet-triplet splittings can also be rationalized by consideration of the corresponding absolute energies, reported in Table 1 and 2 of the supporting information. The relaxed ACI-DSRG-MRPT2 energies computed with truncated references show errors with respect to CASCI-DSRG-MRPT2 ($\sigma = 0$) that are approximately equal to σ, an effect not seen in the unrelaxed energies. The ability of σ to control the error of relaxed energies leads to a cancellation of truncation error in our singlet-triplet splittings, making this quantity almost σ-independent, as seen in the flat error curves of Figure 4.4 and in the exact cancellation of the PT2 corrections. Thus, our only expected error in these splittings can be tied to inaccuracies of the DSRG-MRPT2, which has been shown to be of similar magnitude to other second-order multireference perturbation theories. For the simple case of naphthalene, for example, the relaxed CASCI-DSRG-MRPT2 absolute energy is above the Møller–Plesset second order perturbation theory (MP2) value by only about 8 mE_h due to our finite value of $s = 0.5\ E_\mathrm{h}^{-2}$ used.

The singlet-triplet splittings in Figure 4.4 corresponding to the smallest σ used are summarized in Table 4.1 along with available cc-pVQZ data, for which the largest number of basis functions we could treat was 1350 for tetracene in the cc-pVQZ basis. We also report singlet-triplet splittings for heptacene, requiring a CAS(30,30), although we were restricted to $\sigma = 10$ mE_h due to computational time and memory constraints. While we do see that our relaxed energies are stable with respect to an increasing σ, the results from heptacene are possibly affected by an overly truncated reference. Moreover, the heptacene splittings are the only ones that increase with relaxation, which can be interpreted as sign of an insufficient reference being corrected by relaxation. Generally, we see that relaxation reduces splitting energies by up to 1 kcal mol^{-1}, though decreasingly so with increasing acene size. Increasing the basis set from cc-pVTZ to cc-pVQZ increases the splittings by

over 1 kcal mol^{-1}, indicating the importance of basis set effects in accurately predicting these quantities. The singlet-triplet splitting values we report are all computed with the ENPT2 correction for both relaxed and unrelaxed references. Singlet-triplet gaps without the ENPT2 correction differ from the corrected values by at most 2×10^{-4} kcal mol^{-1} and by about 10^{-6} kcal mol^{-1} in most cases (see Supporting Information for absolute energies with and without the ENPT2 correction). Note also that the ENPT2-corrected absolute energies are exactly identical to the uncorrected ones for $\sigma = 0$.

Table 4.1: Adiabatic singlet-triplet splittings (kcal mol^{-1}) of the acene series computed with ACI and ACI-DSRG-MRPT2 with both unrelaxed and relaxed references.

				ΔE_{ST} (kcal mol^{-1})		
					ACI-DSRG-MRPT2	
n	CAS(n,n)	N_{bf}[a]	σ[b]	ACI	unrelaxed	relaxed
			cc-pVDZ			
2	(10,10)	170	0.0	68.3	63.7	62.3
3	(14,14)	232	0.0	43.6	41.7	40.3
4	(18,18)	294	1.0	30.9	27.7	27.0
5	(22,22)	356	3.0	21.4	18.7	17.7
6	(26,26)	418	5.0	13.6	11.7	11.2
			cc-pVTZ			
2	(10,10)	402	0.0	64.1	62.1	61.4
3	(14,14)	546	0.0	45.6	43.4	42.0
4	(18,18)	690	1.0	33.2	28.9	27.9
5	(22,22)	834	3.0	22.1	18.9	18.0
6	(26,26)	978	5.0	14.8	11.5	11.4
7	(30,30)	1122	10	9.5	7.2	7.7
			cc-pVQZ			
2	(10,10)	790	0.0	64.5	63.1	62.2
3	(14,14)	1070	0.0	47.0	44.4	43.2
4	(18,18)	1350	1.0	32.8	29.2	28.3

[a] Number of non-frozen orbitals.
[b] The ACI energy importance criteria (in mE_h). See eq (4.2).

Additionally in Table 4.2 we summarize experimental and theoretical predictions of ΔE_{ST} from a variety of methods including DFT, CC, various multireference theories, and ACI-DSRG-MRPT2 best estimates.[36,42,76,78,101] None of the values reported in Table 4.2 include zero-point vibrational energy corrections (ZPVEs), which we show computed with UB3LYP/6-31G(d). Aside from UB3LYP, the methods with the least amount of explicitly treated static correlation, coupled cluster with singles, doubles, and perturbative triples

Table 4.2: Comparison of the best ACI-DSRG-MRPT2 adiabatic singlet-triplet splittings (kcal mol^{-1}) of the acene series with selected literature values

	n-acene						
Method	2	3	4	5	6	7	MUD^n
UB3LYP[a]	62.6	41.8	27.7	17.9	10.9	5.6	2.9
CCSD(T)[b]	65.8	48.2	33.5	25.3	17.7	13.4	3.0
pp-RPA@U[c]	66.2	45.7	32.1	22.6	15.2	9.0	1.2
CAS(8,8)-CISD+Q[d]	65.5	48.4	38.5	27.7	24.2	16.6	5.7
GAS-pDFT (FP-1)[e]	70.6	45.5	33.6	25.4	19.7	16.5	3.9
GAS-pDFT (WFP-3)[e]	64.7	43.1	28.8	20.5	15.0	10.0	1.4
DMRG-pDFT[f]	67.1	46.1	31.6	22.6	16.8	14.3	1.7
DMRG-CASPT2[g]	–	39.0	27.2	18.8	13.3	–	3.2
DMRG-CASPT2[h]	–	39.8	29.6	19.8	14.2	–	2.2
This work	62.2	43.2	28.3	18.0	11.4	7.7	2.5
ZPVE	−3.4	−2.3	−1.8	−1.5	−1.3	−1.2	
Exp.	60.9,[i] 61.0[j]	42.6,[i] 43.1[k]	29.4[i]	19.8 ± 0.7[l]	(12.4 ± 1.2)[m]	–	

[a] Ref. 76. [b] Data for $n = 2-6$ taken from ref. 78, value for $n = 7$ computed in this work. [c] Unrestricted geometry. Ref 65. [d] 6-31G basis; see ref 101. [e] tPBE functional and 6-31+G(p,d), Active space partitioning in parentheses defined in Ref. 36. [f] tPBE functional and 6-31+G(p,d) Ref. 39. [g] CAM-B3LYP/6-31G* geometry. Ref. 42. [h] CAS(12,12)-CASPT2-D geometries. Ref. 42. [i] Ref 96. [j] Ref 97. [k] Ref 98. [l] Ref. 99. [m] Ref. 100, based on extrapolated correlations of triplet energies to singlet energies and ionization potentials for lower acenes. [n] Mean unsigned deviation with respect to vibrationally corrected experimental values.

[CCSD(T)], the particle-particle random phase approximation (pp-RPA), and CAS(8,8)-CISD+Q, generally overestimate the splittings with errors increasing with acene length. When ZPVE corrections are included, ACI-DSRG-MRPT2 consistently underestimate the experimental gaps by 1.7–3.3 kcal mol^{-1}, similar on average to the DMRG-CASPT2 results reported by Kurashige and Yanai[42] which show larger (≈ 5 kcal mol^{-1}) absolute errors for the smaller acenes with respect to experiment. The DMRG-pDFT predicts singlet-triplet gaps around 2–5 kcal mol^{-1} larger than our results and are on average closer to the experimental values by 0.8 kcal mol^{-1} compared to ACI-DSRG-MRPT2 despite using a smaller basis set. Interestingly, DMRG-CASPT2 using the DFT-optimized geometry and GAS-pDFT using an active space partitioning which maximizes the number of determinants included both agree well with ACI-DSRG-MRPT2 with an average absolute deviation of about 2 kcal mol^{-1}.

As shown by the DMRG-CASPT2 data in Table 4.2, different geometry optimization

procedures can cause deviations in ΔE_{ST} on the order of 1–3 kcal mol^{-1}, suggesting that a geometry optimization scheme more accurate than DFT is required to enable reliable comparisons with experiment. Additionally, most experimental data shown here involve solid or liquid stabilizing matrices, and in some cases are derived from indirect measurements, both having unpredictable deviations with respect to the zero-temperature, gas-phase results from calculations. In light of these complications in experimental comparisons, the general agreement of the relaxed ACI-DSRG-MRPT2 and the DMRG-CASPT2 results of Kurashige and Yanai[42] when both computations use DFT optimized geometries is particularly encouraging considering that the ACI-DSRG-MRPT2 can be applied to heptacene using a CAS(30,30). Furthermore, the absolute errors of the ACI-DSRG-MRPT2 with respect to experiment do not systematically deviate as a function of acene length, with all errors within a 1.6 kcal mol^{-1} window. This observed consistency would predict an experimental singlet-triplet gap for heptacene to be roughly 2.5 kcal mol^{-1} above our reported value.

4.3.3 Emergent Radical Character

One of the greatest benefits of our approach is that we can analyze the importance of relaxation effects on electronic properties. We emphasize that the relaxed wave functions and densities we present span the π/π^* active spaces used in building the references, and they are optimized in *response* to dynamical effects rather than being built in the full orbital basis of the DSRG-MRPT2. To investigate the emergent radical character, and the importance of relaxation effects in accurately describing it, we compute the effective number of unpaired electrons as defined by Takatsuka et al.,[102,103]

$$\#\text{ of unpaired electrons } = \sum_{i}^{\text{all}} n_i(2-n_i) \tag{4.8}$$

for each natural orbital occupation number (n_i) computed from relaxed and unrelaxed active space densities. In our wave function analysis, we use a constant σ per number of electrons

in order to ensure that each acene is computed to the same relative accuracy, so that our interpretation of trends is unaffected by any potential differences in reference wave function quality.

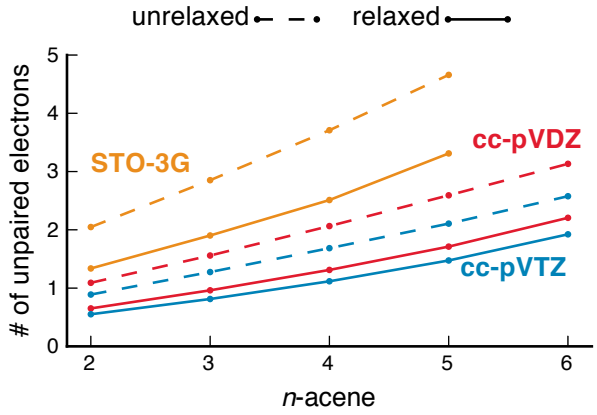

Figure 4.5: Number of unpaired electrons for the ground state singlets of the oligoacenes computed from unrelaxed (dashed line) and relaxed (solid line) ACI-DSRG-MRPT2 wave functions. Sigma values are chosen to produce a constant 190 μE_h error per electron.

Figure 4.5 shows the effective number of unpaired electrons for the acene series computed from unrelaxed and relaxed references of ground state singlets, using STO-3G, cc-pVDZ, and cc-pVTZ basis sets. Improving the dynamical correlation treatment by both increasing the basis set and relaxing the reference reduces the observed radical character dramatically. When used in small basis sets, this metric yields only qualitative information about the relative radical character among acenes and is unable to provide any definitive insight into when the degree of radical character is significant. In computing this metric more accurately, we see quantitative evidence for the emergent diradical character in hexacene, though we are cautious to map this metric directly to a chemical observable. While increasing the correlation treatment and basis set quality is likely to further decrease this metric, we already see relatively close agreement between results using cc-pVTZ and cc-pVDZ basis sets. Our observation of a slower emergence of radical character is consistent with the previously reported notion[84–86] that small basis sets and only an active-space treatment of electron correlation can lead to overestimating the radical character and misinterpreting the nature of the ground state. Ultimately, ACI-DSRG-MRPT2 results do show weak emergent

radical character with acene length.

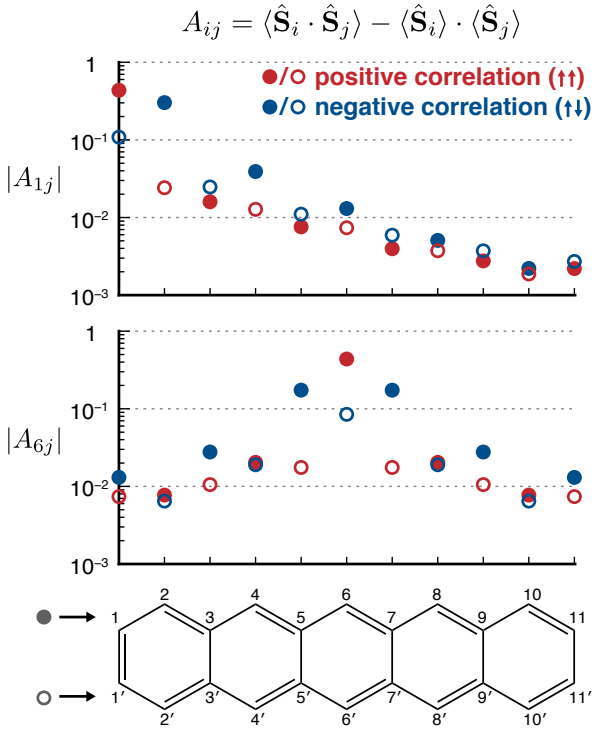

Figure 4.6: Log-plot of the spin-spin correlation function using carbons 1 and 6 as references, computed for the ground state singlet of pentacene with a relaxed ACI-DSRG-MRPT2 wave function.

4.3.4 Analysis of Spin-Spin Correlation

As a final analysis, we characterize spatial correlations of spin by computing the spin-spin correlation function (A_{ij}) between two atomic sites i and j, defined as $A_{ij} = \langle \hat{\mathbf{S}}_i \cdot \hat{\mathbf{S}}_j \rangle - \langle \hat{\mathbf{S}}_i \rangle \cdot \langle \hat{\mathbf{S}}_j \rangle$, where each site is defined as an atom-centered, Pipek–Mezey localized[104] carbon $2p_z$-like molecular orbital (plotted in the Supporting Information), and $\hat{\mathbf{S}}_i$ is the total spin operator for site i. This correlation function depends on the 1- and 2- RDMs of the ACI wave functions, enabling us to understand the effect of reference relaxation on the spin correlations, though it will not include spin correlations outside the π/π^* manifold. As shown in Figure 4.6, spin-spin correlation in pentacene is large at small distances but quickly decays with a pattern characteristic of short-range antiferromagnetic order. Interestingly, opposite-spin correlations are larger than same-spin correlations along the same

edge, but have similar magnitudes along for the opposite edge. This result indicates that any radical character in the acenes is localized along the long axes of the molecule and stabilized with antiferromagnetic ordering, supporting previous hypotheses.[86]

In addition, we also compute the spin-spin correlation density with respect to site i [$A_i(\mathbf{r})$], defined as,

$$A_i(\mathbf{r}) = \langle \hat{\mathbf{S}}(\mathbf{r}) \cdot \hat{\mathbf{S}}_j \rangle - \langle \hat{\mathbf{S}}(\mathbf{r}) \rangle \cdot \langle \hat{\mathbf{S}}_j \rangle \approx \sum_j |\phi_j(\mathbf{r})|^2 A_{ij} \tag{4.9}$$

where $\hat{\mathbf{S}}(\mathbf{r})$ is the total spin operator in real space and the last approximate equality assumes that overlap terms can be neglected due to orbital localization. In Figure 4.7, we use this metric to illustrate the spatial distribution and the effect of reference relaxation on spin-spin correlation in pentacene. Dynamical correlation generally increases same and opposite spin correlations for long range interactions, while decreasing the short-range opposite correlations indicative of bonding. Thus, the relaxation effects enhance long-range effects while reducing short-range ones. Note that our plots of the spin correlation density do not explicitly reflect open shell character, but they do show short-range antiferromagnetic order.

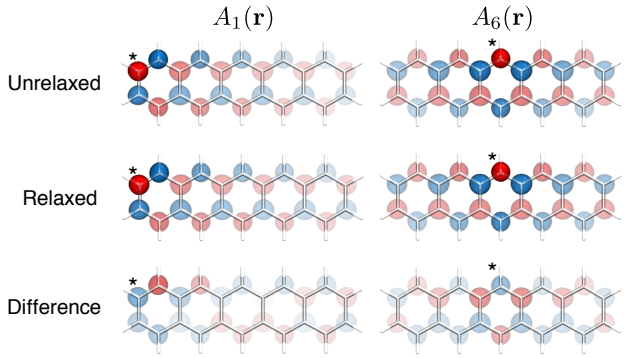

Figure 4.7: Spin correlation densities plotted from unrelaxed and relaxed references, in addition to the difference of relaxed and unrelaxed results. We show two reference sites, marked with "*", corresponding to central and terminal carbons consistent with the labeling in Figure 4.6, with all reference sites plotted in the SI.

4.4 Conclusions

In this work, we have introduced the ACI-DSRG-MRPT2 method for studying large-scale strong correlation. Our approach uses the efficient, tunable ACI to recover static correlation within large active spaces and the intruder-free DSRG-MRPT2 to recover dynamical correlation, which we can use to recompute active space wave functions with consideration of dynamical correlation. We have shown that this strategy can be applied to large active spaces, up to CAS(30,30), and for systems using up to 1350 basis functions on a single node. We find that this procedure provides accurate energies and high-quality wave functions suitable for quantitative analysis. Our application to the oligoacenes has demonstrated that relaxation effects can significantly influence interpretation of chemical properties, with notable reduction of radical character and a shifting of spin correlations to longer distance.

In addition, the ACI-DSRG-MRPT2 is flexible. With reference wave functions formed from determinants, we can easily apply our approach to excited states using state-specific or multistate DSRG approaches.[51] Furthermore, we are not limited to second order perturbation theory, as the higher-order non-perturbative variants of the DSRG still only require at most the 3-RDM. With further development of ACI, we can apply ACI-DSRG theories to ground and excited states of even larger, more complex molecules.

Bibliography

[1] D. K. W. Mok, R. Neumann, and N. C. Handy. "Dynamical and Nondynamical Correlation." *J. Phys. Chem.* **100**, 6225 (1996).

[2] F. A. Evangelista. "Perspective: Multireference coupled cluster theories of dynamical electron correlation." *J. Chem. Phys.* **149**, 030901 (2018).

[3] B. O. Roos, P. R. Taylor, and P. E. M. Siegbahn. "A complete active space SCF method (CASSCF) using a density matrix formulated super-CI approach." *Chem. Phys.* **48**, 157 (1980).

[4] H.-J. Werner and P. J. Knowles. "A second order multiconfiguration SCF procedure with optimum convergence." *J. Chem. Phys.* **82**, 5053 (1998).

[5] J. Olsen. "The CASSCF method: A perspective and commentary." *Int. J. Quant. Chem.* **111**, 3267 (2011).

[6] S. R. White. "Density matrix formulation for quantum renormalization groups." *Phys. Rev. Lett.* **69**, 2863 (1992).

[7] S. R. White and R. L. Martin. "Ab initio quantum chemistry using the density matrix renormalization group." *J. Chem. Phys.* **110**, 4127 (1999).

[8] G. K.-L. Chan and M. Head-Gordon. "Highly correlated calculations with a polynomial cost algorithm: A study of the density matrix renormalization group." *J. Chem. Phys.* **116**, 4462 (2002).

[9] G. K.-L. Chan, J. J. Dorando, D. Ghosh, J. Hachmann, E. Neuscamman, H. Wang, and T. Yanai. "An Introduction to the Density Matrix Renormalization Group Ansatz in Quantum Chemistry." In S. Wilson, P. Grout, J. Maruani, G. Delgado-Barrio, and P. Piecuch, editors, "Frontiers in Quantum Systems in Chemistry and Physics," 49–65. Springer Netherlands (2008).

[10] G. K.-L. Chan and S. Sharma. "The density matrix renormalization group in quantum chemistry." *Annu. Rev. Phys. Chem.* **62**, 465 (2011).

[11] A. E. DePrince III. "Variational optimization of the two-electron reduced-density matrix under pure-state N-representability conditions." *J. Chem. Phys.* **145**, 164109 (2016).

[12] J. Fosso-Tande, D. R. Nascimento, and I. A Eugene DePrince. "Accuracy of two-particle N-representability conditions for describing different spin states and the singlet–triplet gap in the linear acene series." *Mol. Phys.* **114**, 423 (2016).

[13] J. Fosso-Tande, T.-S. Nguyen, G. Gidofalvi, and I. A Eugene DePrince. "Large-Scale Variational Two-Electron Reduced-Density-Matrix-Driven Complete Active Space Self-Consistent Field Methods." *J. Chem. Theor. Comput.* **12**, 2260 (2016).

[14] G. H. Booth, A. J. Thom, and A. Alavi. "Fermion Monte Carlo without fixed nodes: A game of life, death, and annihilation in Slater determinant space." *J. Chem. Phys.* **131**, 054106 (2009).

[15] G. H. Booth and A. Alavi. "Approaching chemical accuracy using full configuration-interaction quantum monte carlo: a study of ionization potentials." *J. Chem. Phys.* **132**, 174104 (2010).

[16] D. Cleland, G. H. Booth, and A. Alavi. "Communications: Survival of the fittest: Accelerating convergence in full configuration-interaction quantum Monte Carlo." *J. Chem. Phys.* **132**, 041103 (2010).

[17] G. Li Manni, S. D. Smart, and A. Alavi. "Combining the complete active space self-consistent field method and the full configuration interaction quantum monte carlo within a super-CI framework, with application to challenging metal-porphyrins." *J. Chem. Theor. Comput.* **12**, 1245 (2016).

[18] S. Sharma, A. A. Holmes, G. Jeanmairet, A. Alavi, and C. J. Umrigar. "Semistochastic heat-bath configuration interaction method: Selected configuration interaction with semistochastic perturbation theory." *J. Chem. Theor. Comput.* **13**, 1595 (2017).

[19] A. A. Holmes, N. M. Tubman, and C. J. Umrigar. "Heat-Bath Configuration Interaction: An Efficient Selected Configuration Interaction Algorithm Inspired by Heat-Bath Sampling." *J. Chem. Theor. Comput.* **12**, 3674 (2016).

[20] J. E. T. Smith, B. Mussard, A. A. Holmes, and S. Sharma. "Cheap and Near Exact CASSCF with Large Active Spaces." *J. Chem. Theor. Comput.* **13**, 5468 (2017).

[21] N. M. Tubman, J. Lee, T. Y. Takeshita, M. Head-Gordon, and K. B. Whaley. "A deterministic alternative to the full configuration interaction quantum Monte Carlo method." *J. Chem. Phys.* **145**, 044112 (2016).

[22] J. B. Schriber and F. A. Evangelista. "Communication: An adaptive configuration interaction approach for strongly correlated electrons with tunable accuracy." *J. Chem. Phys.* **144**, 161106 (2016).

[23] J. B. Schriber and F. A. Evangelista. "Adaptive Configuration Interaction for Computing Challenging Electronic Excited States with Tunable Accuracy." *J. Chem. Theor. Comput.* **13**, 5354 (2017).

[24] Y. Ohtsuka and J.-y. Hasegawa. "Selected configuration interaction method using sampled first-order corrections to wave functions." *J. Chem. Phys.* **147**, 034102 (2017).

[25] T. Zhang and F. A. Evangelista. "A deterministic projector configuration interaction approach for the ground state of quantum many-body systems." *J. Chem. Theor. Comput.* **12**, 4326 (2016).

[26] K. D. Vogiatzis, G. Li Manni, S. J. Stoneburner, D. Ma, and L. Gagliardi. "Systematic Expansion of Active Spaces beyond the CASSCF Limit: A GASSCF/SplitGAS Benchmark Study." *J. Chem. Theor. Comput.* **11**, 3010 (2015).

[27] B. S. Fales, S. Seritan, N. F. Settje, B. G. Levine, H. Koch, and T. J. Martínez. "Large-Scale Electron Correlation Calculations: Rank-Reduced Full Configuration Interaction." *J. Chem. Theor. Comput.* **14**, 4139 (2018).

[28] Y. Garniron, A. Scemama, E. Giner, M. Caffarel, and P.-F. Loos. "Selected configuration interaction dressed by perturbation." *J. Chem. Phys.* **149**, 064103 (2018).

[29] N. M. Tubman, C. D. Freeman, D. S. Levine, D. Hait, M. Head-Gordon, and K. B. Whaley. "Modern Approaches to Exact Diagonalization and Selected Configuration Interaction with the Adaptive Sampling CI Method." *arXiv* https:—-arxiv.org–abs–1807.00821 (2018).

[30] S. Guo, Z. Li, and G. K.-L. Chan. "A Perturbative Density Matrix Renormalization Group Algorithm for Large Active Spaces." *J. Chem. Theor. Comput.* **14**, 4063 (2018).

[31] S. Pathak, L. Lang, and F. Neese. "A dynamic correlation dressed complete active space method: Theory, implementation, and preliminary applications." *J. Chem. Phys.* **147**, 234109 (2017).

[32] E. Xu, M. Uejima, and S. L. Ten-no. "A Full Coupled-Cluster Reduction For Accurate Description Of Strong Electron Correlation." *arXiv* https:—-arxiv.org–abs–1807.05818 (2018).

[33] B. O. Roos and K. Andersson. "Multiconfigurational perturbation theory with level shift — the Cr_2 potential revisited." *Chem. Phys. Lett.* **245**, 215 (1995).

[34] K. Andersson, P.-Å. Malmqvist, and B. O. Roos. "Second-order perturbation theory with a complete active space self-consistent field reference function." *J. Chem. Phys.* **96**, 1218 (1998).

[35] G. L. Manni, R. K. Carlson, S. Luo, D. Ma, J. Olsen, D. G. Truhlar, and L. Gagliardi. "Multiconfiguration pair-density functional theory." *J. Chem. Theor. Comput.* **10**, 3669 (2014).

[36] S. Ghosh, C. J. Cramer, D. G. Truhlar, and L. Gagliardi. "Generalized-active-space pair-density functional theory: an efficient method to study large, strongly correlated, conjugated systems." *Chemical Science* **8**, 2741 (2017).

[37] L. Gagliardi, D. G. Truhlar, G. Li Manni, R. K. Carlson, C. E. Hoyer, and J. L. Bao. "Multiconfiguration Pair-Density Functional Theory: A New Way To Treat Strongly Correlated Systems." *Acc. Chem. Res.* **50**, 66 (2017).

[38] E. Fromager, J. Toulouse, and H. J. A. Jensen. "On the universality of the long-/short-range separation in multiconfigurational density-functional theory." *J. Chem. Phys.* **126**, 074111 (2007).

[39] P. Sharma, V. Bernales, S. Knecht, D. G. Truhlar, and L. Gagliardi. "Density Matrix Renormalization Group Pair-Density Functional Theory (DMRG-PDFT): Singlet-Triplet Gaps in Polyacenes and Polyacetylenes." *arXiv* https://arxiv.org/abs/1808.06273 (2018).

[40] D. Zgid, D. Ghosh, E. Neuscamman, and G. K.-L. Chan. "A study of cumulant approximations to n-electron valence multireference perturbation theory." *J. Chem. Phys.* **130**, 194107 (2009).

[41] Y. Kurashige, J. Chalupsk y, T. N. Lan, and T. Yanai. "Complete active space second-order perturbation theory with cumulant approximation for extended active-space wavefunction from density matrix renormalization group." *J. Chem. Phys.* **141**, 174111 (2014).

[42] Y. Kurashige and T. Yanai. "Theoretical study of the π π* excited states of oligoacenes: A full π-valence DMRG-CASPT2 study." *Bull. Chem. Soc. Japan* **87**, 1071 (2014).

[43] Z. Luo, Y. Ma, X. Wang, and H. Ma. "Externally-Contracted Multireference Configuration Interaction Method Using a DMRG Reference Wave Function." *J. Chem. Theor. Comput.* (2018).

[44] E. Pastorczak and K. Pernal. "Correlation Energy from the Adiabatic Connection Formalism for Complete Active Space Wave Functions." *J. Chem. Theor. Comput.* **14**, 3493 (2018).

[45] K. Pernal. "Electron Correlation from the Adiabatic Connection for Multireference Wave Functions." *Phys. Rev. Lett.* **120**, 013001 (2018).

[46] K. Sivalingam, M. Krupicka, A. A. Auer, and F. Neese. "Comparison of fully internally and strongly contracted multireference configuration interaction procedures." *The Journal of Chemical Physics* **145** (2016).

[47] F. A. Evangelista. "A driven similarity renormalization group approach to quantum many-body problems." *J. Chem. Phys.* **141**, 054109 (2014).

[48] C. Li and F. A. Evangelista. "Multireference driven similarity renormalization group: a second-order perturbative analysis." *J. Chem. Theor. Comput.* **11**, 2097 (2015).

[49] C. Li and F. A. Evangelista. "Towards numerically robust multireference theories: The driven similarity renormalization group truncated to one- and two-body operators." *J. Chem. Phys.* **144**, 164114 (2016).

[50] K. P. Hannon, C. Li, and F. A. Evangelista. "An integral-factorized implementation of the driven similarity renormalization group second-order multireference perturbation theory." *J. Chem. Phys.* **144**, 204111 (2016).

[51] C. Li, P. Verma, K. P. Hannon, and F. A. Evangelista. "A low-cost approach to electronic excitation energies based on the driven similarity renormalization group." *J. Chem. Phys.* **147**, 074107 (2017).

[52] P. Stampfuß and W. Wenzel. "Improved implementation and application of the individually selecting configuration interaction method." *J. Chem. Phys.* **122**, 024110 (2005).

[53] F. A. Evangelista and J. Gauss. "An orbital-invariant internally contracted multireference coupled cluster approach." *J. Chem. Phys.* **134**, 114102 (2011).

[54] M. Hanauer and A. Köhn. "Communication: Restoring full size extensivity in internally contracted multireference coupled cluster theory." *J. Chem. Phys.* **137**, 131103 (2012).

[55] F. A. Evangelista, W. D. Allen, and H. F. Schaefer. "Coupling term derivation and general implementation of state-specific multireference coupled cluster theories." *J. Chem. Phys.* **127**, 024102 (2007).

[56] F. A. Evangelista, A. C. Simmonett, H. F. Schaefer III, D. Mukherjee, and W. D. Allen. "A companion perturbation theory for state-specific multireference coupled cluster methods." *Phys. Chem. Chem. Phys.* **11**, 4728 (2009).

[57] S. Mao, L. Cheng, W. Liu, and D. Mukherjee. "A spin-adapted size-extensive state-specific multi-reference perturbation theory. I. Formal developments." *J. Chem. Phys.* **136**, 024105 (2012).

[58] P. Celani, H. Stoll, H.-J. Werner, and P. J. Knowles. "The CIPT2 method: Coupling of multi-reference configuration interaction and multi-reference perturbation theory. Application to the chromium dimer." *Mol. Phys.* **102**, 2369 (2004).

[59] Y. Garniron, A. Scemama, P.-F. Loos, and M. Caffarel. "Hybrid stochastic-deterministic calculation of the second-order perturbative contribution of multireference perturbation theory." *J. Chem. Phys.* **147**, 034101 (2017).

[60] P.-F. Loos, A. Scemama, A. Blondel, Y. Garniron, M. Caffarel, and D. Jacquemin. "A Mountaineering Strategy to Excited States: Highly Accurate Reference Energies and Benchmarks." *J. Chem. Theor. Comput.* **14**, 4360 (2018).

[61] J. Li, M. Otten, A. A. Holmes, S. S. a. p. arXiv, and 2018. "Fast Semistochastic Heat-Bath Configuration Interaction." *arXiv* .

[62] A. Scemama, A. Benali, D. Jacquemin, M. Caffarel, and P.-F. Loos. "Excitation energies from diffusion Monte Carlo using selected configuration interaction nodes." *J. Chem. Phys.* **149**, 034108 (2018).

[63] A. Scemama, Y. Garniron, M. Caffarel, and P.-F. Loos. "Deterministic Construction of Nodal Surfaces within Quantum Monte Carlo: The Case of FeS." *J. Chem. Theor. Comput.* acs.jctc.7b01250 (2018).

[64] H. F. Bettinger. "Electronic structure of higher acenes and polyacene: The perspective developed by theoretical analyses." *Pure Appl. Chem.* **82**, 905.

[65] Y. Yang, E. R. Davidson, and W. Yang. "Nature of ground and electronic excited states of higher acenes." *Proc. Natl. Acad. Sci. U.S.A.* **113**, E5098 (2016).

[66] I. Paci, J. C. Johnson, X. Chen, G. Rana, D. Popović, D. E. David, A. J. Nozik, M. A. Ratner, and J. Michl. "Singlet fission for dye-sensitized solar cells: can a suitable sensitizer be found?" *JACS* **128**, 16546 (2006).

[67] H. Marciniak, M. Fiebig, M. Huth, S. Schiefer, B. Nickel, F. Selmaier, and S. Lochbrunner. "Ultrafast exciton relaxation in microcrystalline pentacene films." *Phys. Rev. Lett.* **99**, 176402 (2007).

[68] T. S. Kuhlman, J. Kongsted, K. V. Mikkelsen, K. B. Møller, and T. I. Sølling. "Interpretation of the Ultrafast Photoinduced Processes in Pentacene Thin Films." *JACS* **132**, 3431 (2010).

[69] P. M. Zimmerman, F. Bell, D. Casanova, and M. Head-Gordon. "Mechanism for Singlet Fission in Pentacene and Tetracene: From Single Exciton to Two Triplets." *JACS* **133**, 19944 (2011).

[70] M. W. B. Wilson, A. Rao, B. Ehrler, and R. H. Friend. "Singlet Exciton Fission in Polycrystalline Pentacene: From Photophysics toward Devices." *Acc. Chem. Res.* **46**, 1330 (2013).

[71] S. Izadnia, D. W. Schönleber, A. Eisfeld, A. Ruf, A. C. LaForge, and F. Stienkemeier. "Singlet Fission in Weakly Interacting Acene Molecules." *J. Phys. Chem. Lett.* **8**, 2068 (2017).

[72] M. Wibowo, R. Broer, and R. W. A. Havenith. "A rigorous nonorthogonal configuration interaction approach for the calculation of electronic couplings between diabatic states applied to singlet fission." *Comp. Theor. Chem.* **1116**, 190 (2017).

[73] S. Refaely-Abramson, F. H. da Jornada, S. G. Louie, and J. B. Neaton. "Origins of Singlet Fission in Solid Pentacene from an ab initio Green's Function Approach." *Phys. Rev. Lett.* **119**, 267401 (2017).

[74] L. A. Martínez-Martínez, M. Du, R. Florentino Ribeiro, S. Kéna-Cohen, and J. Yuen-Zhou. "Polariton-Assisted Singlet Fission in Acene Aggregates." *J. Phys. Chem. Lett.* 1951–1957 (2018).

[75] M. Bendikov, H. M. Duong, K. Starkey, K. N. Houk, E. A. Carter, and F. Wudl. "Oligoacenes: theoretical prediction of open-shell singlet diradical ground states." *JACS* **126**, 7416 (2004).

[76] J. Hachmann, J. J. Dorando, M. Avilés, and G. K.-L. Chan. "The radical character of the acenes: a density matrix renormalization group study." *J. Chem. Phys.* **127**, 134309 (2007).

[77] B. Hajgató, D. Szieberth, P. Geerlings, F. De Proft, and M. S. Deleuze. "A benchmark theoretical study of the electronic ground state and of the singlet-triplet split of benzene and linear acenes." *J. Chem. Phys.* **131**, 224321 (2009).

[78] B. Hajgató, M. Huzak, and M. S. Deleuze. "Focal point analysis of the singlet-triplet energy gap of octacene and larger acenes." *J. Phys. Chem. A* **115**, 9282 (2011).

[79] W. Mizukami, Y. Kurashige, and T. Yanai. "More π Electrons Make a Difference: Emergence of Many Radicals on Graphene Nanoribbons Studied by Ab Initio DMRG Theory." *J. Chem. Theor. Comput.* **9**, 401 (2013).

[80] J. P. Malrieu, R. Caballol, C. J. Calzado, C. De Graaf, and N. Guihery. "Magnetic interactions in molecules and highly correlated materials: physical content, analytical derivation, and rigorous extraction of magnetic Hamiltonians." *Chem. Rev.* **114**, 429 (2014).

[81] S. Lehtola, N. M. Tubman, K. B. Whaley, and M. Head-Gordon. "Cluster decomposition of full configuration interaction wave functions: A tool for chemical interpretation of systems with strong correlation." *J. Chem. Phys.* **147**, 154105 (2017).

[82] S. Lehtola, J. Parkhill, and M. Head-Gordon. "Cost-effective description of strong correlation: Efficient implementations of the perfect quadruples and perfect hextuples models." *J. Chem. Phys.* **145**, 134110 (2016).

[83] C.-N. Yeh and J.-D. Chai. "Role of Kekulé and non-Kekulé structures in the radical character of alternant polycyclic aromatic hydrocarbons: a tao-dft study." *Sci. Rep.* **6**, 30562 (2016).

[84] J. Lee, D. W. Small, E. Epifanovsky, and M. Head-Gordon. "Coupled-Cluster Valence-Bond Singles and Doubles for Strongly Correlated Systems: Block-Tensor Based Implementation and Application to Oligoacenes." *J. Chem. Theor. Comput.* **13**, 602 (2017).

[85] S. Battaglia, N. Faginas-Lago, D. Andrae, S. Evangelisti, and T. Leininger. "Increasing Radical Character of Large [n]cyclacenes Unveiled by Wave Function Theory." *J. Phys. Chem. A* **121**, 3746 (2017).

[86] N. Dupuy and M. Casula. "Fate of the open-shell singlet ground state in the experimentally accessible acenes: A quantum Monte Carlo study." *J. Chem. Phys.* **148**, 134112 (2018).

[87] S. Lehtola, J. Parkhill, and M. Head-Gordon. "Orbital optimisation in the perfect pairing hierarchy: applications to full-valence calculations on linear polyacenes." *Mol. Phys.* **116**, 547 (2017).

[88] F. Neese. "The ORCA program system." *WIREs: Comp. Mol. Sci.* **2**, 73 (2012).

[89] R. M. Parrish, L. A. Burns, D. G. A. Smith, A. C. Simmonett, A. E. DePrince, E. G. Hohenstein, U. Bozkaya, A. Y. Sokolov, R. Di Remigio, R. M. Richard, J. F. Gonthier, A. M. James, H. R. McAlexander, A. Kumar, M. Saitow, X. Wang, B. P. Pritchard, P. Verma, H. F. Schaefer, K. Patkowski, R. A. King, E. F. Valeev, F. A. Evangelista, J. M. Turney, T. D. Crawford, and C. D. Sherrill. "Psi4 1.1: An Open-Source Electronic Structure Program Emphasizing Automation, Advanced Libraries, and Interoperability." *J. Chem. Theor. Comput.* **13**, 3185 (2017).

[90] L. Bytautas, J. Ivanic, and K. Ruedenberg. "Split-localized orbitals can yield stronger configuration interaction convergence than natural orbitals." *J. Chem. Phys.* **119**, 8217 (2003).

[91] T. H. Dunning Jr. "Gaussian basis sets for use in correlated molecular calculations. I. The atoms boron through neon and hydrogen." *J. Chem. Phys.* **90**, 1007 (1989).

[92] D. E. Woon and T. H. Dunning Jr. "Gaussian basis sets for use in correlated molecular calculations. III. The atoms aluminum through argon." *J. Chem. Phys.* **98**, 1358 (1993).

[93] F. Weigend. "A fully direct RI-HF algorithm: Implementation, optimised auxiliary basis sets, demonstration of accuracy and efficiency." *Phys. Chem. Chem. Phys.* **4**, 4285 (2002).

[94] F. Weigend, A. Köhn, and C. Hättig. "Efficient use of the correlation consistent basis sets in resolution of the identity MP2 calculations." *J. Chem. Phys.* **116**, 3175 (2002).

[95] C. Hättig. "Optimization of auxiliary basis sets for RI-MP2 and RI-CC2 calculations: Core–valence and quintuple-ζ basis sets for H to Ar and QZVPP basis sets for Li to Kr." *Phys. Chem. Chem. Phys.* **7**, 59 (2005).

[96] W. Siebrand. "Radiationless Transitions in Polyatomic Molecules. II. Triplet-Ground-State Transitions in Aromatic Hydrocarbons." *J. Chem. Phys.* **47**, 2411 (1967).

[97] J. B. Birks. *Photophysics of Aromatic Molecules*. Wiley-Interscience, London (1970).

[98] J. Schiedt and R. Weinkauf. "Photodetachment photoelectron spectroscopy of mass selected anions: anthracene and the anthracene-H_2O cluster." *Chem. Phys. Lett.* **266**, 201 (1997).

[99] J. Burgos, M. Pope, C. E. Swenberg, and R. R. Alfano. "Heterofission in pentacene-doped tetracene single crystals." *Physica Status Solidi (b)* **83**, 249 (1977).

[100] H. Angliker, E. Rommel, and J. Wirz. "Electronic spectra of hexacene in solution (ground state. Triplet state. Dication and dianion)." *Chem. Phys. Lett.* **87**, 208 (1982).

[101] S. Horn, F. Plasser, T. Müller, F. Libisch, J. Burgdörfer, and H. Lischka. "A comparison of singlet and triplet states for one- and two-dimensional graphene nanoribbons using multireference theory." *Theor. Chem. Acc.* **133**, 183 (2014).

[102] K. Takatsuka, T. Fueno, and K. Yamaguchi. "Distribution of odd electrons in ground-state molecules." *Theoret. Chim. Acta* **48**, 175 (1978).

[103] M. Head-Gordon. "Characterizing unpaired electrons from the one-particle density matrix." *Chem. Phys. Lett.* **372**, 508 (2003).

[104] J. Pipek and P. G. Mezey. "A fast intrinsic localization procedure applicable for abinitio and semiempirical linear combination of atomic orbital wave functions." *J. Chem. Phys.* **90**, 4916 (1989).

Chapter 5

Real-Time Propagation of Selected Configuration Interaction Wave Functions Applied to Charge Migration

5.1 Introduction

In recent years, the development of high-intensity attosecond laser pulses[1] has enabled chemists to probe the dynamics of electrons with unprecedented detail.[2–6] Attosecond dynamics in molecules involves only electronic motion, as the dynamics of the much heavier nuclei occur at femtosecond timescales. Unlike charge transfer processes which typically involve the coupled motion of nuclei and electrons, *charge migration* is defined as the ultrafast electronic motion that occurs before the onset of nuclear effects. In principle, ultrashort laser pulses can induce charge migration resulting in a new distribution of charge in a molecule, which then causes motion in the nuclei in response to the new electronic field. The notion of controlling chemical reactions by tuning attosecond charge migration is commonly referred to as “attochemistry" and can potentially induce chemical reactions or bond rearrangements that are typically hard to control.[2–4,7–13] Due to the difficulty and high cost[10] of experimentally probing charge migration, theoretical models are required to determine how the electron dynamics proceed. For theoretical methods, computation of the dynamics can be difficult due to the potentially many electronic states required to accurately model the charge migration.

One way to initiate charge migration is by ultrafast ionization, where the sudden re-

moval on an electron can create a superposition of cationic states that form a time-evolving wave packet.[11,14,15] Cederbaum and Zoberly introduced the idea that attosecond charge migration in this context is driven by electron correlation manifested in the number of energetically similar cationic states and the degree to which they couple.[14,16–19] Correlation-driven dynamics has since been theoretically observed from core, valence, and inner-valence ionizations in a number of studies employing Green's function techniques based on the non-Dyson intermediate-state representation of the third- or fourth- order algebraic diagrammatic construction [ADC(3), ADC(4)].[6,11,20–28] Work by Bruner *et al.*[29] employed time-dependent density functional theory (TD-DFT)[30,31] to study charge migration, where they also report correlation-driven dynamics following core ionization. Very recently, a time-dependent density matrix renormalization group (TD-DMRG) method was able to reproduce experimentally observed hole oscillations in ionized iodoacetylene.[32]

ADC(3), ADC(4), and TD-DFT can affordably capture charge migration effects in many cases, but they inherently depend on a single-reference description of correlation effects. A single-reference method is appropriate if the ionization spectrum of a molecule shows only a few energetically-separated and weakly-coupled cationic states that are related by single or double excitations.[33] However, a single-reference theory may fail if the ionization spectrum has many coupled satellite states, and in the extreme case a large density of states, corresponding to numerous near-degenerate cationic states that are no longer simple hole excitations from a dominant state. This situation is most likely to occur for inner-valence ionizations and cases with many degenerate orbitals. TD-DMRG is well-suited to treat dynamics involving any combination of cationic states as it does not rely on a single-reference ansatz. However, TD-DMRG uses a matrix product state (MPS) formalism to compress the information in the full CI (FCI) wave function, and propagation of a MPS wave function comes with many difficulties. For example, many propagation schemes involve the addition of multiple intermediate wave functions which is not a well-defined function for MPSs and requires costly workarounds.[34,35] Also, propagation meth-

ods usually require many products of the Hamiltonian with the wave function, which scales as $\mathcal{O}(N_A^4 M^2 + N_A^3 M^3)$ for virtual bond dimension M and N_A correlated orbitals.[36]

As an alternative, we propose to use our selected CI variant, called the adaptive CI (ACI),[37–39] to study the attosecond charge migration resultant from ultrafast ionization. ACI is based on the very old idea of selected CI[40–60] and is one of numerous new manifestations of these techniques.[61–77] To the best of our knowledge, a real-time variant of any selected CI method has not appeared in the literature, perhaps surprisingly. The novelty of ACI lies in its ability to compute a compact wave function with a tunable, approximately predeterminable energy error. This property was also extended to to electronically excited states,[38] and as a result, we see the ACI as being an efficient means of approximating the cationic Hamiltonian used in charge migration dynamics studies. In particular, ACI is well-suited to describe all relevant cationic states compactly and with equal accuracy, regardless of coupling or presence of strongly correlated electrons in these states. With details of the algorithm presented elsewhere,[37–39] ACI wave functions are constructed in a basis of Slater determinants, making the definition of ionized initial states trivial, unlike in DFT where only the initialization of core-ionized states is feasible.[29]

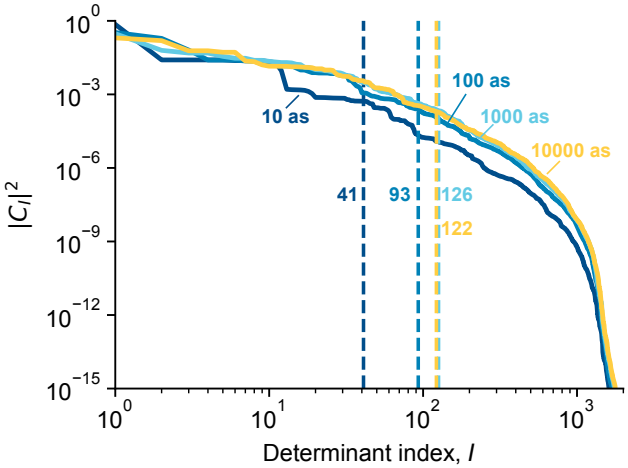

Figure 5.1: Sorted squared magnitudes of all determinants in the FCI wave function. The wave function is computed for a lithium dimer separated by 1.0 Å, computed with the STO-3G basis and propagated using the exact exponential propagator. Each curve shows the coefficients at 10, 100, 1000, and 10000 as snapshots. We also plot a labeled vertical dotted line at the number of determinants that recover 99% of the exact FCI wave function.

The success of a time-dependent ACI (TD-ACI) in treating charge migration relies on the exact wave function being sparse throughout propagation. To test the sparsity of propagated wave functions, we analyze the squared magnitude of FCI coefficients ($|c_I|^2$) computed at four time steps in the evolution of a core-ionized lithium dimer in Figure 5.1. We will present more theoretical details in later sections, but the relevant dynamics in this model system involve a core hole migrating from one lithium atom to another with a frequency of around 250 as. Also shown in Figure 5.1 is the number of determinants required to recover 99% of the FCI wave function. We see that as the propagation proceeds, the sparsity is reduced only slightly, requiring at most 126 determinants out of a total of 5400 throughout a 10 fs simulation. This result is promising, and suggests that the entire wave function may not be necessary to recover the relevant dynamics.

5.2 Theory

5.2.1 Time-Dependent ACI

Studying ultrafast dynamics of electrons requires the solution to the time-dependent Schrödinger equation (in atomic units),

$$i\frac{\partial}{\partial t}|\Psi(t)\rangle = \hat{H}|\Psi(t)\rangle, \tag{5.1}$$

which dictates how a wave function, $\Psi(t)$, evolves in time according to the Hamiltonian ($\hat{H}$). For a time-independent $\hat{H}$, the evolution of a wave function can be written exactly,

$$|\Psi(t+\Delta t)\rangle = e^{-i\hat{H}\Delta t}|\Psi(t)\rangle, \tag{5.2}$$

where Δt is the timestep over which the wave function evolves. Many time-dependent variants of methods in electronic structure theory have been proposed to approximate equations 5.1-5.2, including real-time versions of Hartree–Fock,[78,79] configuration interaction,[80–85] multiconfigurational self consistent field,[86–88] density functional theory,[30,89–91] and coupled-cluster theories.[92–96]

To study charge migration following ionization, we first perform a ground-state ACI computation, producing an N-electron wave function, $|\Psi_0^N\rangle$, in an associated selected determinantal space, M,[37–39]

$$|\Psi_0^N\rangle = \sum_{\Phi_\mu^N \in M} |\Phi_\mu^N\rangle\, c_\mu \tag{5.3}$$

The quality of the ACI energy, and to some extent the wave function, is controlled by a user-defined parameter, σ, which controls the error in the computed energy, E_{ACI}, with respect to the exact value, E_{FCI},

$$|E_{\mathrm{ACI}} - E_{\mathrm{FCI}}| \approx \sigma. \tag{5.4}$$

In our dynamics studies, we invoke the commonly-used *sudden ionization approximation*, where the initial wave function for the simulation $[\Psi^{N-1}(t=0)]$ is defined immediately after the ionization process by annihilating an electron in spin orbital ϕ_i,

$$|\Psi^{N-1}(t=0)\rangle = \frac{\hat{a}_i\,|\Psi_0^N\rangle}{\langle\Psi_0^N|\,\hat{a}_i^\dagger \hat{a}_i\,|\Psi_0^N\rangle}. \tag{5.5}$$

In propagating this cationic wave function, we need to build a cationic Hamiltonian. The basis, M^{N-1}, for the cationic Hamiltonian is constructed from a set of cationic determinants, $\{\Phi_I^{N-1}\}$, defined by applying a single annihilation to all determinants in the original basis M,

$$M^{N-1} = \{\Phi_I^{N-1} : \Phi_I^{N-1} = \hat{a}_i\,|\Phi_\mu^N\rangle\,,\ \forall i \in \mathbf{A} \text{ and } \forall \Phi_\mu^N \in M\}, \tag{5.6}$$

where $\mathbf{A}$ denotes the set of all active orbitals. We then define the TD-ACI wave function, where the time-dependence is entirely encoded in the expansion coefficients $[c_I(t)]$,

$$|\Psi^{N-1}(t)\rangle = \sum_{\Phi_I^{N-1} \in M_c} c_I(t)\,|\Phi_I^{N-1}\rangle\,, \tag{5.7}$$

and the wave function can be determined at any time t using the propagator from equation 5.2. The number of determinants in the initial wave function is typically smaller than $|M^{N-1}|$, and contributions from determinants in M^{N-1} are added as the propagation pro-

ceeds.

Defining M^{N-1} using a selected CI procedure enables efficient representation of the exact dynamics, but the cationic Hamiltonian will generally still be too large to use in exact propagation. Specifically, evaluating the exponential in equation 5.2 requires computation of all eigenvalues and eigenvectors of $\hat{H}$, which is impractical for most computations. As a result, we use the fourth-order Runge–Kutta technique for integrating differential equations, which is equivalent to approximating the exact exponential propagator using a Taylor series truncated to fourth order so long as $\hat{H}$ is time-independent. The fourth order Runge–Kutta integrator approximates the exact propagator using a series of intermediates,

$$|k_1\rangle = -i\hat{H}\,|\Psi^{N-1}(t)\rangle \tag{5.8}$$

$$|k_2\rangle = -i\hat{H}(|\Psi^{N-1}(t)\rangle + \frac{1}{2}\Delta t\,|k_1\rangle) \tag{5.9}$$

$$|k_3\rangle = -i\hat{H}(|\Psi^{N-1}(t)\rangle + \frac{1}{2}\Delta t\,|k_2\rangle) \tag{5.10}$$

$$|k_4\rangle = -i\hat{H}(|\Psi^{N-1}(t)\rangle + \Delta t\,|k_3\rangle), \tag{5.11}$$

for a finite time step Δt. The wave function at $t+\Delta t$ is then written as,

$$|\Psi^{N-1}(t+\Delta t)\rangle = |\Psi^{N-1}(t)\rangle + \frac{\Delta t}{6}(|k_1\rangle + 2\,|k_2\rangle + 2\,|k_3\rangle + |k_4\rangle) + \mathscr{O}(\Delta t^5). \tag{5.12}$$

One drawback of the Runge–Kutta integrator is that it does not preserve the norm as the wave function propagates in time, requiring a renormalization at each time step that could potentially affect the accuracy of the wave function. As we can see from equations 5.8-5.12, fourth order Runge–Kutta also requires four matrix-vector products between the Hamiltonian and the CI coefficients, which comprise the most computationally demanding part of the algorithm. A key advantage of the Runge–Kutta method is that these matrix-vector products can performed extremely efficiently by using the σ-vector algorithms from direct Davidson–Liu diagonalization procedures. Furthermore, these products are computationally less demanding than Lanczos methods if more than four Krylov subspace vectors are needed, as those require additional orthogonalization and diagonalization steps.

In TD-ACI, the main source of error is not expected to result from the approximation of the exponential propagator but rather from the truncated basis, M^{N-1}, of the cationic Hamiltonian. While $\Psi^{N-1}(t=0)$ can be constructed from a singly-annihilated ground-state ACI wave function, M^{N-1} needs to consider the determinants most important to describe the various cationic states that drive the dynamics. These cationic states can be described as simple hole states, defined with a single annihilation of the ground state, or they can have more complex structure if they involve single annihilations coupled with electronic excitations. This second class of cationic state can be built from annihilating electronically excited states of the neutral species, and they can be challenging to identify but necessary to produce correct dynamics.[14,17,19,28,33] In a previous work, we showed that time-independent ACI can be successfully applied to electronically excited states using algorithms that either optimize individual sets of determinants for each state, or build a single set of determinants for all states of interest.[38] In TD-ACI, a single set of determinants is required to describe many cationic states in H, so we define M^{N-1} with equation 5.6 and choose M such that its determinants can be used accurately for the ground and lowest-lying excited states. To build M, we use the state-averaged ACI (SA-ACI), which finds an optimal set of determinants to describe multiple roots by using a determinant importance criterion averaged over each state of interest.

To analyze the dynamics from a TD-ACI computation, we monitor the migration of the hole throughout the molecular orbitals used. Specifically, we can define a *hole occupation number*, n_i for an orbital i, as the difference between the occupation of orbital i in the ground state and the ionized state at time t,

$$n_i(t) = \langle \Psi_0^N | \hat{a}_i^\dagger \hat{a}_i | \Psi_0^N \rangle - \langle \Psi^{N-1}(t) | \hat{a}_i^\dagger \hat{a}_i | \Psi^{N-1}(t) \rangle . \tag{5.13}$$

The hole can occupy multiple orbitals and migrate among them as the propagation proceeds, all dictated by the degree of correlation in $\Psi^{N-1}(t)$.

In this work, we focus on valence and near-valence ionization-induced charge migra-

tion. Consequently the cationic states required for a reasonably accurate simulation can be well-approximated using a complete active space (CAS) form of the wave function, where only the subset of the orbital basis most important in defining the cationic states is used to build the wave function. Using TD-ACI, we are able to study dynamics using active spaces much larger than the FCI limit, and we will show that our flexible ansatz is capable of efficiently characterizing the relevant cationic states required for correct dynamics.

5.3 Results and Discussion

In the following section, we apply TD-ACI to charge migration triggered by valence and inner-valence ionization in both benzene and iodoacetylene. Our application to benzene will serve as a benchmark to understand the behavior of TD-ACI, after which we will compute hole migration dynamics in iodoacetylene, comparing to recent theoretical and experimental data.

5.3.1 Valence Ionization of Benzene

To understand the effects of basis truncation and approximate propagation, we study the charge migration following a valence ionization in benzene. The dynamics of the ionized state is characterized by hole migration within the π/π^* manifold, with weak hole-occupation of a nearby σ-bonding orbital. A complete active space containing the six π/π^* valence orbitals and electrons and the energetically nearest σ/σ^* bonding/antibonding pair is thus required, resulting in a CAS(8,8) shown in Figure 5.2.[28] This active space is small enough to use both FCI and the exact propagator, making it a good model system to test our approximations.

The benzene geometry was optimized using density functional theory (DFT) with a B3LYP functional and the cc-pVDZ basis set using the PSI4 program.[97] The TD-ACI uses the aforementioned CAS(8,8) active space computed within the cc-pVDZ basis using density fitted integrals using the cc-pVDZ-JKFIT basis in computing the RHF references.[98]

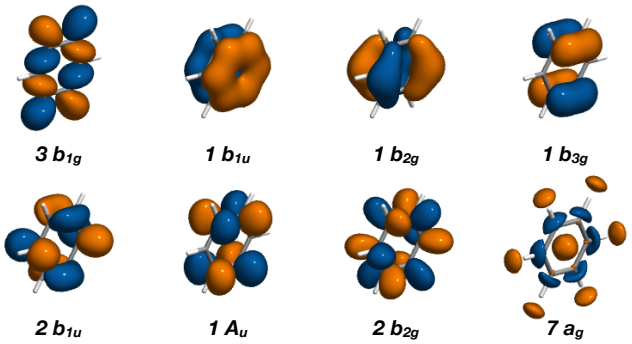

Figure 5.2: Active space used in all benzene computations. Orbitals are computed with restricted Hartree–Fock using C_1 symmetry, though we use D_{2h} labels here for convenience.

The computation was run using C_1 symmetry, but we plot the active orbitals in Figure 5.2 using corresponding D_{2h} labels for clarity. In the TD-ACI simulation, we use a time step of 0.05 as for total simulation time of 2 fs, and the initial state is prepared by annihilating the alpha spin orbital corresponding to the lowest energy π-bonding orbital, with symmetry label $1b_{1u}$.

Upon ionization of the $1b_{1u}$ orbital, the hole migrates between a superposition of the degenerate b_{2g} and b_{3g} orbitals occupied in the initial state and the original $1b_{1u}$ orbital. Using a simplified CAS(8,8) model, this oscillation occurs smoothly and with a frequency of roughly 750 as. This hole oscillation is faster by about 200 as compared to those previously reported[28] because our use of a CAS(8,8) excludes configurations that serve to slow the dynamics and create more complex interference patterns. Nonetheless, our model will be effective in determining the utility of determinant selection in TD-ACI because the oscillating hole occupations will likely require determinants different in character from those that define the ground state.

We test three different schemes to build M^{N-1} based on either single-state or state-averaged ACI algorithms, where M is built to optimize one, two, or four roots of the neutral species. These time-independent computations are run with varying values of σ, which are selected to produce similar dimensions of M^{N-1} to facilitate comparisons. With the various M^{N-1} bases, we propagate the initial wave functions using the fourth-order Runge-

Kutta algorithm, and we plot the error in the overlap of these propagated wave functions with respect to the FCI result in Figure 5.3. These overlap errors contain only truncation

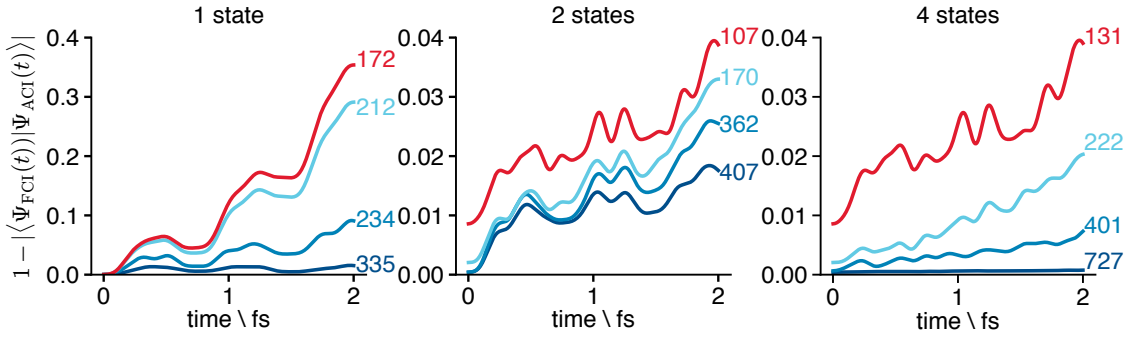

Figure 5.3: Error in propagated wave functions computed with various σ values using one, two, or three reference states in computing the cationic basis. The error is defined as the deviation between unity and the overlap of the approximate wave function with the exact wave function, for which $|M^{N-1}| = 3920$ determinants. Each error curve is labeled with the number of determinants in the cationic space. The exact wave functions are propagated with the exact propagator, and TD-ACI wave functions are propagated with the fourth order Runge–Kutta propagator.

errors, and we see that the observed error is not necessarily correlated with the number of determinants in each computation. For example, the propagations with the single-state M^{N-1} (left plot) show errors that grow up to 0.3 at 2 fs when the cationic space is defined by about 200 determinants. With a similar dimension, the two-state variant already shows an approximate 10-fold increase in accuracy, and the four-state method shows the least error for a given number of determinants, with only minor improvements to the two-state scheme. This result can be rationalized by consideration of the cationic states that couple strongly in the Hamiltonian. Specifically, this particular dynamics in benzene has been reported to involve strong coupling of two-hole/one-particle states in addition to hole-excited states.[28] The cationic Hamiltonian therefore needs states characterized by the initial hole state, states with the hole located in different orbitals, and most importantly hole states that also have single or higher electronic excitations. This third type of state is more efficiently reached when building M^{N-1} with the SA-ACI procedure because the states considered have single, double, or higher excitation character with respect to the ground state.

As mentioned, the dynamics under study involves a rapid hole migration from the $1b_{1u}$ orbital to a superposition of b_{2g} and b_{3g} orbitals. This dynamics is shown in Figure 5.4, where the exact hole occupations are shown in light grey in each panel. The exact hole occupation of the $1b_{1u}$ orbital is shown in each plot starting at unity, and the b_{2g} and b_{3g} hole occupations start from zero and are always identical. In the upper four panels, we show hole occupations computed with TD-ACI using the exact propagator and various numbers of optimized roots in defining M^{N-1} in addition to various sizes of M^{N-1}. The lower panels show the same data, but instead using the fourth-order Runge–Kutta propagator. Our first observation is that the TD-ACI dynamics are indistinguishable when using either exact or Runge–Kutta propagations in this case, showing that our expected propagation errors are negligible even with determinant selection so long as an appropriate time step is chosen. When the M^{N-1} is optimized with respect to one root, the hole occupation oscillates too quickly and does not transfer from the $1b_{1u}$ orbital (red) to the b_{2g} and b_{3g} orbitals (blue and green) with enough magnitude. Interestingly, the hole occupations of the b_{2g} and b_{3g} orbitals are correctly always identical. Using the two-state procedure to build a similarly-sized M^{N-1}, the magnitude of the hole occupation numbers is much more accurate, though the dynamics is slightly too fast and the occupations of the b_{2g} and b_{3g} orbitals are now different. Finally, the four-state procedure gives nearly exact dynamics, and with a larger M^{N-1} space, gives occupations nearly indistinguishable from the exact result.

These results indicate that TD-ACI is a viable technique in studying charge migration resultant from ionization, particularly if the basis for the cationic Hamiltonian is truncated using importance criteria that can consider multiple roots. This use of an SA-ACI computation to build the basis enables a faster convergence to the $\sigma = 0$ limit, and does not bias the determinantal makeup of cationic Hamiltonian towards the ground cationic state.

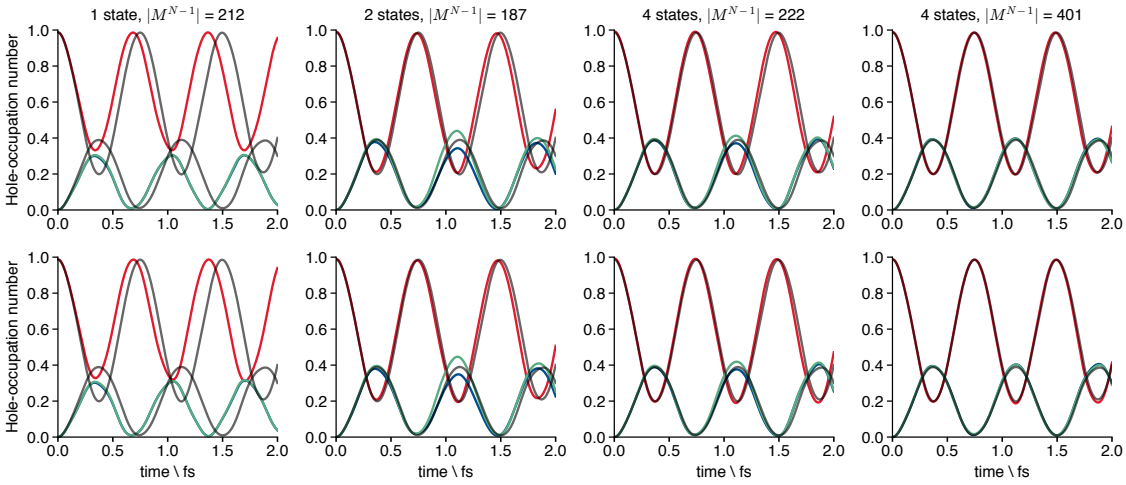

Figure 5.4: Hole occupations of $1b_{1u}$ (red), $1b_{2g}$ (blue), and $1b_{3g}$ (green) orbitals computed using TD-ACI with various sizes of M^{N-1} optimized for 1, 2, and 4 states. The top row shows occupations computed using the exact propagator, and the bottom row used the fourth order Runge–Kutta propagator. Each plot shows the exact occupations with a grey line.

5.3.2 Charge Migration in Iodoacetylene

Iodoacetylene has been a valuable model of charge migration for theorists and experimentalists alike. Recently, Kraus *et. al* have used high-harmonic generation pulses to achieve 100 as resolution and control over charge migration following ionization.[5,10] The dynamics following ionization was reproduced theoretically by a TD-DMRG study using a CAS(16,36) active space.[32] In iodoacetylene, two cationic states drive the dynamics, one characterized by a hole in the $5p$-like orbitals of iodine perpendicular to the molecular axis, and the other having a hole in the two π-bonding orbitals in the acetylene triple bond. These states have considerable degeneracies and thus a multiconfigurational time-dependent approach may be required.

Driven by the two aforementioned cationic states, the dynamics of ionized iodoacetylene involve the ionized hole migrating between the iodine and acetylene groups with a measured frequency of about 0.93 fs. Our final test of TD-ACI will be to reproduce this migration frequency using a truncated determinantal basis of cationic determinants. We optimize the geometry with DFT using a PBE0 functional and def2-SVP basis set. This basis

was used in all iodoacetylene computations with an effective core potential that contains 28 electrons. Within the remaining 59 orbitals, we use a CAS(16,22), which includes all molecular orbitals generated from the $2p$-like orbitals in the acetylene group, and $4d$ and $5p$-like molecular orbitals from the iodine. In the dynamics simulations, we use a timestep of 0.02 as for a total simulation time of 2 fs. The initial state is prepared by annihilating a valence $5p$-like orbital on the iodine atom, and all computations are run in C_1 symmetry with split-localized orbitals in the active space.

Our first simulation uses a single-state ACI computation with $\sigma = 8\ mE_\mathrm{h}$ to generate a cationic basis containing $93,554$ determinants, where the Hilbert space defined from our CAS(16,22) contains roughly 10^{11} determinants. We plot the hole occupation numbers for the ionized $5p$-like orbital on the iodine and the in-plane π-bonding orbital of the acetylene in Figure 5.5 for the 2 fs simulation. The hole migrates from the iodine to the acetylene and back in about 0.9 fs, agreeing closely with the experimental frequency of 0.93 fs. We also see that this migration still leaves some degree of hole occupation on each moiety. To further analyze the charge migration dynamics, we can compute a representation of the density of the ionized hole (ρ_H) by weighting the Hartree–Fock orbitals by the corresponding hole occupation,

$$\rho_H = \sum_i |\phi_i|^2 n_i, \tag{5.14}$$

which we show in the lower panel in Figure 5.5. Interestingly, the relatively good agreement between our computed frequency of hole migration and the experimental value suggests that the single-state ACI procedure is building an adequate space of determinants to describe the relevant cationic states. The cationic states that drive the dynamics, namely those characterized by valence ionizations of acetylene and iodine, therefore do not involve a significant coupling between the hole excitation and additional electronic excitations.

We can more rigorously test this conclusion by comparing the hole migration frequencies computed from similarly sized determinantal spaces optimized for one, two, and three electronic states. In Table 5.1, we show the time required for the hole to migrate to the

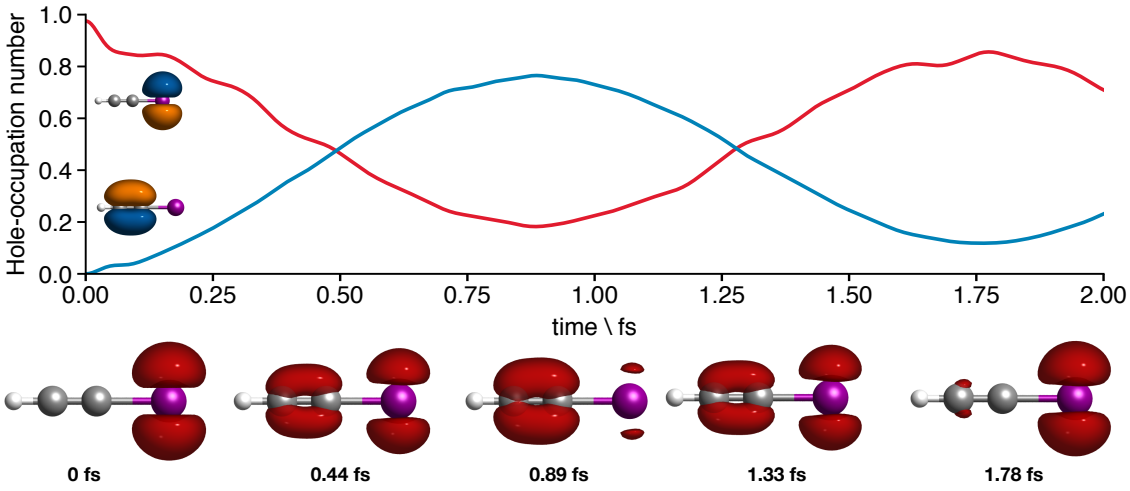

Figure 5.5: Hole occupations of the $5p$-like molecular orbital on iodine (red) and the π on the acetylene (blue) in the same plane. Below the plot we show the migration of the hole using the representation of the hole density defined in the text. The snapshots selected for the densities shown correspond to maxima, minima and intersection of the hole occupation curves.

acetylene group and then back to the iodine from three computations using roughly 10^4 determinants in M^{N-1}. We also show the migration times resultant from the TD-ACI computation using a larger cationic determinantal basis optimized for one state that was used for Figure 5.5. For a nearly constant size of M^{N-1}, we see that increasing the number of states used to generate the cationic basis has a negligible effect on the hole migration times. Only when the total number of cationic determinants is increased, even when optimized for the neutral ground state, do we see the migration times approach the experimental and TD-DMRG values. This result depends solely on the determinantal makeup of the cationic states most important in forming the evolving wave packet. In this case, these states are simple cationic hole states with the hole located on the iodine or acetylene moieties, and no coupled electronic excitations are as significant as they were for our previous study on benzene. As a result, the dominant contribution for both hole states comes from different annihilations of the ground state and not from annihilations of excited states. A very appeal-

Table 5.1: Hole migration times (as) for various dimensions of M^{N-1} optimized with respect to one, two, or three electronic states.

		Time for maximum hole occupation (as)	
Number of states	$\lvert M^{N-1}\rvert$	acetylene	iodine
1	10127	862	1684
2	10827	864	1660
3	10759	868	1610
1	93554	886	1780

ing property of our TD-ACI approach is that we can effectively optimize M^{N-1} regardless of the character of the relevant cationic states, whether simple or complex

5.4 Conclusions and Future Challenges

In this work, we have used ground and excited state ACI algorithms to solve the time-dependent Schrödinger equation. TD-ACI is able to effectively model the real-time propagation of the exact wave function using a truncated space of determinants selected by the time-independent ACI algorithm. We apply this methodology to charge migration dynamics that follow ultrafast ionization. We find that ACI is well-suited to find determinants relevant to the initial state, and determinants important at later points in time can be initially identified in excited state computations to reduce systematic increases in error as the wave function evolves. We also find that the single-state ACI computation can recover these determinants if a sufficiently large value of σ is used. Due to the short time scale of charge migration, we did not encounter significant issues in using approximations to the exact time propagator, though these effects could be important in longer simulations. Propagation error and truncation errors were studied using a charge migration model in benzene, where we found that cationic spaces optimized for multiple roots are needed to efficiently capture dynamics in which two-hole one-particle states are relevant. This type of state is not always relevant to the dynamics in propagating our initial state, as we saw in our application to hole migration in iodoacetylene. Using various schemes to build our cationic basis, we were able to compute hole migration times between acetylene and iodine

groups that match experimental results. As we have shown, TD-ACI is an extremely flexible option for studying charge migration because it can determine an optimal cationic basis regardless of the character of the dominant cationic states.

Following the success of this initial TD-ACI study, we anticipate numerous future directions of study. While the SA-ACI procedure was successful in building a determinantal space for the entire dynamics, we envision an even more efficient scheme where the selection and removal of determinants can be done during the simulation itself. For example, one can imagine an algorithm that estimates the importance of a determinant at a future timestep using low-order approximate propagation. Additionally, integration of the current TD-ACI scheme with a time-dependent Hamiltonian would enable *ab initio* studies of molecules interacting with fluctuating electric or magnetic fields. Finally, we envision including dynamical correlation effects beyond our active space treatment by combining an effective Hamiltonian theory with a time-dependent reference wave function.

Bibliography

[1] F. Krausz and M. Ivanov. "Attosecond physics." *Rev. Mod. Phys.* **81**, 163 (2009).

[2] M. Nisoli, P. Decleva, F. Calegari, A. Palacios, and F. Martín. "Attosecond Electron Dynamics in Molecules." *Chem. Rev.* **117**, 10760 (2017).

[3] S. R. Leone, C. W. McCurdy, J. Burgdörfer, L. S. Cederbaum, Z. Chang, N. Dudovich, J. Feist, C. H. Greene, M. Ivanov, R. Kienberger, U. Keller, A. Stolow, U. Thumm, and M. J. J. Vrakking. "What will it take to observe processes in'real time'?" *Nat. Photon.* **8**, 162 (2014).

[4] F. Lépine, M. Y. Ivanov, and M. J. J. Vrakking. "Attosecond molecular dynamics: fact or fiction?" *Nat. Photon.* **8**, 195 (2014).

[5] P. M. Kraus and H. J. Wörner. "Perspectives of Attosecond Spectroscopy for the Understanding of Fundamental Electron Correlations." *Angewandte Chemie International Edition* **57**, 5228 (2018).

[6] V. Despré, N. V. Golubev, and A. I. Kuleff. "Charge Migration in Propiolic Acid: A Full Quantum Dynamical Study." *Phys. Rev. Lett.* **121**, 203002 (2018).

[7] A. D. Bandrauk, S. Chelkowski, and G. L. Yudin. "Chirped photoelectron attochemistry." In "Femtochemistry VII," 553–562. Elsevier (2006).

[8] P. Salières, A. Maquet, S. Haessler, J. Caillat, and R. Taïeb. "Imaging orbitals with attosecond and Ångström resolutions: toward attochemistry?" *Rep. Prog. Phys.* **75**, 062401 (2012).

[9] A. E. Boguslavskiy, J. Mikosch, A. Gijsbertsen, M. Spanner, S. Patchkovskii, N. Gador, M. J. J. Vrakking, and A. Stolow. "The Multielectron Ionization Dynamics Underlying Attosecond Strong-Field Spectroscopies." *Science* **335**, 1336 (2012).

[10] P. M. Kraus, B. Mignolet, D. Baykusheva, A. Rupenyan, L. Horný, E. F. Penka, G. Grassi, O. I. Tolstikhin, J. Schneider, F. Jensen, L. B. Madsen, A. D. Bandrauk, F. Remacle, and H. J. Wörner. "Measurement and laser control of attosecond charge migration in ionized iodoacetylene." *Science* **350**, 790 (2015).

[11] N. V. Golubev, V. Despré, and A. I. Kuleff. "Quantum control with smoothly varying pulses: general theory and application to charge migration." *Journal of Modern Optics* **64**, 1031 (2017).

[12] H. J. Wörner, P. C. H. o. H.-r. Spectroscopy, and 2011. "Attosecond spectroscopy." *ethz.ch* .

[13] H. J. Wörner, C. A. Arrell, N. Banerji, A. Cannizzo, M. Chergui, A. K. Das, P. Hamm, U. Keller, P. M. Kraus, E. Liberatore, P. Lopez-Tarifa, M. Lucchini, M. Meuwly, C. Milne, J.-E. Moser, U. Rothlisberger, G. Smolentsev, J. Teuscher, J. A. van Bokhoven,

and O. Wenger. "Charge migration and charge transfer in molecular systems." *Structural Dynamics* **4**, 061508 (2017).

[14] L. S. Cederbaum and J. Zobeley. "Ultrafast charge migration by electron correlation." *Chem. Phys. Lett.* **307**, 205 (1999).

[15] K.-J. Yuan and A. D. Bandrauk. "Ultrafast X-ray Photoelectron Imaging of Attosecond Electron Dynamics in Molecular Coherent Excitation." *J. Phys. Chem. A* **123**, 1328 (2018).

[16] H. Hennig, J. Breidbach, and L. S. Cederbaum. "Electron Correlation as the Driving Force for Charge Transfer: Charge Migration Following Ionization in N-Methyl Acetamide." *J. Phys. Chem. A* **109**, 409 (2005).

[17] J. Breidbach and L. S. Cederbaum. "Universal attosecond response to the removal of an electron." *Phys. Rev. Lett.* **94**, 033901 (2005).

[18] A. I. Kuleff and L. S. Cederbaum. "Ultrafast correlation-driven electron dynamics." *J. Phys. B: At. Mol. Opt. Phys.* **47**, 124002 (2014).

[19] A. I. Kuleff, N. V. Kryzhevoi, M. Pernpointner, and L. S. Cederbaum. "Core Ionization Initiates Subfemtosecond Charge Migration in the Valence Shell of Molecules." *Phys. Rev. Lett.* **117**, 093002 (2016).

[20] M. Wormit, D. R. Rehn, P. H. P. Harbach, J. Wenzel, C. M. Krauter, E. Epifanovsky, and A. Dreuw. "Investigating excited electronic states using the algebraic diagrammatic construction (ADC) approach of the polarisation propagator." *Mol. Phys.* **112**, 774 (2014).

[21] A. Dreuw and M. Wormit. "The algebraic diagrammatic construction scheme for the polarization propagator for the calculation of excited states." *WIREs Comput Mol Sci* **5**, 82 (2014).

[22] A. I. Kuleff and L. S. Cederbaum. "Charge migration in different conformers of glycine: The role of nuclear geometry." *Chem. Phys.* **338**, 320 (2007).

[23] S. Lünnemann, A. I. Kuleff, and L. S. Cederbaum. "Ultrafast charge migration in 2-phenylethyl-N,N-dimethylamine." *Chem. Phys. Lett.* **450**, 232 (2008).

[24] S. Lünnemann, A. I. Kuleff, and L. S. Cederbaum. "Charge migration following ionization in systems with chromophore-donor and amine-acceptor sites." *J. Chem. Phys.* **129**, 104305 (2008).

[25] A. I. Kuleff and A. Dreuw. "Theoretical description of charge migration with a single Slater-determinant and beyond." *J. Chem. Phys.* **130**, 034102 (2009).

[26] S. Lünnemann, A. I. Kuleff, and L. S. Cederbaum. "Ultrafast electron dynamics following outer-valence ionization: the impact of low-lying relaxation satellite states." *J. Chem. Phys.* **130**, 154305 (2009).

[27] A. I. Kuleff, S. Lünnemann, and L. S. Cederbaum. "Ultrafast Charge Migration Following Valence Ionization of 4-Methylphenol: Jumping over the Aromatic Ring †." *J. Phys. Chem. A* **114**, 8676 (2010).

[28] V. Despré, A. Marciniak, V. Loriot, M. C. E. Galbraith, A. Rouzée, M. J. J. Vrakking, F. Lépine, and A. I. Kuleff. "Attosecond Hole Migration in Benzene Molecules Surviving Nuclear Motion." *J. Phys. Chem. Lett.* **6**, 426 (2015).

[29] A. Bruner, S. Hernandez, F. Mauger, P. M. Abanador, D. J. LaMaster, M. B. Gaarde, K. J. Schafer, and K. Lopata. "Attosecond Charge Migration with TDDFT: Accurate Dynamics from a Well-Defined Initial State." *J. Phys. Chem. Lett.* **8**, 3991 (2017).

[30] K. Lopata and N. Govind. "Modeling Fast Electron Dynamics with Real-Time Time-Dependent Density Functional Theory: Application to Small Molecules and Chromophores." *J. Chem. Theor. Comput.* **7**, 1344 (2011).

[31] K. Lopata, B. E. Van Kuiken, M. Khalil, and N. Govind. "Linear-Response and Real-Time Time-Dependent Density Functional Theory Studies of Core-Level Near-Edge X-Ray Absorption." *J. Chem. Theor. Comput.* **8**, 3284 (2012).

[32] L.-H. Frahm and D. Pfannkuche. "Ultrafast ab-initio Quantum Chemistry Using Matrix Product States." *J. Chem. Theor. Comput.* acs.jctc.8b01291 (2019).

[33] J. Breidbach and L. S. Cederbaum. "Migration of holes: numerical algorithms and implementation." *J. Chem. Phys.* **126**, 034101 (2007).

[34] F. Verstraete and J. I. Cirac. "Renormalization algorithms for Quantum-Many Body Systems in two and higher dimensions." (2004).

[35] J. Ren, Z. Shuai, and G. Kin-Lic Chan. "Time-Dependent Density Matrix Renormalization Group Algorithms for Nearly Exact Absorption and Fluorescence Spectra of Molecular Aggregates at Both Zero and Finite Temperature." *J. Chem. Theor. Comput.* **14**, 5027 (2018).

[36] G. K.-L. Chan and M. Head-Gordon. "Highly correlated calculations with a polynomial cost algorithm: A study of the density matrix renormalization group." **116**, 4462 (2002).

[37] J. B. Schriber and F. A. Evangelista. "Communication: An adaptive configuration interaction approach for strongly correlated electrons with tunable accuracy." *J. Chem. Phys.* **144**, 161106 (2016).

[38] J. B. Schriber and F. A. Evangelista. "Adaptive Configuration Interaction for Computing Challenging Electronic Excited States with Tunable Accuracy." *J. Chem. Theor. Comput.* **13**, 5354 (2017).

[39] J. B. Schriber, K. P. Hannon, C. Li, and F. A. Evangelista. "A Combined Selected Configuration Interaction and Many-Body Treatment of Static and Dynamical Correlation in Oligoacenes." *J. Chem. Theor. Comput.* **14**, 6295 (2018).

[40] M. J. M. Bernal and S. F. Boys. "Electronic Wave Functions. VIII. A Calculation of the Ground States NaFormula, Ne and FFormula." *Philosophical Transactions of the Royal Society A: Mathematical, Physical and Engineering Sciences* **245**, 139 (1952).

[41] Z. Gershgorn and I. Shavitt. "An application of perturbation theory ideas in configuration interaction calculations." *Int. J. Quant. Chem.* **2**, 751 (1968).

[42] A. Pipano and I. Shavitt. "Convergence studies in configuration interaction calculations." *Int. J. Quant. Chem.* **2**, 741 (1968).

[43] C. F. Bender and E. R. Davidson. "Studies in Configuration Interaction: The First-Row Diatomic Hydrides." *Phys. Rev.* **183**, 23 (1969).

[44] J. L. Whitten and M. Hackmeyer. "Configuration Interaction Studies of Ground and Excited States of Polyatomic Molecules. I. The CI Formulation and Studies of Formaldehyde." *J. Chem. Phys.* **51**, 5584 (1969).

[45] B. Huron, J. P. Malrieu, and P. Rancurel. "Iterative perturbation calculations of ground and excited state energies from multiconfigurational zeroth-order wavefunctions." *J. Chem. Phys.* **58**, 5745 (1973).

[46] R. J. Buenker and S. D. Peyerimhoff. "Individualized configuration selection in CI calculations with subsequent energy extrapolation." *Theoret. Chim. Acta* **35**, 33.

[47] R. J. Buenker and S. D. Peyerimhoff. "Energy extrapolation in CI calculations." *Theoret. Chim. Acta* **39**, 217 (1975).

[48] S. Evangelisti, J.-P. Daudey, and J. P. Malrieu. "Convergence of an improved CIPSI algorithm." *Chem. Phys.* **75**, 91 (1983).

[49] R. Cimiraglia. "Second order perturbation correction to CI energies by use of diagrammatic techniques: An improvement to the CIPSI algorithm." *J. Chem. Phys.* **83**, 1746 (1985).

[50] P. J. Knowles and N. C. Handy. "A new determinant-based full configuration interaction method." *Chem. Phys. Lett.* **111**, 315 (1984).

[51] R. J. Harrison. "Approximating full configuration interaction with selected configuration interaction and perturbation theory." *J. Chem. Phys.* **94**, 5021 (1991).

[52] A. O. Mitrushenkov. "Passing the several billions limit in FCI calculations on a minicomputer." *Chem. Phys. Lett.* **217**, 559 (1994).

[53] A. L. Wulfov. "Passing the one-quadrillion limit in FCl extrapolations on a personal computer." *Chem. Phys. Lett.* (1996).

[54] M. Hanrath and B. Engels. "New algorithms for an individually selecting MR-CI program." *Chem. Phys.* (1997).

[55] P. Stampfuß, K. Hamacher, and W. Wenzel. "Massively parallel individually selecting configuration interaction." *J. Mol. Struct.:THEOCHEM* **506**, 99 (2000).

[56] J. Ivanic, K. R. T. C. Accounts, and 2001. "Identification of deadwood in configuration spaces through general direct configuration interaction." *Springer* **106**, 339 (2001).

[57] P. Stampfuß and W. Wenzel. "Improved implementation and application of the individually selecting configuration interaction method." *J. Chem. Phys.* **122**, 024110 (2005).

[58] L. Bytautas and K. Ruedenberg. "A priori identification of configurational deadwood." *Chem. Phys.* **356**, 64 (2009).

[59] J. C. Greer. "Estimating full configuration interaction limits from a Monte Carlo selection of the expansion space." *J. Chem. Phys.* **103**, 1821 (1995).

[60] J. C. Greer. "Monte Carlo Configuration Interaction." *Journal of Computational Physics* **146**, 181 (1998).

[61] J. P. Coe and M. J. Paterson. "Development of Monte Carlo configuration interaction: natural orbitals and second-order perturbation theory." *J. Chem. Phys.* **137**, 204108 (2012).

[62] J. P. Coe and M. J. Paterson. "State-averaged Monte Carlo configuration interaction applied to electronically excited states." *J. Chem. Phys.* **139**, 154103 (2013).

[63] P. J. Knowles. "Compressive sampling in configuration interaction wavefunctions." *Mol. Phys.* **113**, 1655 (2015).

[64] J. R. McClean and A. Aspuru-Guzik. "Compact wavefunctions from compressed imaginary time evolution." *RSC Advances* (2015).

[65] C. F. Bunge. "Selected configuration interaction with truncation energy error and application to the Ne atom." *J. Chem. Phys.* **125**, 014107 (2006).

[66] F. A. Evangelista. "Adaptive multiconfigurational wave functions." **140**, 054109 (2014).

[67] N. M. Tubman, J. Lee, T. Y. Takeshita, M. Head-Gordon, and K. B. Whaley. "A deterministic alternative to the full configuration interaction quantum Monte Carlo method." *J. Chem. Phys.* **145**, 044112 (2016).

[68] N. M. Tubman, C. D. Freeman, D. S. Levine, D. Hait, M. Head-Gordon, and K. B. Whaley. "Modern Approaches to Exact Diagonalization and Selected Configuration Interaction with the Adaptive Sampling CI Method." *arXiv* https:—-arxiv.org–abs–1807.00821 (2018).

[69] Y. Ohtsuka and J.-y. Hasegawa. "Selected configuration interaction method using sampled first-order corrections to wave functions." *J. Chem. Phys.* **147**, 034102 (2017).

[70] E. Giner, A. Scemama, and M. Caffarel. "Using perturbatively selected configuration interaction in quantum Monte Carlo calculations." *Can. J. Chem.* **91**, 879 (2013).

[71] E. Giner, R. Assaraf, and J. Toulouse. "Quantum Monte Carlo with reoptimised perturbatively selected configuration-interaction wave functions." *Mol. Phys.* **114**, 910 (2016).

[72] P.-F. Loos, A. Scemama, A. Blondel, Y. Garniron, M. Caffarel, and D. Jacquemin. "A Mountaineering Strategy to Excited States: Highly Accurate Reference Energies and Benchmarks." *J. Chem. Theor. Comput.* **14**, 4360 (2018).

[73] A. A. Holmes, N. M. Tubman, and C. J. Umrigar. "Heat-Bath Configuration Interaction: An Efficient Selected Configuration Interaction Algorithm Inspired by Heat-Bath Sampling." *J. Chem. Theor. Comput.* **12**, 3674 (2016).

[74] S. Sharma, A. A. Holmes, G. Jeanmairet, A. Alavi, and C. J. Umrigar. "Semistochastic heat-bath configuration interaction method: Selected configuration interaction with semistochastic perturbation theory." *J. Chem. Theor. Comput.* **13**, 1595 (2017).

[75] A. A. Holmes, C. J. Umrigar, and S. Sharma. "Excited states using semistochastic heat-bath configuration interaction." *J. Chem. Phys.* **147**, 164111 (2017).

[76] V. A. Neufeld and A. J. W. Thom. "Exciting determinants in Quantum Monte Carlo: Loading the dice with fast, low memory weights." *J. Chem. Theor. Comput.* **15**, 127 (2018).

[77] J. Li, M. Otten, A. A. Holmes, S. Sharma, and C. J. Umrigar. "Fast semistochastic heat-bath configuration interaction." *J. Chem. Phys.* **149**, 214110 (2018).

[78] K. C. Kulander. "Time-dependent Hartree-Fock theory of multiphoton ionization: Helium." *Phys. Rev. A* **36**, 2726 (1987).

[79] X. Li, S. M. Smith, A. N. Markevitch, D. A. Romanov, R. J. Levis, and H. B. Schlegel. "A time-dependent Hartree–Fock approach for studying the electronic optical response of molecules in intense fields." *Physical Chemistry Chemical Physics* **7**, 233 (2005).

[80] N. Rohringer, A. Gordon, and R. Santra. "Configuration-interaction-based time-dependent orbital approach for ab initio treatment of electronic dynamics in a strong optical laser field." *Phys. Rev. A* **74**, 043420 (2006).

[81] H. B. Schlegel, S. M. Smith, and X. Li. "Electronic optical response of molecules in intense fields: Comparison of TD-HF, TD-CIS, and TD-CIS(D) approaches." *J. Chem. Phys.* **126**, 244110 (2007).

[82] P. Krause, T. Klamroth, and P. Saalfrank. "Molecular response properties from explicitly time-dependent configuration interaction methods." *J. Chem. Phys.* **127**, 034107 (2007).

[83] P. Krause, J. A. Sonk, and H. B. Schlegel. "Strong field ionization rates simulated with time-dependent configuration interaction and an absorbing potential." *J. Chem. Phys.* **140**, 174113 (2014).

[84] W.-T. Peng, B. S. Fales, and B. G. Levine. "Simulating Electron Dynamics of Complex Molecules with Time-Dependent Complete Active Space Configuration Interaction." *J. Chem. Theor. Comput.* **14**, 4129 (2018).

[85] I. S. Ulusoy, Z. Stewart, and A. K. Wilson. "The role of the CI expansion length in time-dependent studies." *J. Chem. Phys.* **148**, 014107 (2018).

[86] H. D. Meyer, U. Manthe, and L. S. Cederbaum. "The multi-configurational time-dependent Hartree approach." *Chem. Phys. Lett.* **165**, 73 (1990).

[87] M. Nest, T. Klamroth, and P. Saalfrank. "The multiconfiguration time-dependent Hartree-Fock method for quantum chemical calculations." *J. Chem. Phys.* **122**, 124102 (2005).

[88] R. P. Miranda, A. J. Fisher, L. Stella, and A. P. Horsfield. "A multiconfigurational time-dependent Hartree-Fock method for excited electronic states. I. General formalism and application to open-shell states." *J. Chem. Phys.* **134**, 244101 (2011).

[89] J. Theilhaber. "Ab initiosimulations of sodium using time-dependent density-functional theory." *Phys. Rev., B Condens. Matter* **46**, 12990 (1992).

[90] K. Yabana and G. F. Bertsch. "Time-dependent local-density approximation in real time." *Phys. Rev., B Condens. Matter* **54**, 4484 (1996).

[91] R. Baer and R. Gould. "A method for ab initiononlinear electron-density evolution." *J. Chem. Phys.* **114**, 3385 (2001).

[92] E. Dalgaard and H. J. Monkhorst. "Some aspects of the time-dependent coupled-cluster approach to dynamic response functions." *Phys. Rev. A* **28**, 1217 (1983).

[93] C. Huber and T. Klamroth. "Explicitly time-dependent coupled cluster singles doubles calculations of laser-driven many-electron dynamics." *J. Chem. Phys.* **134**, 054113 (2011).

[94] S. Kvaal. "Ab initio quantum dynamics using coupled-cluster." *J. Chem. Phys.* **136**, 194109 (2012).

[95] D. R. Nascimento and A. E. DePrince. "Linear Absorption Spectra from Explicitly Time-Dependent Equation-of-Motion Coupled-Cluster Theory." *J. Chem. Theor. Comput.* **12**, 5834 (2016).

[96] D. R. Nascimento and A. E. DePrince III. "Simulation of Near-Edge X-ray Absorption Fine Structure with Time-Dependent Equation-of-Motion Coupled-Cluster Theory." *J. Phys. Chem. Lett.* **8**, 2951 (2017).

[97] R. M. Parrish, L. A. Burns, D. G. A. Smith, A. C. Simmonett, A. E. DePrince, E. G. Hohenstein, U. Bozkaya, A. Y. Sokolov, R. Di Remigio, R. M. Richard, J. F. Gonthier, A. M. James, H. R. McAlexander, A. Kumar, M. Saitow, X. Wang, B. P. Pritchard, P. Verma, H. F. Schaefer, K. Patkowski, R. A. King, E. F. Valeev, F. A. Evangelista, J. M. Turney, T. D. Crawford, and C. D. Sherrill. "Psi4 1.1: An Open-Source Electronic Structure Program Emphasizing Automation, Advanced Libraries, and Interoperability." *J. Chem. Theor. Comput.* **13**, 3185 (2017).

[98] F. Weigend. "A fully direct RI-HF algorithm: Implementation, optimised auxiliary basis sets, demonstration of accuracy and efficiency." *Phys. Chem. Chem. Phys.* **4**, 4285 (2002).

Chapter 6

Conclusions and Future Directions

In this dissertation, we have outlined the initial development of a novel selected CI method and have presented various algorithmic extensions enabling the computation of excited states, dynamical correlation effects, and time-dependent quantities. Our method, the Adaptive CI (ACI), represents a large step towards increasing the applicability of multireference methods to more diverse problems in chemistry.

Our first study was devoted to the initial development of the ACI algorithm. The goal of ACI is to exploit the sparsity in a full CI (FCI) wave function by estimating the importance of determinants in Hilbert space, and then keeping a certain number of these determinants such that the energy error of the total wave function matches a user-defined parameter. This algorithm was achieved by iteratively screening, adding, and removing determinants as more of the FCI wave function is deterministically sampled. The novelty in ACI is that the desired error in the energy can be reliably predicted before the computation, as the algorithm can efficiently add the correct determinants to approximately achieve this error. We tested this error control and tunability on the dissociation of N_2, where we saw potential energy curves that paralleled the FCI result nearly exactly, with flat error curves located at or near the predefined error. We then applied ACI as a replacement for complete active space CI (CASCI) to enable the use of very large active spaces. We computed the singlet-triplet splittings in the oligoacene series, which required active spaces containing up to 42 electrons in 42 orbitals [CAS(42,42)]. Due to the reliable error prediction achieved by the

ACI algorithm, the singlet-triplet splittings were within a kcal mol^{-1} of DMRG benchmark data, with some computations using around 3×10^6 determinants from a Hilbert space with dimension on the order of 10^{14}.

Following the initial development of the ground state ACI method, we explored several new algorithmic extensions designed to compute excited states. The goal of an excited state ACI method is twofold: (1) to achieve predictive error control for arbitrary numbers of electronic states with diverse determinantal makeups and (2) to preserve orthogonality among computed states. To fulfill these requirements, we considered strategies either where each state is described by an individual set of determinants or where one set of determinants is used for multiple roots. By modifying the determinant importance criteria to consider multiple roots in the reference, we were able to test numerous algorithms for computing excited states. The best performance came from the orthogonality constrained ACI (OC-ACI), which uses a state-specific criterion to generate a determinantal space optimized for each state of interest. Starting with the ground state, these roots are sequentially optimized such that the previously computed states are projected out of the solution of the current state, ensuring orthogonality and avoiding variational collapse. OC-ACI was able to accurately compute the singlet excited states of methylene, the avoided crossing in the lithium fluoride dissociation, and excited states of long polyenes using up to a CAS(24,24). For example, OC-ACI computed excitation energies of polyenes up to octatetraene with errors on the order of 0.01 eV. An interesting alternative to OC-ACI is to define the determinant importance criterion as an average over several states, as is done in the state-averaged ACI (SA-ACI) method. While slightly less accurate and flexible than OC-ACI, SA-ACI does not require multiple ACI computations and is in principle not considerably more expensive than a ground state ACI computation. In future applications connecting ACI to theories of dynamical correlation, the SA-ACI method may be more convenient in state-averaged treatments.

The aim of the first two projects was to develop necessary parts of the ACI algorithm

to be affordably applicable to ground and excited states. While ACI can efficiently sample FCI wave functions in small to medium sized molecules, any selected CI method with be too expensive for cases where thousands of orbitals are desired. Thus, we use ACI as a replacement for CASCI in combination with a multireference theory of dynamical correlation. Specifically, we use the second-order perturbative driven similarity renormalization group (DSRG-MRPT2) optimized for density fitted integrals because it can recover dynamical correlation very affordably and without susceptibility to intruder states. Part of this affordability is due to DSRG requiring only the three-particle reduced density matrix (RDM), whereas similar multireference perturbation theories require the 4-RDM and thus cannot make use of techniques that enable large active spaces. We apply the ACI-DSRG-MRPT2 again to the oligoacenes to reveal the effect of dynamical correlation on both the singlet triplet splittings and on properties of the wave function. Using up to a CAS(30,30) and 1350 basis functions, ACI-DSRG-MRPT2 was able to produce singlet-triplet splittings in oligoacenes within a few kcal mol^{-1} of available experimental data. Furthermore, ACI-DSRG-MRPT2 allows for computation of reference wave function properties, including effective numbers of unpaired electrons and spin-spin correlations, with dynamical correlation effects included. We find that treating only the active orbitals tends to overestimate the computed number of effectively unpaired electrons, and dynamical correlations serve to reduce this number significantly. Analysis of these relaxed wave functions also shows an antiferromagnetic ordering of the electron spin in the π/π^* manifold. A very promising extension of this work is to connect ACI with the nonperturbative variants of DSRG that can produce coupled-cluster accuracy with only moderate cost.

In the final component of this work, we used ACI to solve the time-dependent Schrödinger equation. Motivated by the general lack of real-time dependent multireference methods, we formulate a time-dependent ACI (TD-ACI) method in which we propagate an ACI wave function in a selected determinantal basis. Starting with a set of determinants optimized for either the ground state or a few of the lowest-lying states, we are able to build an initial hole

state by removing an electron and propagate it using a Hamiltonian built from the set of all selected cationic determinants. This procedure allows us to study the attosecond-scale charge migration that can occur immediately following ultrafast ionization of a molecule. We applied TD-ACI to model the dynamics within the π/π^* manifold in benzene, where using a state-averaged ACI (SA-ACI) procedure in selecting cationic determinants led to improved accuracy of the wave function. This improved accuracy was resultant from the ability of SA-ACI to build a determinantal basis capable of describing complex cationic states that are characterized by simultaneous hole and electronic excitations. To further benchmark the method, we then applied TD-ACI to the charge dynamics in iodoacetylene. TD-ACI successfully and efficiently reproduces the experimentally determined hole migration frequency between the iodine and acetylene groups. We attribute the success of TD-ACI in reproducing these dynamics to the optimal and compact set of cationic determinants generated from ACI and SA-ACI.

By reformulating the very old idea of selected CI as a tool to describe strongly correlated electrons, we are able to extend the applicability of multireference methods. Despite the advances made in this work, new directions involving ACI are diverse. New algorithmic developments could lead to ACI computations in active spaces larger than our current limit of approximately 42 electrons in 42 orbitals. These developments would need to avoid simultaneous storage of all candidate determinants during the screening step. Additionally, ground and excited state ACI algorithms can be connected to state-specific or multistate theories of dynamical correlation to obtain a complete correlation treatment of electronically excited states. Furthermore, we envision ACI-DSRG treatments more accurate than second-order perturbation theory, including hybrid approaches that use high-order, non-perturbative DSRG methods to handle the most important excitations in the dynamical correlation treatment. Such an extension could set the new standard for accuracy among multireference methods.